

TALLINN UNIVERSITY OF TECHNOLOGY
DOCTORAL THESIS
11/2018

**The Composition and Reactivity of
Different Oil Shales and the Products
Formed During Thermal Treatment**

BIRGIT MAATEN



TALLINN UNIVERSITY OF TECHNOLOGY

School of Engineering

Department of Energy Technology

This dissertation was accepted for the defence of the degree 03/04/2018

Supervisor:

Professor Andres Siirde
School of Engineering
Tallinn University of Technology
Tallinn, Estonia

Co-supervisor:

Professor Alar Konist
School of Engineering
Tallinn University of Technology
Tallinn, Estonia

Opponents:

Prof Eric Suuberg
School of Engineering
Chemical and Biochemical Engineering Faculty
Brown University

Dr. Jüri Truusa
Environmental Management Department
Ministry of the Environment

Defence of the thesis: 07/05/2018, Tallinn

Declaration:

Hereby I declare that this doctoral thesis, my original investigation and achievement, submitted for the doctoral degree at Tallinn University of Technology, has not been previously submitted for doctoral or equivalent academic degree.

Birgit Maaten

signature



European Union
European Regional
Development Fund



Investing
in your future

Copyright: Birgit Maaten, 2018

ISSN 2585-6898 (publication)

ISBN 978-9949-83-228-6 (publication)

ISSN 2585-6901 (PDF)

ISBN 978-9949-83-229-3 (PDF)

TALLINNA TEHNIKAÜLIKOOL
DOKTORITÖÖ
11/2018

**Erinevate põlevkivide koostis
ja reaktiivsus ning nende termilisel
töötlusel tekkivad produktid**

BIRGIT MAATEN

Contents

List of Publications	6
Author's Contribution to the Publications	7
Introduction	9
Abbreviations	11
Terms	12
1 LITERATURE OVERVIEW	13
1.1 Oil shale.....	13
1.2 Pyrolysis	15
1.3 Characterization of solid residues and utilization of oil shale ash	18
1.4 Oil shale beneficiation.....	19
1.5 Thermogravimetric analysis	20
1.6 Kinetic computations	23
2 EXPERIMENTAL.....	26
2.1 Equipment and procedures.....	26
2.1.1 Apparatus.....	26
2.1.2 Compositional analysis.....	26
2.2 Characterization of the materials used	27
2.3 Kinetic calculations.....	29
3 RESULTS AND DISCUSSION	30
3.1 Thermal analysis.....	30
3.2 Evolution of sulfur-containing compounds.....	31
3.3 Kinetic computations and calculation of conversion	33
3.3.1 Kinetic calculations.....	33
3.3.2 Calculation of conversion for isothermal conditions	35
3.4 Possible catalytic effect of the minerals in the oil shale	37
4 CONCLUSIONS	41
List of Figures	43
List of Tables	44
References	45
List of other publications	52
Lühikokkuvõte.....	54
Abstract.....	55
Appendix 1	57
Appendix 2	77
Appendix 3	87
Curriculum vitae.....	95
Elulookirjeldus.....	97

List of Publications

The list of author's publications, on the basis of which the thesis has been prepared:

- I **B. Maaten**, L. Loo, A. Konist, D. Nešumajev, T. Pihu, I. Külaots, D. Neshumayev, T. Pihu, and I. Külaots, "Decomposition kinetics of American, Chinese and Estonian oil shales kerogen," *Oil Shale*, vol. 33, no. 2, pp. 167–183, 2016
- II **B. Maaten**, L. Loo, A. Konist, T. Pihu, and A. Siirde, "Investigation of the evolution of sulphur during the thermal degradation of different oil shales," *J. Anal. Appl. Pyrolysis*, vol. 128, pp. 405–411, 2017
- III **B. Maaten**, L. Loo, A. Konist, and A. Siirde, "Mineral matter effect on the decomposition of Ca-rich oil shale," *J. Therm. Anal. Calorim.*, vol. 131, no. 3, pp. 2087–2091, 2018

Author's Contribution to the Publications

Contribution to the publications in this thesis are:

- I The author was responsible for planning and conducting the experiments, analyzed the results and was the first and corresponding author of the publication.
- II The author procured most of the samples, was responsible for planning and conducting the experiments (except the kinetic calculations), calculated the conversion curves for isothermal conditions, analyzed the results and was the first and corresponding author of the publication.
- III The author was responsible for planning and conducting the experiments, analyzed the results and was the first and corresponding author of the publication. The results were presented at the conference "1st Journal of Thermal Analysis and Calorimetry Conference and 6th V4 (Joint Czech-Hungarian-Polish-Slovakian) Thermoanalytical Conference".

Introduction

Oil shale has been used for power production in Estonia since the beginning of the 20th century [1], [2]. Although the first large shale oil extraction plant for processing of Estonian oil shale was proposed in 1910 the processing only started in the 1920s [3], [4]. However, some records suggest an earlier origin; therefore, in 2016, the Estonian oil shale industry celebrated its 100th anniversary. Although the world is turning to alternative sources of energy, many countries still use fossil fuels. To date, Estonia is highly dependent on oil shale and ~90% of its electricity is still produced in oil shale power plants [5], [6]. Since the beginning of the so-called oil shale period chemical analysis has evolved significantly and thus, its complexity and precision are immense. New and improved analytical techniques have opened up possibilities for new areas of research such as kinetics of decomposition, highly accurate structural analysis, and characterization.

The goal of this thesis is to characterize the composition of oil shales of different origin. Thus, the samples were subjected to thermogravimetric analysis (TGA) under pyrolysis conditions. Based on the thermal analysis data the following questions were answered:

- What are the differences in the evaporating gases produced during the pyrolysis process of different oil shales?
- How can the decomposition of organic matter be described via the kinetic triplet?
- How do the acquired kinetic parameters describe the nature of the samples?
- How can these kinetic parameters be put into practical use rather than be purely theoretical?
- As there is significant data on the effect of inherent minerals on the decomposition of oil shales of other origin, do the minerals in Estonian oil shale affect the decomposition of organic matter during the pyrolysis process?

Samples from Estonia, China and the USA were analyzed. The Estonian sample is the mean laboratory sample of the energetic oil shale used in power production. The samples from China and the USA are also locally used. However, the sample from Kentucky (USA) has not been described to date. Several analytical techniques were employed, namely TGA coupled with mass spectrometry (TGA-MS), wavelength dispersive X-ray fluorescence (WD-XRF), X-ray diffraction (XRD), and elemental analysis (CHNS).

This dissertation is divided into four chapters. Chapter 1 offers a literature overview describing the nature of the oil shale, pyrolysis process, and the types of solid residues produced and how to utilize them. It also presents the history and use of TGA and the basics of kinetic computations. Chapter 2 describes the experimental details, including the type of analyzed samples, the analytical procedure and reagents employed, and the results of the different analytical techniques (**Publications I–III**). The third chapter focuses on the afforded results. The differences of the samples are described based on the results from thermal analysis (**Publications I and II**). Focus is drawn towards the evolution of sulfur compounds and how the oil quality could be improved in light of the sulfur content (**Publication II**). The kinetic analysis data is applied to elucidate the isothermal decomposition of organic matter (**Publication II**). Finally, the catalytic effect of inherent minerals for the Estonian sample is investigated (**Publication III**). Chapter 4 concludes the results of the research.

This thesis is limited to the following conditions:

1. Oil shale samples from only three countries are investigated, namely Estonia, China and the USA. Nevertheless, the samples are of different composition and offer sufficient data to allow conclusions to be drawn.
2. The possible catalytic effect is only investigated for the Estonian sample and its compositional variations. To draw a more general conclusion, samples of other origins should also be analyzed. These are possible topics for future publications.

Future studies to address the limitations of this research are suggested: other physical properties of oil shale, for example the specific surface area should be investigated before and after pyrolysis to provide more knowledge on the reactivity of the sample. Moreover, samples of other origins should be analyzed to reach more general conclusions on the possibility of the catalytic effect of the minerals in oil shale.

Abbreviations

CHNS	Elemental Analysis (Carbon, Hydrogen, Nitrogen, Sulphur)
CM	Mineral Carbon Dioxide Content
C ^{total}	Total Carbon Content
DAEM	Distributed Activation Energy Model
DTA	Differential Thermal Analysis
DTG	Derivative of Mass Loss
EGA	Evolved Gas Analysis
GHC	Gaseous Heat Carrier technology
HHV	High Heating Value
HR	Heating Rate
HV	Heating Value
LHV	Low Heating Value
LOI	Loss On Ignition
OM	Organic Matter
OS	Oil Shale
SHC	Solid Heat Carrier technology
S _{organic}	Organic Sulphur Content
S _{sulfide}	Sulfide Sulfur Content
S _{sulfate}	Sulfate Sulfur Content
S ^{total}	Total Sulfur Content
temp.	Temperature
TGA	Thermogravimetric Analysis
TGA-FTIR	Thermogravimetric Analysis Coupled with Fourier Transformation Infrared Spectroscopy
TGA-MS	Thermogravimetric Analysis Coupled with Mass Spectrometry
XRD	X-ray Diffraction
WD-XRF	Wavelength Dispersive X-ray Fluorescence Spectroscopy

Terms

$A_{(d)}$	ash content (dry basis), wt%
amu	atomic mass unit
d_m	median diameter of particles, μm
E_a	apparent activation energy, kJ/mol
E	activation energy of a reaction, kJ/mol
FC	fixed carbon, wt%
k	rate constant
m_0	initial mass, mg
m/z	mass-to-charge ratio
R	universal gas constant, 8.314 J/(mol*K)
t	time, s
T	temperature, °C or K
$VM_{(d)}$	volatile matter (dry basis), wt%
wt%	weight percent

Greek symbols

α	conversion of organic matter
β	heating rate, °C/min

1 LITERATURE OVERVIEW

1.1 Oil shale

Oil shale is a complex fine-grained sedimentary rock consisting of an organic part, referred to as kerogen, and a mineral part comprising a variety of minerals [7]–[10]. Oil shale can be used in various ways to generate electricity, produce oil and other petrochemicals, and as fertilizer [9], [11], [12]. Beneficial uses are found even for its waste products, for example oil shale ash is used to produce cement and concrete and to landfill mines [13]. As oil shale is one of the World's largest hydrocarbon reserves, it has attracted worldwide scientific interest. Total shale oil reserves are estimated to be as high as 4.8 trillion barrels [9].

Oil shale deposits are widely spread across the world with known deposits in every continent [14]. There are two major types of oil shale in Estonia – Dictyonema argillite (claystone with a low organic content and a pyrite content <9%) and kukersite (main type, sedimentary rock of the Kukruse stage) [15]. Although first articles in the literature on kukersite date back to 1777, oil shale has been mined since 1916 in Estonia [16]. Permanent mining started once Estonia acquired its sovereignty in 1918. Until the end of the 1990s, oil shale mines annually produced between 12 and 13 million tons of product. Most of the mined oil shale was utilized in power plants; thus in 2007 alone, power plants consumed 11 million tons OS, while shale oil plants consumed 3.3 million tons [17].

The amount of organic matter in oil shale varies greatly. For example, in Estonian oil shale the organic matter content ranges from 20 to 60% [18]. Kerogen, contrary to oil and bitumen, is insoluble in commonly used organic solvents and is globally the largest source of petroleum and natural gas [19]. Its average molecular weight is in the order of 3000 and its empirical formula is $C_{200}H_{300}SN_5O_{11}$ [20]. The possible kerogen structure is illustrated in Figure 1 [21]. Kerogen is tightly mixed with the minerals in oil shale, making its separation a complicated procedure [22]. Organic matter in oil shale is divided into several classes depending on its composition and origin. This is usually accomplished by using van Krevelen diagrams, plots of the H/C vs O/C atomic ratios of carbon compounds [23]. Type I and II kerogen have a relatively high H/C and lower O/C ratios and are the source of most of the world's crude oil [24]. Estonian oil shale has a relatively high amount of carbonate minerals with H/C and O/C atomic ratio ranges of 1.4-1.5 and 0.16-0.2, respectively. Thus, it is hard to establish whether it comprises Type I or Type II kerogen [23], [25].

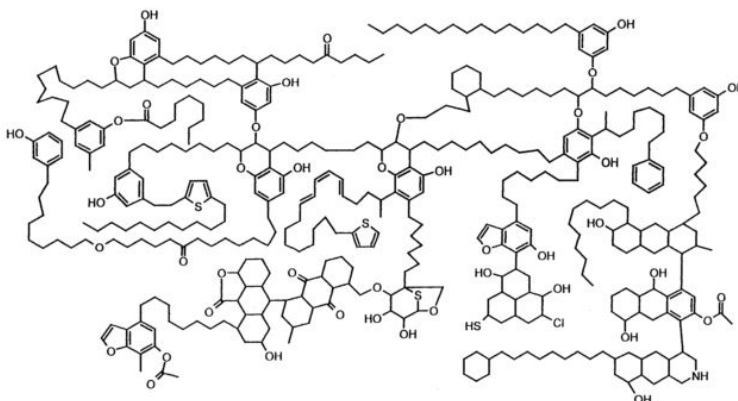


Figure 1. Possible structure of kerogen [21]

Similar to kerogen, the mineral part of oil shale also varies in amount and content. The most common minerals in oil shale are carbonates (calcite and some dolomite), quartz, feldspar and clay [8], [10], while other minerals such as pyrite and silicates can also be present [26], [27]. In addition to minerals, compounds containing copper, cobalt, nickel, molybdenum and vanadium are present in limited quantities [8]. Notably, the solid organic matter is well dispersed in the inorganic matrix [17]. The analytical techniques that are often used to identify the components of mineral matter are infrared (IR) spectroscopy, (XRD), scanning electron microscopy and X-ray power spectroscopy.

As the composition of oil shale is highly dependent on its origin, a comparison of the composition (ultimate and proximate analysis) of some oil shales from the US, China, Estonia and Pakistan is presented in Table 1. These results clearly illustrate the varying compositions of different types of oil shale. For example, Green River oil shale contains 26% more ash than its Estonian equivalent.

Table 1. Proximate and ultimate analytical results of some oil shales, wt%

	Green River ^{a,b} [28], [29]	Kukersite ^b [30]	China ^{c,d} [31]	Pakistani ^e [32]
Moisture	1.6	1.3	2.5–6.0	1–5.5
Volatile matter	n.d.*	46.2	9.7–39.4	29.0–34.4
Fixed carbon	n.d.*	4.6	1.6–13.6	3.2–4.1
Ash	74.0	47.9	56.9–89.3	61.3–67.7
C ^{total}	17.6–25.4	30.5	9.7–29.2	24.4–32.2
H	1.5–2.7	2.7	1.0–4.3	2.9–3.0
N	0.3–0.7	0.2	0.3–0.8	0.1–0.5
S	0.3–0.9	0.5	4.4–5.7	0.0–0.4

*n.d., not determined, ^a Mahogany zone oil shales, ^b as received basis, ^c concludes the results of Huadian, Fushun, and Nongan samples, ^d air-dry basis, ^e samples from Kark, Dharangi, and Malgeen

Another important property of oil shale that needs to be analyzed is its heating value (HV), i.e. the amount of heat produced from the complete combustion of oil shale. The HV of oil shale mainly depends on its organic matter content and composition. The mineral matter also affects the HV as minerals may decompose, dehydrate, and oxidize during the combustion process [17]. Two types of HV are usually reported in the literature, namely high (HHV) and low (LHV) HV. The difference lies in the water produced during the combustion process and hence, whether it is condensed into the liquid phase or not (HHV and LHV, respectively). The HVs for oil shales may vary from 3.6 to 13.4 MJ/kg depending on the origin and therefore the composition of the oil shale. The HV of Estonian oil shale (LHV 8–11 MJ/kg) is among the highest in the world, partly explaining its wide utilization [30], [33]. In addition to chemical determination, empirical correlations for biomass have been created to predict the HHV and elemental composition from the proximate analysis data [34]. To the best of the author's knowledge no such correlations have been reported for oil shale to date.

The most commonly used parameters for the proximate analysis of oil shale (Table 1) are moisture, volatile matter, ash, and fixed carbon content (wt%) together with the previously described HV (MJ/kg). Table 1 illustrates the large differences between the samples. Estonian oil shale (kukersite) contains a high amount of volatile matter and has a lower ash content. The advantage of a "relatively" low ash content is that less waste is produced. However, in practice, half of it still goes to waste. The potential uses of this ash are discussed in chapter 1.3. The ultimate analytical results also vary, with the total carbon content (comprising carbonate minerals) ranging from 9 to 30%. Interestingly, in

this example the sulfur content of Estonian oil shale is shown as quite low, although this study has shown it to be <1.5% (**Publication II**, Table 1). A high sulfur content results in high SO₂ emissions that are harmful to the environment.

1.2 Pyrolysis

Thermal decomposition of oil shale has been investigated since the 1920s [35]. Although extensive literature is available, the kinetics and mechanism of the process remain unclear.

Pyrolysis is defined as thermal degradation in oxygen-free conditions. Hence, oil shale retorting takes place at temperatures of 450-550 °C in the absence of air, however such temperatures do not decompose the mineral matter. In the case of oil shale, pyrolysis is used to produce shale oil. Shale oil is often considered as the perfect alternative to crude oil. This is due to the high H/C atomic ratio of its organic matter (for some shales as high as 1.7) that is similar to that of petroleum [36]. The H/C atomic ratios for different fuels and the resultant final products are illustrated in Figure 2 [37]:

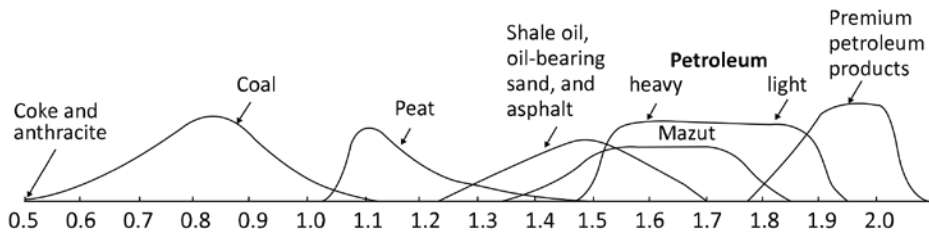


Figure 2. H/C atomic ratios in various hydrocarbon materials [37]

Figure 2 reveals that the H/C atomic ratio in coal (~0.8) is significantly different from that of the desired products (~2, marked as premium petroleum products in Figure 2).

In the literature, the word “pyrolysis” is used quite liberally and while for solid fuels terms such as dry distillation, semicoking, and coking are also used [38] according to the temperature of the process. The retorting (heating) process can tentatively be categorized into three parts: first, heat is transferred from the surface of the oil shale particle to its interior. The second part consists of pyrolysis, whereby thermal decomposition produces shale oil, shale gas, and char. Finally, in the third part, the evolved shale oil vapor and shale gas are transported to the retort surface [17].

Many mechanisms for the pyrolysis of oil shale have been proposed. Han et al. presented a system in which the residual moisture is first evaporated. Next kerogen is converted to bitumen, which subsequently degrades to shale oil, gas, carbonaceous residues and pyrolytic water [39]. A similar mechanism was described by Bhargava et al. [40], who also included the decomposition of some minerals in the 200-600 °C temperature region, as well as by Williams [41]. In their mechanism, some combined water is released, and part of the mineral matter also decomposes to form carbon dioxide. The flow diagram for the mechanism proposed by Han et al. [39] is illustrated in Figure 3.

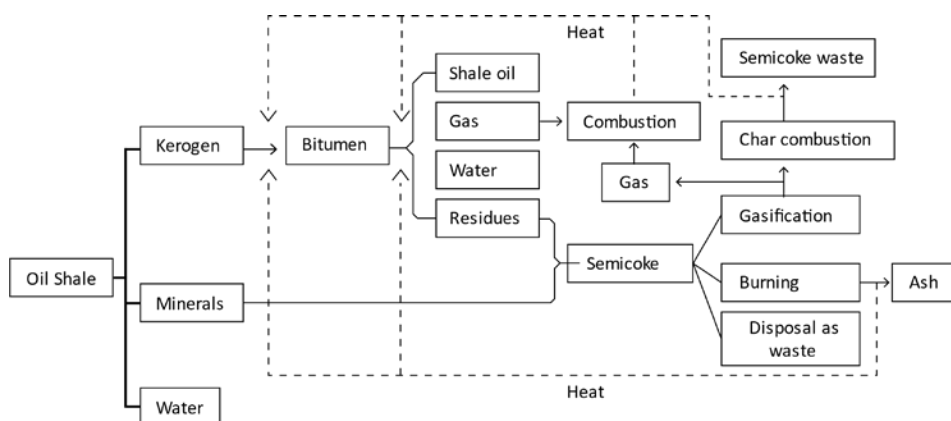


Figure 3. Flow diagram illustrating the mechanism of oil shale retorting [39]

On the other hand, Burnham and Braun have shown that a sequential reaction for oil formation is incompatible with the isothermal pyrolysis results since the maximum oil and gas generation rate are observed at the initial time of the process [24]. A single approach is difficult to determine, as oil shales of different origin and composition may have different thermal decomposition pathways. The properties of the produced shale oil might also differ. The oil composition and yield depend on many factors, including the type and origin of the organic matter, processing temperature, residence time, and particle size [38]. In addition, not all the organic matter is converted into shale oil and gas – usually 40–60% (on oil shale basis 18–20%) of the organic matter is converted into shale oil [38]. For Estonian oil shale, 75–89% kerogen may be converted into oil [42]. These values indicate that the optimal process conditions can be improved.

The shale oil produced by pyrolysis is very similar to crude oil. However it differs in unsaturated hydrocarbon (such as olefins) as well as nitrogen-, sulfur-, and oxygen-containing non-hydrocarbon richness [17]. Since the composition of the products is highly dependent on the starting material, shale oils around the world have different properties. For example, the oil produced from kukersite oil shale is characterized by a high oxygen content and therefore valuable chemicals can be produced from it [17]. The oxygen-containing compounds from shale oil production include phenols, resorcinols (both substituted and non-substituted forms), aldehydes, and ketones [19], [43], [44].

In addition to the raw material, the pyrolysis products also depend on several parameters, the most important of which are the heating temperature, heating time, heat-up rate and oil shale (particle or lump) size [17]. Temperature is the key factor to shale oil and gas yields. Increasing the constant heating temperature has been reported to increase the shale oil and gas yields and decrease the yield of residue-char. Thus, for Fushun oil shale the shale oil and produced gas increased from 1.3% and 559 mL/100 g to 7.4% and 1955 mL/100 g, respectively, with an increase in temperature from 350 °C to 450 °C. At temperatures >450 °C, the increase in oil yield for the Fushun sample was moderate [17]. The relationship between the heating time and oil yield is similar to that of temperature, i.e., the shale oil yield increases with heating time, even at relatively low temperatures. As most reactions are temperature-dependent, the relationship of time and temperature with respect to both time and maximal yield should also be considered. Thus, the higher the heating temperature, the faster the process and the shorter the time needed to obtain maximum oil yield [17]. Nazzal has studied the shale oil yield dependence on particle size (smaller particles 0.2-0.6 mm; larger particles 3.3-5.6 mm)

for Jordan oil shale [45]. He revealed that at a final pyrolysis temperature of 520 °C, a higher oil yield was obtained when larger particles were employed. However, this study only investigated Jordan oil shale, and the dependence of oil shales of other origins might be different. Therefore, further investigation is needed to establish a broader perspective.

In addition to pyrolysis, several other methods that convert oil shale to shale oil with the least possible amount of waste have been investigated. These include solvent extraction [46]–[48], subcritical water extraction [49], [50], and supercritical water extraction [51].

Qian and Yin suggested that the decomposition temperature range is highly dependent on the oil shale. A comparison of initial, final, and peak decomposition temperatures (characteristic temperatures determined by differential thermal analysis, DTA) is presented in Table 2 [17]. The data illustrates that characteristic temperatures for oil shales of different origin can be significantly different. For example, the initial pyrolysis temperature for Australian oil shale is about 100 °C higher than that of the Jordan sample. This is an indication of the importance of analysis of different oil shales, otherwise no general conclusions can be drawn.

Table 2. Oil shale pyrolysis temperatures [17]

<i>Oil Shale</i>	<i>Initial pyrolysis temp., °C</i>	<i>Final pyrolysis temp., °C</i>	<i>Pyrolysis temp. range, ΔT, °C</i>	<i>Pyrolysis peak temp., °C</i>
Fushun, Liaoning	403	507	104	470
Maoming, Guangdong	396	517	121	-
Stuart, Australia	431	464	33	-
Lajjun, Jordan	330	510	180	-
Green River, USA	340	520	180	440

Oil shale pyrolysis has been investigated for quite some time and therefore its research interest has been waning. Nowadays, it is not sufficient to offer the pyrolysis characteristics of a single material. Researchers are investigating the co-pyrolysis of fossil fuels with numerous other materials due to possible advantages including lower emission and pollutant levels, and higher HVs. For example, Lin et al. reported that when sewage sludge is combined with oil shale, thermal degradation of oil shale is promoted and thus, the absorption of hydrocarbons becomes stronger [52]. Since plastics contribute towards the highest proportion of municipal solid waste, the co-pyrolysis of oil shale and polyethylene has also been investigated to utilize the solid residues. In this case, the thermal stability of both components increased, while the residue yield of the mixture was lower than that of oil shale itself [53]. Cordero et al. investigated the co-pyrolysis of coal and biomass and reported an improved desulfurization efficiency and a char product with good HVs [54].

The main environmental problem that may arise during shale oil production is air, water and soil pollution. The amount and concentration of emissions depends on whether the method employed makes use of a gaseous (GHC) or solid heat carrier (SHC). The main pollutants are CO₂, CO, N₂O, NO, NO₂, particulate matter, SO_x and H₂S [55]. Depending on the methodology employed, some ammonia, carbonyl sulfide, benzene,

and hydrogen chloride may also be produced. The pyrolytic water that is produced during the process contains several different aromatic organic compounds, mainly phenols. The separation of phenols is reasonable only for the water produced from GHC technology, as the pyrolytic water from SHC technology contains three times less water-soluble phenols [56]. The separated phenols are in turn used as starting materials in the chemical industry.

Due to its complex composition, the pyrolysis of oil shale is significantly different from that of other materials (Figure 1 and Table 1). During oil shale retorting semicoke (shale char) is also produced. This is considered as a potentially harmful waste since it often contains toxic organic compounds and heavy metals. Thus, its disposal might result in environmental contamination [39]. Moreover, if the char is openly deposited, pollutants may be distributed as dust in the air or leach through aqueous surroundings [17].

1.3 Characterization of solid residues and utilization of oil shale ash

Compared to other fuels, the ash (waste) content in oil shale can be quite high. Significant amounts of oil shale ash are produced every day. The pyrolysis process produces semicoke as waste with values reaching up to 600 kg semicoke per ton of oil shale [57]. Semicoke is characterized by a considerable carbon content (10–12%), an HV of up to 4 MJ/kg, and a high content of mineral matter (up to 70%) [57]. Thus, the Estonian shale oil industry considers semicoke as one of its biggest problems. The produced semicoke contains a considerable amount of contaminants. Analyses of the leachates from semicoke dumps have revealed that the leachates contain 300–500 mg/L phenols, sulfide ions, polyaromatic hydrocarbons and other toxic compounds [58]. In general, the properties of the produced semicoke depend on the retorting process employed. However, in addition to the aforementioned components, most samples also contain a significant amount of total dissolved solids, sulfates, carbonates, other inorganic ions, and to a lesser extent trace elements [42]. In addition to the contaminants distributed through aqueous media, the open deposition of semicoke also pollutes the air, for example through dust. Due to its high carbon content, semicoke can be potentially used for combustion. The semicoke from Kiviter retorts is usually stored as waste (dumped), whereas semicoke from units utilizing solid heat carrier technology is burnt, thereby producing ash as the final product instead of semicoke [59]. The firing of semicoke may give rise to additional complications. When semicoke is mixed with oil shale, the fuel consumption must be increased to maintain the same level of heat production in the boiler (since the gross and net efficiency of the boiler will be lowered). This in turn increases the amount of combustion products [59]. Additionally, the amount of produced semicoke might exceed the capacity of the mixed firing system. Therefore, this alternative is considered as mitigation method rather than a solution to the problem. Semicoke has also been used for the manufacturing of different products ranging from cement to mineral wool [57].

In 2002, Narva power plants generated about five million tons of oil shale ash from oil shale combustion. A big advantage of Estonian oil shale is that the Ca-to-S molar ratio is typically in the range of 5–10; therefore, the fuel itself contains enough Ca to capture the SO₂ produced during firing [60]. The ash properties are well analyzed in several studies [2], [10], [60], [61], with different usages proposed to reduce the quantity of waste. The typical ash composition of Estonian oil shale is presented in Table 3 [62].

Table 3. Oil shale ash composition, wt% on dry basis [62]

Component	SiO ₂	Fe ₂ O ₃	Al ₂ O ₃	CaO	MgO	K ₂ O	Na ₂ O	Ash _{815°C}
Amount	30.7	4.8	6.1	39.0	8.7	1.8	0.1	47.0

In Estonia oil shale ash is commonly used in the building material industry, road construction, agricultural utilization, chemical industry (producing phosphates) and mining engineering [17].

The production of construction materials from oil shale ash is prevalent in Estonia. The ash composition (mainly due to clay minerals) is similar to that of the raw material of cement [15] and therefore, both light and heavy concrete can be produced from different types of oil shale ash [17].

Another very interesting example of ash utilization is the application of the combination of ash and straw mulch to revegetate extracted peatlands. This is possible because the ash from Estonian oil shale power plants corresponds to fertilizer requirements in terms of quality and safety [63]. Additionally, the soil in Estonia is acidic, while the ash is basic due to its high CaO content (see Table 3). Therefore, oil shale ash can also be used as a soil ameliorator to increase plant harvest.

Shale ash is also commonly used in mining engineering, specifically for landfilling excavated underground mines. However, application to the construction and chemical industries is more beneficial.

The oil shale industry produces a vast amount of by-products and waste, which if not disposed properly, could lead to environmental pollution problems. When oil shale ash is utilized in a beneficial way, the whole production chain is more profitable and environmentally friendly. Different methods have therefore been proposed to valorize oil shale and produce less waste.

1.4 Oil shale beneficiation

As previously described, oil shale contains a significant amount of ballast in the form of different minerals (50–85%[64]). These usually have no use and may pose several problems. To the best of the author's knowledge, the first paper that referred to the demineralization process of oil shale was published in 1983 [65]. Silicate minerals have been shown to exhibit an inhibiting effect on the pyrolysis of oil shale; for example, following the removal of silicates in Green River oil shale, the volatile yield increased by 40% [66]. There are numerous similar examples in the literature [22], [43], [67], [68].

The removal of minerals provides useful information on the interactions of the organic part and mineral matrix as well as the overall behavior of the material. The separation of organic matter from the mineral matrix can significantly extend its industrial applicability; for example, the calorific value of kerogen, the structure of which has not been elucidated, is ~35 MJ/kg [15], [69]. It has also introduced the possibility to separate dicarboxylic acids from kerogen to produce plastics and other products [69]. Moreover, since some of the minerals might exhibit a catalytic effect, the yield of the different products should depend on the composition of the sample [27]. Additionally, the minerals in the oil shale could affect the occurring reactions both physically and chemically [70]. The debate on a possible catalytic effect is ongoing and to date, there are publications defending both the existence and non-existence of this effect. The results seem to be highly dependent on the sample and its composition, as well as the preparation method. Therefore, this topic needs further research.

There are several methods for the demineralization of oil shale that can be divided into two main groups – chemical and physical. Physical methods depend on the difference in specific gravity of the organic matter and minerals and on the differential wettability by water and hydrocarbons [19]. For example, Palvadre and Ahelik combined flotation and hydrocycloning and reported the production of a concentrate containing 90% organic matter [69]. This procedure does not remove all the minerals from the original oil shale. Chemical methods, on the other hand, abolish the major minerals via different acids or their combinations. The most common method employs HCl and HF to respectively remove most of the carbonates and silicates. HCl is known to destroy carbonates, sulfides, sulfates and hydroxides, while the subsequent use of HF eliminates clay minerals, quartz, and silicates [19]. Any residual minerals (e.g., pyrite) can be removed with the addition of HNO_3 [71]. There is much uncertainty on whether the use of HNO_3 alters the structure of the remaining kerogen [72]. The process for removing minerals is illustrated in Figure 4 (modified version of Figure 1 in [71]). These guidelines have been widely employed by different researchers.

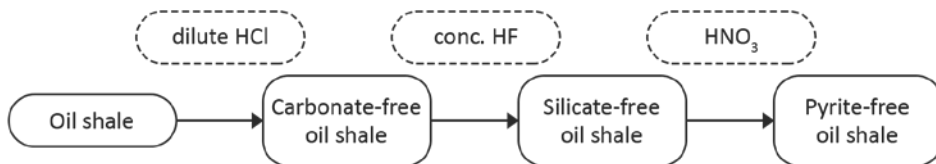


Figure 4. Demineralization process of oil shale

The demineralization of oil shale is often used to determine whether the inherent and removed minerals have a catalytic effect on the decomposition of the organic matter. There are plenty of results on both its existence and non-existence depending on the analyzed sample. Yan et al. revealed that the decomposition and release of organic matter is promoted by the minerals present in oil shale from the Dachengzi mine in China [70]. Al-Harashshah et al. concluded that the minerals enhance catalytic cracking for El-Lajjun (Jordan) oil shale [73]. Karabakan and Yürüm reported both inhibiting and catalytic effects of silicate and carbonate minerals in Turkish and Green River oil shales, respectively [22], [66]. Vučelić et al. reported a very low catalytic effect in Aleksinac (Yugoslavia) oil shale [27], while Pan et al. suggested that there is no significant effect on the decomposition of organic matter [74]. Therefore, no general conclusions can be drawn as the results are highly dependent on the sample employed.

In summary, the advantages of oil shale demineralization include enhanced oil and gas recovery [75], improved performance, and higher HVs [76]. However, one should bear in mind that the results are highly dependent on the oil shale and general conclusions regarding other oil shales cannot be drawn.

1.5 Thermogravimetric analysis

Thermal analysis is associated with thermally stimulated processes, namely processes that are initiated by a change in temperature [77]. This includes a variety of methods which all involve changing the temperature of the sample. The physical quantities that are measured range from states of the sample (temperature, mass, and volume) to changes in the sample material properties (composition, crystalline structure, etc.) [78]. Moreover, such analysis can be employed to determine properties including heat capacity and thermal stability.

Thermogravimetry is the observation of changes in mass as a function of time and/or temperature [79]. Historically, thermogravimetric analyzers with milligram balances were first developed to determine the moisture content of textile fibers [79]. The first mention of thermogravimetry as we know it today dates back to 1833 when thermobalances were used for quality control in the Chinese silk industry [80]. Nowadays, the use of thermogravimetric analyzers ranges from determining phase transitions and investigating oxidation processes to detecting polymorphic forms in pharmaceuticals.

The results afforded by TGA depend on the operational parameters (heating rate and atmosphere) and sample parameters (mass, structure, etc.) [78]. Thermal analysis can be used to study both solid and liquid materials, even very viscous materials. As the sample is heated in a defined gaseous atmosphere under continuous conditions, an apparent mass gain is observed. This is caused by a buoyancy effect and is corrected by subtracting a blank measurement curve from the sample measurement [77]. The samples are analyzed in sample pans made from thermally stable inert materials. The most common are Al₂O₃ crucibles due to their good stability and relatively low price. The sample pans are usually cylindrical with a height-to-diameter ratio <1 to ensure efficient removal of the evolving gases [81]. TGA measurements are also in good accordance with green analytical chemistry guidelines – since small sample sizes are used, few parallel measurements are needed, minimal waste amounts are produced, minor sample treatment is necessary, and different analytical processes can be integrated [82].

Another advantage of TGA is its ease of coupling with other analytical techniques. The most common are MS and Fourier transformation infrared (FTIR) spectroscopy. This allows data on the evaporating substances to be collected, thereby providing a precise overview of sample degradation. For example, Beneš et al. employed TGA-FTIR to study the thermal degradation of polyvinyl chloride under different atmospheres and used the TGA data to determine the kinetic parameters and the FTIR information to establish the mechanism of the reaction [83]. Tiwari and Deo used TGA-MS for the compositional analysis of oil shale pyrolysis [84]. They identified compounds of up to 300 atomic mass units (amu) and noticed that the alkanes were released at lower temperatures than their equivalent aromatics, thereby giving insight on the variability of the pyrolysis products. Additionally, coupled methods can be combined with other analytical techniques to attain even more information. The chemical formula of a formerly unknown bismuth oxalate was established by using TGA-MS and TGA-FTIR combined with quantitative chemical analysis [85]. Coupled methods can be especially useful when simultaneously investigating several materials. Lin et al. investigated the co-pyrolysis of sewage sludge and oil shale using TGA-FTIR [52]. The results of their study can be used to create theoretical groundwork for the co-pyrolysis technology of those materials and to develop their thermochemical conversion systems. The author of this thesis and her colleagues have studied the combustion characteristics of oil shale in air and oxy-fuel atmospheres using TGA-MS [62]. We found that combustion is delayed under an oxy-fuel atmosphere and that an increase in the oxygen content decreases the CO₂ emissions.

TGA has been widely used to investigate the combustion and pyrolysis of oil shale [53], [62], [74], [86]–[90]. A typical thermogram of Estonian oil shale is displayed in Figure 5.

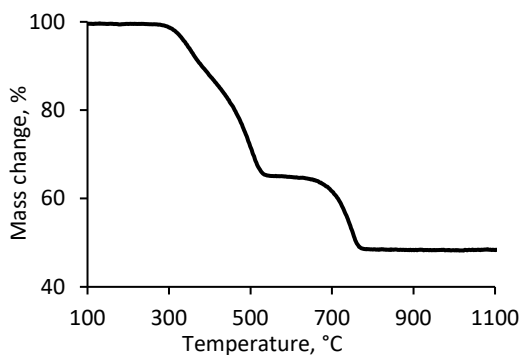


Figure 5. Thermogram of Estonian oil shale

The thermogram presents the decomposition profile (mass change, % vs. temperature, °C) of Estonian oil shale and its dependence on temperature (measured under 80% N₂ and 20% O₂). Two major mass loss steps can be identified, the first at a temperature range of 300–550 °C accounts for the combustion of organic matter and the decomposition of pyrite, while the second at a temperature range of 650–830 °C, represents the decomposition of the carbonate minerals. Moreover, clay minerals have been shown to release structural water at temperatures <550 °C [32].

As previously stated, oil shale contains a relatively large amount of different minerals, some of which might contribute towards the thermal decomposition profile. For Estonian oil shale, the minerals that contribute to the mass loss are mainly calcite, dolomite (carbonate minerals), and pyrite. The thermochemical properties of common minerals are listed in Table 4. As these properties were published in 1979, there are several components present in oil shale; for example, kaolinite and hydrous mica, that are not listed in the table.

Table 4. Thermochemical properties of common minerals in oil shale deposits [91]

Mineral	Chemical formula	Type of chemical reaction	DTA ^a peak temp. (°C)
Calcite	CaCO ₃	dissociation	860–1010
Dolomite	CaCO ₃ ·MgCO ₃	dissociation	790, 940
Analcite	NaAlSi ₂ O ₆ ·H ₂ O	dehydration, dissociation	150–400
Shortite	Na ₂ Ca ₂ (CO ₃) ₃	dissociation	470
Trona	Na ₂ CO ₃ ·NaHCO ₃ ·2H ₂ O	dissociation, dehydration	170
Pyrite	FeS ₂	oxidation, dissociation	550
K-feldspar	KAlSi ₃ O ₈	dissociation	–
Gaylussite	CaNa ₂ (CO ₃) ₂ ·5H ₂ O	dehydration, crystallographic transformation, melting	145, 175, 325, 445, 720–982
Illite	Empirical*	dehydroxylation	100–150, 550, 900
Plagioclase	NaAlSi ₃ O ₈ –CaAl ₂ Si ₂ O ₈	dissociation	–
Nahcolite	NaHCO ₃	dissociation	170
Dawsonite	NaAl(OH) ₂ CO ₃	dehydroxylation, dissociations	300, 440
Gibbsite	γ-Al(OH) ₃	dehydroxylation	310, 550
Ankerite	Ca(Mg, Mn, Fe)(CO ₃) ₂	dissociation	700, 820, 900
Siderite	FeCO ₃	oxidation, dissociation	500–600, 830
Albite	NaAlSi ₃ O ₈	dissociation	–
Quartz	SiO ₂	crystallographic transformation	~575

*Illite empirical formula: K_{0.6}(H₃O)_{0.4}Al_{1.3}Mg_{0.3}Fe²⁺_{0.1}Si_{3.5}O₁₀(OH)₂·(H₂O), ^a differential thermal analysis

Table 4 reveals the decomposition of pyrite peaks at a temperature of 550 °C, which falls within the range of the decomposition of organic materials (Figure 5). The author and her colleagues have previously shown that during the combustion of Estonian oil shale, pyrite decomposes at a temperature range of 400–500 °C [62]. As previously mentioned (Chapter 1.5), MS coupling allows the user to acquire knowledge on the evaporating gases, with oil shale sulfur usually being the element of interest. The sulfur content of the produced oil is of crucial importance due to current regulations (described in Chapter 3.2) and thus, sulfur-containing compounds are investigated during oil shale pyrolysis. Pan et al. used TGA-MS to study the decomposition of Jimsar oil shale. They revealed that at a temperature range of 510–650 °C, pyrites react with organic matter to form H₂S and SO₂ [74]. Lan et al. demonstrated the change in the content of sulfur-containing gases when the retorting temperature is increased [92]. These results are a clear indication of the significance of the analysis of the evaporating gases. Therefore, based on these data, recommendations can be made to improve the retorting process and the quality of the resultant products.

1.6 Kinetic computations

The theory of chemical reactions states that most reactions have to overcome an energy barrier for one structure to change into another [93]. The speed of these reactions depends on how many molecules can pass that barrier. This is known to be temperature-dependent – the higher the temperature, the more molecules can pass the necessary barrier. This was first described by the Swedish scientist Svante Arrhenius in 1889 who stated that the increase of the rate constants depends on the temperature [Equation (1)] [94]:

$$k = Ae^{-E/RT} \quad (1)$$

where A is the frequency factor, E is the activation energy of the reaction, R is the universal gas constant and T is the absolute temperature. Equation (1) has been vastly applied to determine the rate of different chemical reactions and is used to calculate the activation energy. Additionally, this equation has led the way to the kinetic computations employed nowadays. As TGA provides information on the overall reaction kinetics instead of the individual reactions, the activation energy values derived from the TGA data are referred to as apparent activation energy values [40].

By definition, kinetics deals with measurement and parameterization of process rates [77]. The period between 1975 to 1995 has seen a huge leap in the derivation of chemical kinetics capable of extrapolating time scales ranging from hundreds of millions of years to milliseconds for application to different fields spanning from geology to combustion [95]. Usually, the kinetic triplet is presented as a result of kinetic calculations. This consists of the activation energy (E_a) and pre-exponential factor (A) value, and the function of reaction mechanism [$f(\alpha)$]. Each of these parameters has a specific theoretical concept: E_a is associated with the energy barrier, A with the frequency of vibrations of the activated complex, and $f(\alpha)$ with the reaction mechanism [77].

Burnham and Braun stated that the best suited method for calculating kinetic parameters for a complex material such as oil shale is the distributed activation energy model (DAEM) [24]. This method assumes that devolatilization occurs through several simultaneous first-order reactions [96], [97]. The derivation of the formula can be found

in the study by Burnham et al. [24]. The DAEM method is widely used to describe the pyrolysis of biomass, coal, and other materials of energetic value [31].

The rate of the reaction considers three main variables, namely the temperature, T , extent of conversion, α , and pressure, P (usually ignored) [77]:

$$\frac{d\alpha}{dT} = k(T)f(\alpha)h(P) \quad (2)$$

Therefore, most kinetic methods used in thermal analysis consider the rate to be a function of only two variables, T and α :

$$\frac{d\alpha}{dT} = k(T)f(\alpha) \quad (3)$$

where $k(T)$ is the rate constant and represents the dependence of the process rate on temperature and $f(\alpha)$ represents the dependence on the extent of conversion. The conversion of organic matter at any time t is defined as the fractional weight loss:

$$\alpha = \frac{W_0 - W_t}{W_0 - W_f} \quad (4)$$

where W_0 is the initial weight of the sample, W_t is the weight of the sample at time t , and W_f is the final mass at the end of reaction.

A large number of researchers offer kinetic triplets that are calculated from TGA data as the temperature can be easily controlled and both isothermal ($T=\text{const.}$) and non-isothermal ($T=T(t)$) profiles can be used. For the non-isothermal program, the temperature changes linearly with time according to Equation (5):

$$\beta = \frac{dT}{dt} = \text{const} \quad (5)$$

where β is the heating rate.

As stated by Burnham, for a single unimolecular decomposition reaction, the activation energy is equal to the bond energy of the bond to be broken [93]. However, such a simple situation is rarely observed and the reactions of practical interest often include several sequential or parallel reactions. Therefore, more computationally complex methods are required to determine the activation energy for the decomposition of compounds such as fuels and polymers as accurately as possible. This has led to the development of methods for almost every type of material and process. A model-free analysis that allows the determination of the activation energy without the assumption of a kinetic process has also been developed [98]. This, however, might provide irrelevant results for simultaneously running parallel reactions.

Burnham and Braun have illustrated that for complex materials (oil shale) the most suited approximation for decomposition kinetics is the parallel reaction model [24]. This model employs a set of independent, parallel reactions, each of which has a frequency factor and activation energy. The information provided by the activation energy values is diverse. In addition to the results used in simulations, it also provides some preliminary information about the structures being decomposed. For example, low activation energy values indicate the rupture of weak chemical bonds (C–O and S–O) or branched functional groups, medium values are associated with the breaking of side chains in the β -site of aromatics and normal alkanes of large molecular weight, and high values indicate dehydrogenation and rupture of heterocyclic compounds and combination of aromatic rings [99]–[101].

Kinetic analysis can have both a practical and a theoretical purpose. A considerable practical advantage is the prediction of process rates and material lifetimes [77]. From a

practical point of view, kinetic equations are useful in predicting and modelling coal and other fuel conversion processes in boilers [102]. Understanding the kinetics is critical to design an efficient retorting process. For example, TGA measurements and subsequent calculations can be used to predict the behavior of a fuel particle in isothermal conditions (**Publication II**). Although comparison with literature shows that kinetic parameters are unique to each individual sample, this eliminates the need for industrial scale experiments, thereby saving both time and money. Additionally, it is possible to use such preliminary results for the design of different retorts.

2 EXPERIMENTAL

Oil shale is usually described according to its complex heterogeneous nature (Tables 1 and 2). Hence, it is difficult to attain coinciding experimental results for nominally similar samples. The same experimental technique, starting from the procurement of the sample and its preparation to the analytical method and data treatment should be employed to acquire comparable results [53].

2.1 Equipment and procedures

2.1.1 Apparatus

The chemical composition of the samples was determined by XRF. The analysis was performed with a Rigaku Primus II WD-XRF spectrometer. The X-ray source comprised a Rhodium anode 4 kW X-Ray tube with a 30 μm window. The list of crystals in use was as follows: RX25, PET, LiF(200), LiF(220), RX61F, RX75, Ge, RX4, and RX40. For the mineralogical composition, the XRD analysis was performed on a Bruker Advance D8 system using Cu $K\alpha$ radiation in the 2 θ range of 3°–72°, with a step size of 0.02° 2 θ and a counting time of 0.1 s per step using a LynxEye detector. The X-ray tube was operated at 40 kV and 40 mA. Elemental analysis was performed on an Elementar Analyser System Vario MACRO CHNS analyzer, while TG analysis was conducted on a NETZSCH STA 449 F3 Jupiter® TG-DSC analyzer coupled with a NETZSCH QMS Aëolos® mass spectrometer. The samples were heated under pure nitrogen. A protective gas flow of 50 mL/min high-purity nitrogen was employed. Prior to each pyrolysis test, the TGA system was flushed with high-purity N₂ gas to remove any residual air. Constant heating rates of 2, 5, 10, 20, 35 and 50 °C/min were applied in a temperature range of 40–850 °C. To eliminate any buoyancy effects (apparent mass gain), correction runs with empty crucibles were run and the afforded data was subtracted from the measured data. The samples were analyzed in Pt/Rh alloy crucibles with removable Al₂O₃ thin-walled liners. An isothermal step at 105 °C was used to remove moisture. Temperature calibration was performed using In, Sn, Zn, Al and Au standards. Measurements were repeated at least twofold to ensure reproducibility (temperature difference <1.6 °C). For comparison with the MS data, measurements with a heating rate of 5 °C/min were chosen to ensure that there were no overlaps between the peaks. To correctly interpret the results, the intensity ratio of the mass-to-charge-ratio (m/z) of 34 to that of 33 was checked to be 2.38 to ensure that the compound was indeed H₂S. An m/z of 34 was selected for comparison due to its higher intensity. For the analysis of SO₂ m/z values of 64 and 48 were investigated. The data was normalized starting from 200 °C to remove background noise and smoothed with a five-point moving average.

2.1.2 Compositional analysis

For proximate analysis, the following standards were used: for the determination of total sulfur and sulfate sulfur content, gravimetric analysis was based on EVS 664:2017. Size analysis by sieving was performed according to ISO 1953:2015; DIN 66165 1, part 2. The ash content (A_d) was measured according to ISO 1171:2010. For the moisture content, EVS 668-96 was employed. The HV was determined using a gross calorimetric bomb according to EVS-ISO 1928:2016. To determine the amount of volatile matter (VM_d), gravimetric analysis based on the ISO 5071-1:2013 method was employed. For the determination of loss on ignition (LOI) EVS-EN 196-2 p.7:2013 was followed. The fixed carbon amount was calculated from the equation: $FC (\%) = 100 - A_d - VM_d$.

2.2 Characterization of the materials used

Oil shale samples used in this investigation were named according to their location as follows: Estonian – from an underground mine called “Estonia” in Estonia; Colorado – from the Green River shale formation, Colorado, U.S.A.; Green River – from the Green River shale formation, U.S.A.; Kentucky – from the New Albany shale formation, Kentucky, U.S.A.; Chinese 1 and Chinese 2 – from the Maoming mine, Guangdong Province, Southwest China with local classifications of C and A, respectively. The Estonian sample is the mean energetic sample used in the industry. The sample from Kentucky depicts the undiscovered potential of its origin as it has not been investigated before.

All oil shale samples used in the pyrolysis tests were previously dried, crushed (if needed), and sieved (1 mm opening). The median diameter (d_m) for Estonian oil shale was 180 μm . The results from the elemental analysis of the tested oil shales are presented in Table 5, while the proximate analysis data are presented in Table 6 (**Publications I and II**).

Table 5. Ultimate analysis results, wt%, dry base

Sample	N	C ^{total}	H	S ^{total}	S _{sulfide}	S _{sulfate}	S _{organic}
Estonia	0.1	27.3	2.7	1.46	0.96	0.07	0.43
Colorado	0.9	27.7	3.2	1.39	0.67	0.30	0.42
Green River	0.4	17.2	1.7	0.81	0.20	0.03	0.58
Kentucky	0.5	15.4	1.7	1.76	0.76	0.33	0.67
Chinese 1	0.9	23.3	2.4	2.16	1.17	0.30	0.69
Chinese 2	0.9	23.0	3.0	1.96	1.26	0.23	0.47

Table 6. Proximate analysis results, as-received basis

Sample	Ash (wt%)	Moisture (wt%)	Volatile matter (wt%)	Fixed carbon (wt%)	HHV (MJ/kg)
Estonia	51.3	0.5	47.5	1.3	9.85
Colorado	61.9	1.9	26.9	11.2	11.34
Green River	66.8	0.3	33.2	0.0	5.51
Kentucky	76.6	0.9	14.9	8.6	6.41
Chinese 1	56.1	0.6	42.8	1.2	11.40
Chinese 2	61.0	1.2	28.9	10.1	10.14

In addition to oil shales originating from different countries and deposits, oil shale samples with different amounts of organic matter were analyzed to determine the existence of the catalytic effect of the inherent minerals on the decomposition of organic matter. The raw oil shale sample was dried at 105 °C, crushed and sieved to a particle size <1 mm (median diameter = 180 μm). This was labelled as sample OM30 (30 % organic matter, Table 10). This is the same Estonian sample that was used for the investigation of sulfur and in the kinetic analysis. From another sample with an initial particle size of <8 mm the fraction of below 90 μm was separated (sieved) to establish whether there was a difference in its composition and reactivity. This was labelled as sample OM49. Two samples from another batch of oil shale, comprising 68 and 88% organic matter were prepared via flotation and with subsequent HNO₃ washing. These were labelled as OM68 and OM88, respectively. Thus, the raw material for the prepared samples was of three different origins. The preparation of the samples is illustrated in Figure 6.

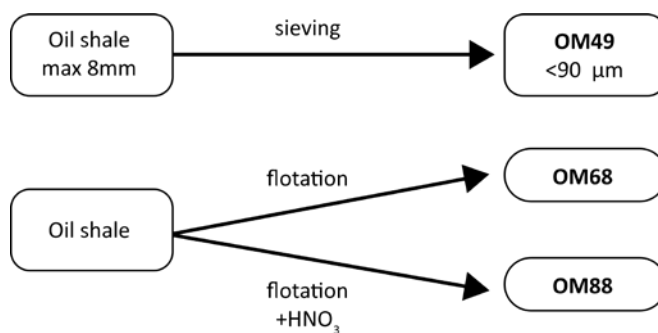


Figure 6. Preparation of the samples

The results from the mineral composition and elemental analyses are listed in Tables 7–9 (**Publication III**). Additionally, the characteristic temperatures of TGA and derivative mass loss (DTG) are presented in Table 10 (**Publication III**). These comprise the onset of mass loss, T_{onset} , the temperature of maximal devolatilization (maximal mass loss), T_{max} , and the temperature at the end of decomposition, T_{end} . T_{onset} and T_{end} were set as the intersection of the tangents as shown in **Publication I**. The organic matter (OM) and mineral carbon dioxide (CM) amounts are also included to provide further information on the composition of the samples.

Table 7. Mineral composition of the analyzed samples, wt%

Component	OM30	OM49	OM68	OM88
Dolomite	22.2	26.3	11.7	1.5
Calcite	31.7	17.8	26.6	tr.*
Quartz	11.8	11.5	12.1	6.7
K-feldspar	8.5	11.7	12.5	15.2
Illite	17.5	22.0	25.1	59.9
Chlorite	2.1	3.3	5.1	12.3
Kaolinite	4.4	4.3	4.5	tr.*
Anatase	tr.*	0.6	0.5	1.2
Apatite	tr.*	0.9	0.0	tr.*

tr.* <0.5 mass%

Table 8. XRF analysis results of the analyzed samples, wt%

Component	OM30	OM49	OM68	OM88
Na ₂ O	0.13	0.17	0.14	0.08
MgO	3.69	3.43	1.41	0.47
Al ₂ O ₃	5.02	4.36	2.79	1.42
SiO ₂	15.35	12.98	8.71	3.73
P ₂ O ₅	0.10	0.07	0.05	0.02
SO ₃	1.98	2.10	2.41	0.24
K ₂ O	1.87	1.82	0.84	0.86
CaO	20.71	11.96	7.33	0.85
TiO ₂	0.32	0.24	0.18	0.10
MnO	0.04	0.03	0.02	0.00
Fe ₂ O ₃	2.21	2.24	1.14	0.39
LOI ^a	48.54	60.54	74.92	91.82

*n/d – not detected, ^a – Loss on ignition at 920 °C

Table 9. Elemental composition of oil shales with different amounts of organic matter, wt%

Sample	C^{total}	H	N	S^{total}
OM30	27.3	2.7	0.07	1.46
OM49	40.1	4.1	0.08	2.24
OM68	54.3	6.4	0.23	1.58
OM88	68.8	8.3	0.32	1.42

Table 10. Characteristic parameters of TGA measurements

Sample	T_{onset}	T_{max}	T_{end}	OM^a , wt%	CM^a , wt%
OM30	417	466	489	30.3	18.4
OM49	415	461	485	49.0	11.5
OM68	419	464	492	68.3	5.0
OM88	419	472	496	88.3	0.0

^a – data obtained from results of thermal analysis under an atmosphere of 80% N₂ and 20% O₂

2.3 Kinetic calculations

The publications presented herein offer kinetic calculation results based on two fundamentally different procedures. The results presented in **Publication I** are calculated using the Arrhenius plot method and the Coats-Redfern integral method. As the reaction mechanism of organic matter decomposition remains unclear, the Arrhenius equation [Equation (1)] and fractional weight loss [Equation (4)] were used to determine whether one or several temperature zones are present during decomposition. **Publication I** reveals that a breaking point was determined, confirming the existence of two consecutive zones. The pre-exponential factor and activation energy value for both temperature zones were calculated using both methods using Equations (4–6) in **Publication I**. These methods are outdated as they are based on single heating rate data. The kinetic calculations and recreation of the modelled curves presented in **Publication II** were accomplished using Kinetics2015. This program uses time-dependent temperature and numerically integrates the calculated rate over the thermal history, thereby offering precise results. DAEM was chosen as the calculation method as it assumes that the reactivity distribution corresponds to a set of independent and parallel reactions; additionally, an activation energy value and a frequency factor are calculated for each case [24]. As the reliable determination of the Arrhenius parameters requires measurements at three or more heating rates [81], data from heating rates of 2, 5, 10, 20 and 35 °C/min were used to calculate the kinetic parameters. The activation energy distributions are calculated in 4.184 kJ/mol (1 kcal/mol) steps. The activation energy value of the highest weighing (percentage) reaction was chosen to compare the data of the different samples.

3 RESULTS AND DISCUSSION

The results represented and discussed in this chapter are the sum of the findings published in **Publications I, II, and III**. The results are divided into topics of interest based on the main findings.

3.1 Thermal analysis

The samples were subjected to pyrolysis (under nitrogen atmosphere to avoid oxidation of the sample) in a thermogravimetric analyzer. The tests were run using several heating rates; however, for comparison the thermograms obtained from a heating rate of 20 °C/min were used (Figure 7, modified version of Figure 2 in **Publication I**). Strictly isothermal measurements are not possible due to a finite non-isothermal heat-up time. Hence, some mass loss may occur during the heat-up process, resulting in inaccurate estimation of the kinetic parameters. Therefore, the parameters were measured using non-isothermal TGA [77].

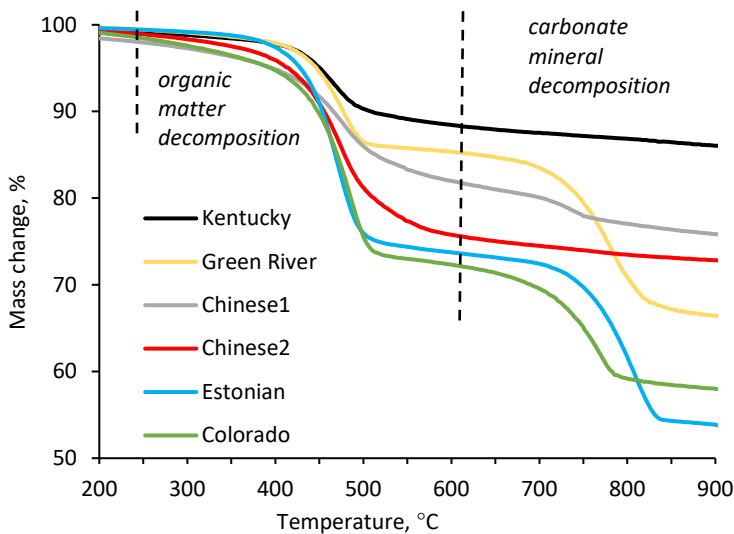


Figure 7. Thermograms of the analyzed oil shale samples

Oil shale pyrolysis consists of three main steps [103], [104]: first, water evaporates at lower temperatures (<200 °C). This is followed by the pyrolysis of kerogen, which usually occurs at a temperature range of 200–600 °C. The beginning of the pyrolysis process is highly dependent on the origin of the sample (Chapter 1.2). The final step is the decomposition of carbonate minerals at temperatures >700 °C. As the best kinetic analysis available is no better than the data is analyses [24], it is crucial to be accurate in the temperature measurements. The curves of mass vs. temperature should display an almost parallel shift toward higher temperatures with an increase in the heating rate. Thus, as a rule of thumb, increasing the heating rate by the same amount should result in a nearly constant shift in temperature on the TG curve [81]. This phenomenon was observed in this research too.

As the oil shales from different parts of the world vary in composition and properties, it is difficult to establish a single approach towards thermal treatment of oil shale. The same process parameters are difficult to implement for different samples as the resulting

products are highly dependent on the starting material. Therefore, to draw general conclusions, samples of different origin need to be thoroughly analyzed.

The results reported in **Publications I–III** agree with the data found in the literature. Estonian oil shale exhibits the greatest mass loss (47%) at 900 °C. This is in good accordance with the proximate analysis results (Table 5) in which the ash content for the Estonian sample is 51.3%. As the ash content was determined from a different analytical technique, the results can be considered as overlapping. Regarding the similarities of the decomposition profiles, the sample from Colorado exhibits a similar degradation pattern with a total mass loss of 42%. The Green River sample has similarities with the two previously mentioned samples, however, with a lower the total mass loss of 35%. The samples from China and Kentucky contain significantly less organic matter and little or no carbonate minerals. The Green River sample exhibits mass loss steps for the decomposition of organics and carbonate minerals with values of 14 and 19%, respectively. The samples from China contain no carbonate minerals and organic matter contents of 18 and 24%, respectively. The decomposition profiles of the Chinese samples also differ in curve steepness, whereby the mass loss steps display a very slanting profile, indicating the in contrast to the other samples, the start of the reaction in these samples is relatively slow. This strongly suggests that the reactions are more temperature-dependent, and unevenly distributed and that there may be several competing reactions rather than one dominant reaction.

The thermal analysis results are in good accordance with data found in the literature. Yörük et al. reported similar weight loss data for Estonian oil shale under CO₂ and argon environments [105]. Yao et al. investigated the co-combustion of oil shale and hydrochar and presented a 40% mass loss for Maoming oil shale [106]. Moreover, the analyzed sample also did not contain any carbonate minerals. Extensive data has been reported for the US samples, with different results based on the sampling location. For example, Tiwari and Deo demonstrated mass loss steps of 12 and 20% for the decomposition of organics and carbonate minerals, respectively [107].

3.2 Evolution of sulfur-containing compounds

The sulfur contents in oil shale and the produced shale oil have received significant attention over the past few years. In Estonia, oil is produced at temperatures of 450–500 °C [108]. Solid heat carrier technology (used since 1980) utilizes lower temperatures than gaseous heat carrier technology (first used in 1924) making it the preferred technology [3]. The different sulfur contents in oil shales of diverse origin raise queries on the differences in the evolution of sulfur-containing compounds and the conclusions that can be made from the gathered data. Thus, TGA-MS was employed to study the evolution of sulfur-containing gases.

Before analyzing the sulfur compounds, general observations were made based on the MS data. All the analyzed samples displayed peaks at m/z 12, 16, 17, 18 and 44 in the organic decomposition phase. Water ($m/z = 18$ and 17) was detected with high intensities for all samples except Chinese1 and 2. The carbon, oxygen, and carbon dioxide fragments ($m/z = 12$, 16 and 44, respectively) were also detected for all samples but with considerably smaller intensities. The peaks at m/z 39, 41, 42, 43, 55 and 56 had very high intensities during the organic decomposition phase. These account for the release of organic compounds, probably hydrocarbons such as butane, pentane, and their isomers. This is in good accordance with data found in the literature [84].

H₂S and SO₂ were chosen in this study to determine the differences in the release of sulfur-containing compounds between the analyzed samples.

Evolution of the hydrogen sulfide fragment was investigated using m/z values of 33 and 34 as these have the respective relative intensities of 100% and 42%. The heteroatomic species exhibited significantly different evolution profiles than the hydrocarbons and water. The conclusions drawn are based on the data from m/z = 34 as this is the more intense signal.

Figure 5 in **Publication II** reveals that in the Colorado sample the peak at m/z = 34 is only detected in the organic decomposition region. This result clearly differs from that of other samples. The Green River sample does not exhibit a distinguishable peak and its signal is noisy even after smoothing. This is to be expected as the Green River sample has the lowest total sulfur content with most of the sulfur being in the organic form (Table 4). In contrast to these samples, the Estonian sample exhibits two major peaks, the first in the organic decomposition temperature range (320–500 °C) and the second sharp and narrow peak at temperatures of 520–570 °C. This is due to the composition of the sample in which most of the sulfur is in the sulfide and organic form. The samples from China and Kentucky exhibit a similar H₂S evolving profile. However, for these samples the intensity is lower during the organic matter decomposition phase. The second sharp peak is found at a temperature range of 500–600 °C. The sharp peak is shifted towards higher temperatures for the Chinese 2 sample. This is again in good accordance with the composition of the samples, with the Chinese samples containing a relatively high amount of sulfur in sulfide form (1.17 and 1.26% for Chinese 1 and 2, respectively). As previously demonstrated, pyrite decomposes at temperatures of 450–650 °C. Therefore, the sharp peaks are attributed to the decomposition of pyrite. This is also supported by the data observed for m/z = 64 (SO₂).

SO₂ exhibits different evolving profiles. For the Green River sample, an overlapping peak is detected in the region of 350–600 °C with a peak temperature of 450 °C. The samples from Colorado and Estonia display a similar profile, while in the Estonian sample the peaks are shifted towards higher temperatures. The samples from China and Kentucky exhibit profiles that are fairly similar to that of the evolving H₂S. The only difference is that the peaks at the lower temperatures are less sharp and intense. Interestingly, in the Chinese 2 sample, SO₂ is already detected already at 270 °C. Moreover, similar to H₂S, there is also a peak at a temperature range of 500–600 °C. However, in this case, the peak is wider and flatter.

Hu et al. revealed that when pyrite is removed from oil shale, sulfur will only evolve in the form of SO₂ [71]. This is in good accordance with the data presented herein, as both H₂S and SO₂ fragments are detected. Notably, the thermal analysis results should be treated cautiously as they include contributions of other minerals that are not removed from the sample. As previously discussed (Chapter 1.4), the catalytic effect of minerals has been both proven and rebutted in the literature. Pyrite is among the minerals which has received significant attention. As the Estonian sample also contains pyrite, its effect (or lack of it) on the decomposition of organic matter should be investigated. This is discussed in more detail later (Chapter 3.4).

Strizhakova and Usova reported that liquid products produced from thermal treatment of oil shale are thermodynamically unstable and contain large amounts of N-, O-, and S-containing organic compounds [38]. Additionally, Riboulleau suggested that organic sulfur is mostly present as di(poly)sulfides and sulfides and that flash pyrolysis produces short-chain alkylthiophenes [109]. Thus, the afforded products require

treatment and cannot be directly used as fuels. For example the presence of nitrogen in shale oil decreases the stability of the obtained fuel [38]. Thus, nowadays, catalysts are used to effectively remove sulfur- and nitrogen-containing compounds from the shale oil [110]. Therefore, it would be reasonable to produce shale oil of the highest quality to improve its characteristics and decrease the need (or extent) for further treatment.

The results presented herein are important to allow conclusions on the pyrolysis process of different oil shales to be made. As the samples exhibited both similarities and differences, the only general conclusion that can be drawn is that the pyrolysis temperatures could be lowered so that the produced oil would contain less sulfur. Based on the gathered data, the optimal temperature for oil production (depending on the sample) was determined as 400–450 °C. From the figures presented in **Publication II**, one can conclude that the temperature should be kept below 480 °C. At temperatures >450 °C the evolution of sulfur intensifies, resulting in higher sulfur concentrations in the product. Nonetheless, lowering the temperature is not effective for the Estonia and Colorado samples since maximal evolution occurs at ~400 °C. As the reduction of the global maximum fuel sulfur content from 4.5% to 0.5% (for some countries to 0.1% by 2015) by 2020 has been mandated by the International Maritime Organization, the sulfur contents of fuels must be decreased [111], [112]. Such reductions have been shown to have highly significant environmental benefits. For example, for one particular ship the particulate matter emissions were reduced by 67%, SO₂ emissions by 80% and the volatile organic compound emissions were also reduced [113].

As the results obtained from research are based only on lab-scale experiments, further research on large-scale application is necessary.

3.3 Kinetic computations and calculation of conversion

As described by Moukhina, the number of reaction steps in reactions with unknown or poorly described mechanisms is also unknown [98]. Processes with several chemical reaction steps can still produce a single peak on the thermoanalytical curve. In such cases, this single peak is the only peak that can be analyzed. Thus, the kinetic parameters can be correctly determined only for this peak. Moukhina offers an explanation as to how a process with two consecutive steps can be perceived as a single-step process. She suggests that one of the reactions may be slow enough to produce a peak on the thermoanalytical curve, while the second reaction is fast enough for the “intermediate” product to be quickly converted into the final product. Moukhina explained that kinetic parameters can be determined only for reaction steps that are visible as steps in the TG curves [98].

Notably, TGA often includes unreactive residue, in this case ash, comprising a variety of mineral. This error is eliminated by differentiating the data so that the data is converted into reaction rates [24]. To validate the kinetic analysis, modeled curves were constructed to compare the experimental results (**Publication II**). As the decomposition of the organic matter during the pyrolysis of oil shale is shown as a single mass loss step, the activation energy distributions are calculated for that step.

3.3.1 Kinetic calculations

The apparent activation energy values of oil shale organic matter decomposition found in the literature cover an extensive range (13 to 215 kJ/mol) [8], [73], [114]–[116]. Notably, the results are sample-dependent and solely describe the sample for which they were calculated. These results are usually calculated from TGA data. Thus, to correctly

compare the samples, the measurements and subsequent calculations need to be performed following precisely the same conditions. Additionally, regardless of the sophistication of the algorithms, the kinetic predictions are always limited in both precision and accuracy [77].

Yongjiang et al. investigated the kinetic parameters of oil shale pyrolysis determined from both isothermal and non-isothermal measurement analysis [117]. They discovered that the average results of the parameters acquired from non-isothermal measurements were similar to those attained from isothermal measurements. As the non-isothermal analysis enables a fast scan of the whole range of interest and is therefore preferred from an analytical point of view and in material characterization, data from non-isothermal measurements was employed for the kinetic calculations.

The results presented in **Publication I** only offer a single apparent activation energy value for two temperature zones. As described in Chapter 1.6, the presence of a “breaking point” in the data enables the determination of different temperature zones. This work assumes temperature zones, lower and higher zone, with fundamentally different kinetic parameters of decomposition. The values lie in the range of 14 to 31 kJ/mol and 70 to 149 kJ/mol, for the lower and higher temperature zone, respectively. The lower values for the first zone indicate that the bonds that are broken during decomposition are weak. As the methods use different approaches for the calculations, the results also indicated that the direct Arrhenius plot method yields higher apparent activation energy values.

Although the results reported in this research are similar to those found in the literature (**Publication I**), the presented methods have become outdated since newer and more precise methods have become available. As described by Burnham, the use of a single heating rate was common in the past; however, nowadays, several heating rates are being used. Additionally, the use of specific software (e.g., Kinetics2015, used in this research) enables the fitting of a wide range of global kinetic models [118]. Common mistakes include the assumption of a first order reaction when in practice there are consecutive and sequential reactions, using an insufficient range of heating rates, and temperature and random measurement errors. In addition to offering guidelines for collecting experimental thermal analysis data [81], the Kinetics Committee of the International Confederation for Thermal Analysis and Calorimetry (ICTAC) has also offered recommendations on how to perform kinetic computations based on thermal analysis data. They have also demonstrated that fossil fuels follow distributed reactivity models, a process that consists of a set of independent, parallel reactions the contributions of which are controlled by the mathematical distribution function [77]. As the actual reactivity distributions tend to be asymmetric rather than the symmetric Gaussian distributions, a discrete distribution is also introduced. The results in **Publication II** are therefore calculated using the DAEM.

Figure 8 (Figure 3 in **Publication II**) illustrates the activation energy distributions for the analyzed samples. For the samples from China and Kentucky (group 1) the weight percentages of the single reactions are <30% and the count of the single reactions is quite high. The single reactions are quite evenly distributed. The activation energy distributions of the samples from Estonia, Colorado and Green River (group 2) are also presented in Figure 3 of **Publication II**. These samples all display one dominant reaction with a relatively high weight (68–74%). The value distribution is more uneven, while the amount of independent reactions is smaller (e.g., Chinese 2 30 reactions). For the first group, the dominant reaction exhibits a slightly higher activation energy value than those

of the second group. The top three energy values account for only 35–46% of the overall yield for the second group, whereas for the first group the top three account for 79–88% of the yield.

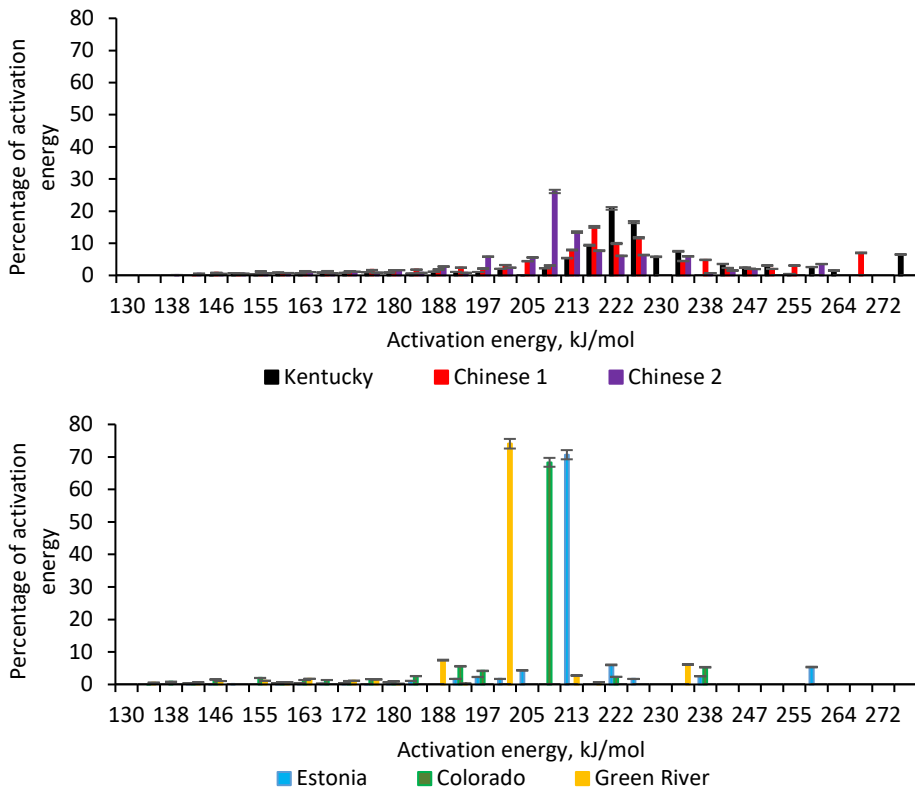


Figure 8. Activation energy distributions for the analyzed samples

The activation energy value distributions clearly describe the decomposition profiles obtained by using TGA. As discussed before (Chapter 3.1), the curves exhibited different steepness. For the Chinese 2 sample there is a large amount of parallel and consecutive reactions with similar apparent activation energy values which might be complete at different times. This is also why the TGA decomposition profile has no distinguishable mass loss step. Conversely, the beginning and end of organic matter decomposition in the Estonian sample are highly distinguishable. This is also logical as there is only one dominant reaction and other, less “weighing” reactions will not have a noticeable effect on the course of the dominant reaction.

The results presented here are in good accordance with data found in the literature. In their review, Raja et al. have demonstrated that most principal activation energy values fall within the range of 200 to 242 kJ/mol, with most samples values falling within the middle of the range. They also revealed that the frequency factors are in the 10^{12} – 10^{16} s^{-1} range, with most values again in the middle of the range [95].

3.3.2 Calculation of conversion for isothermal conditions

For the practical use of these kinetic parameters, the results were also used to calculate the isothermal decomposition curves of the same samples. The calculations were performed using the Arrhenius equation [Equation (1)]. Notably, these are only

valid for the same samples with the same preparation methods and properties. The calculated results at 450 °C and 480 °C are illustrated in Figures 9 and 10, respectively.

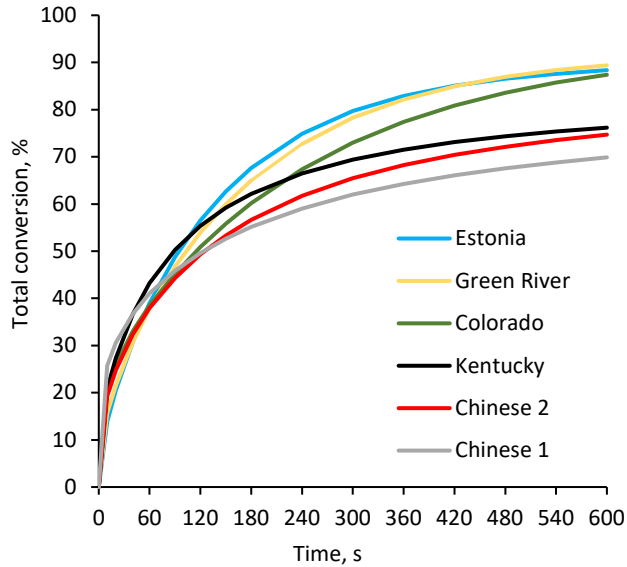


Figure 9. Calculated conversions of the organic matter at 450 °C

Figure 9 illustrates that the calculated curves for decomposition at 450 °C exhibit some differences. At 450 °C the reactions would not yet have reached their maximum rate and therefore the curves are better suited for comparison. The total conversion during the first 10 minutes varies from 70 to 89%. The samples from Estonia, Green River, and Colorado reach a similar total conversion during the first 10 minutes. On the other hand, the Colorado sample displays a smaller conversion during the first few minutes. The Chinese 1 sample exhibits the highest conversion (26%) in the first 10 seconds. This is an indication of a very high initial reactivity. However, the rest of the course of the reaction remains modest so that this sample has the lowest total conversion of the tested samples (70% in 10 minutes). Conversely, the samples from Estonia and Green River display the highest total conversions of all the samples at 13.8% and 15.7% in the first 10 seconds, respectively. The Chinese 2 and Kentucky samples reach a conversion of nearly 75% in 10 minutes. The results indicate the fundamental difference between the samples. Additionally, at a temperature of 450 °C it is difficult to reach total conversion over a reasonable amount of time.

The conversions at 480 °C were also calculated to compare the temperature effect and to study the change in conversion (Figure 10).

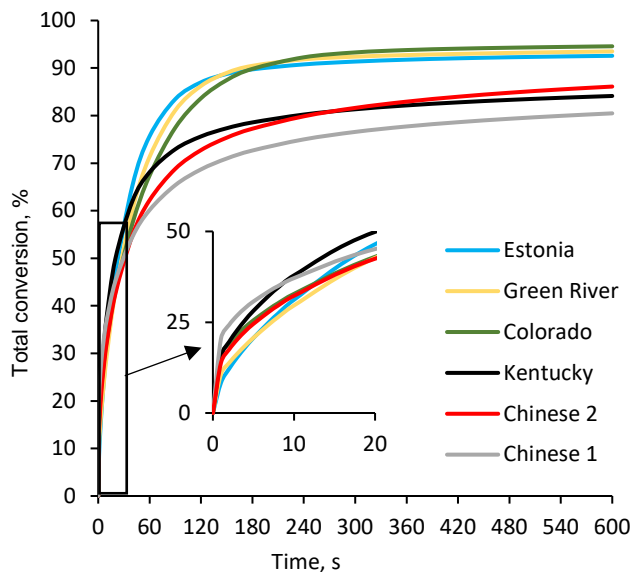


Figure 10. Calculated conversions of the organic matter at 480 °C

As expected, the reactions at 480 °C are significantly faster than those at 450 °C. The total conversions are also higher, ranging from 80 to 95%. The beginning of the reaction is very fast for all the samples. In the first 5 seconds, the samples reach a conversion of 21 to 31%. Chinese 1 has the highest initial reactivity, reaching a conversion of ~31%. The slowest start is for the Estonian and Green River samples, with conversions of only 21%. In the first minute, the conversions are in the range of 60 to 76%. Interestingly, at this temperature Chinese 1 displays the lowest total conversion, while the highest conversion is observed in the Estonian sample. This is an indication that the Estonian sample has a more even conversion profile, while the Chinese 1 displays a quick start and then subsequently slows down.

The results presented in Figure 10 suggest that a higher temperature (compared to the previously analyzed 450 °C) would result in a much faster process with a higher decomposition range. However, a higher temperature would also result in higher sulfur concentrations in the products. This clearly illustrates that products of better quality might take more time to produce.

The curves presented in Figures 9 and 10 are a good indication of how using the results from the kinetic studies can be applied. The results presented herein are also illustrative of how the course of the process for different oil shales would change, if the pyrolysis temperature was lowered, as explained in the previous chapter.

3.4 Possible catalytic effect of the minerals in the oil shale

This thesis has illustrated that the existence of the catalytic effect of minerals in oil shale highly depends on the nature of the sample. As the composition and quantitative ratios of oil shale products depend directly, among other parameters, on the composition of the sample, its effect should be thoroughly investigated. While data on other oil shales is available in the literature, data on the possible catalytic effect on Estonian oil shale is scarce. As Estonia is highly dependent on oil shale the Estonian sample and variations of it were chosen as the test subjects.

To confirm the presence of a catalytic effect, four samples with different amounts (30, 49, 68 and 88%; OM30, OM49, OM68, and OM88, respectively) of organic matter were chosen. The respective mineral matter was analyzed by XRD (Table 8). Table 9 illustrates that OM49 exhibits a higher amount of sulfur than the other samples. As this sample is not treated with acids, its sulfur content is predictably higher than for those of OM68 and OM88. When compared to the sulfur content of OM30, the explanation is that sulfur seems to be in the very fine fraction (<90 μm) instead of the bigger particles. The thermograms of the samples analyzed are displayed in Figure 11 (modified version of Figure 1 in **Publication III**).

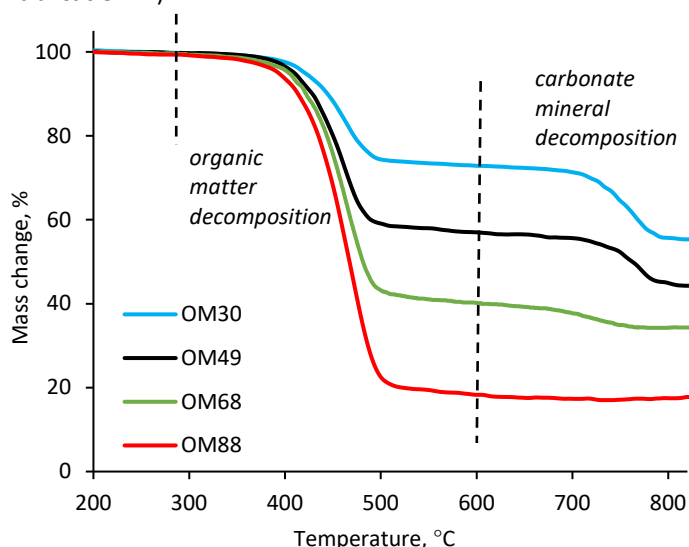


Figure 11. Thermograms of the Estonian samples

The thermograms reported herein illustrate the variations in the selected sample compositions and are in very good accordance with data found in the literature (Chapter 3.1). The main mass loss step for all the samples was observed at a temperature range of 370–500 °C. This accounts for the decomposition of organic matter, as discussed in previous chapters. The decomposition of carbonate minerals was also observed in all the samples, except for sample OM88 which does not contain any carbonate minerals, as expected.

To better understand the possible differences, derivatives of mass loss (DTG) data were also studied. These provide more insight on the course of the reaction. The DTG curves are illustrated in Figure 12 (Figure 2 in **Publication III**). DTG data is used to determine whether there is a shift in the peak of the maximal mass loss. This in turn provides an insight on the effect of the sample composition on the decomposition process. Thus, in the presence of a catalytic effect, marked changes in the peak maximum would be observed.

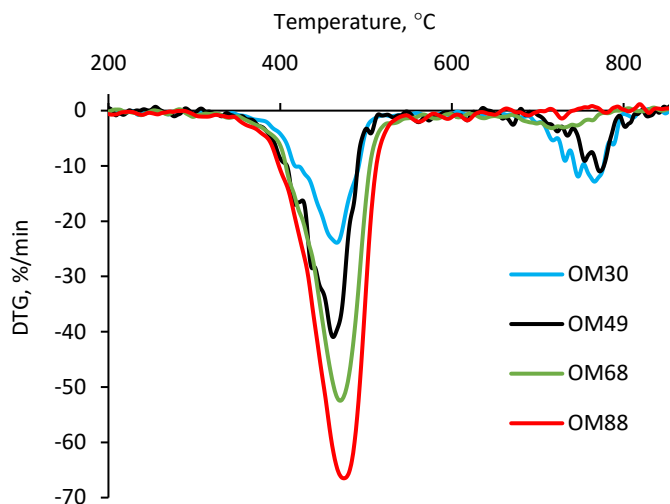


Figure 12. Derivatives of thermograms.

To study the existence of the catalytic effect, only TGA data was used. As it is quite difficult to compare the TGA graphs due to the differences in the extent of the major mass loss step, the conversion of organic matter was plotted against temperature. This simplifies the visual comparison of the acquired results. The conversion (fractional mass loss at any time) was calculated from Equation (4) (Chapter 1.6). The conversion was calculated as 0 from a temperature of 200 °C to avoid any possible effects of moisture. Moreover, as only the decomposition of organic matter was of interest, the graphs are presented up to temperatures of 700 °C to exclude the decomposition of carbonate minerals. This allows comparing the thermal behavior of the organic matter only. Any differences between the four conversion curves would be sufficient evidence of the existence of the catalytic effect. The results of the conversion comparisons are displayed in Figure 13.

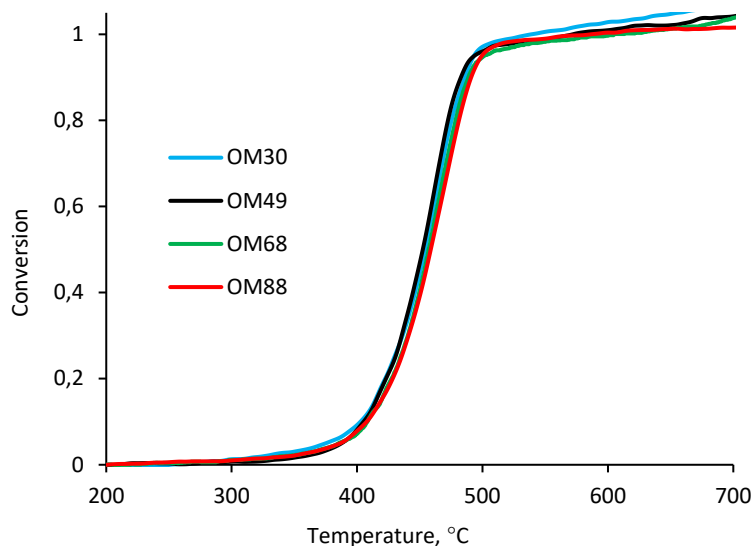


Figure 13. Organic matter conversion curves

The acidic minerals in coal are known to catalyze the decomposition of organic sulfur. On the other hand, its alkaline mineral matter can react with sulfur-containing gases, thereby hindering sulfur emissions [119]. Fan et al. reported that after demineralization, no confinement by the mineral matrix was observed and the pyrolysis of shale char started at lower temperatures than those observed for the untreated sample [120]. This is important knowledge aids the determination of the optimal temperatures for retorting. As further comparison, Chang et al. investigated the oil yield of demineralized Huadian oil shale, removing carbonate and silicate minerals and compared it to the results of untreated oil shale [43]. They also illustrated that the elimination of carbonate minerals decreased the nitrogen- and oxygen-containing compounds of the produced oil and that the silicate minerals had the opposite effect on the oxygenated compounds. In both cases, there was a decrease in the H/C ratio of the shale oil. The results reveal that the mineral effect directly influences the quality of the oil products. This highlights the importance of studying the mineral matter effect on the pyrolysis process.

The data presented herein reveals that the beginning of the process is not affected by the sample composition. Thus, T_{onset} varies by a very small range (only 4 °C). This is also supported by the conversion curves, which do not display any differences at low temperatures. The beginning of the decomposition process is dominated by the breaking of weaker bonds, which does not seem to be affected by the sample composition. Notably, the samples with a higher mineral matter content had a lower T_{end} value. This might account for some catalytic effect, albeit very small. In practice, the difference between the characteristic temperatures reported herein for raw oil shale and upgraded oil shale is less than 10 °C. The inhibiting effect of silicate minerals was also not confirmed as there seems to be no correlation between SiO_2 content and the characteristic decomposition temperatures. The T_{max} values vary only by a range of 6 °C. The T_{max} value shifted to a lower temperature for sample OM49 but not for sample OM68. As this latter sample contains significantly less mineral matter, there is no reason to believe that a change as small as this would result in a noticeable effect. The possible reason for the lower T_{max} value of sample OM49 is that during the sieving process the small particles of mineral matter particles remained bound to the organic matter. This would decrease the porosity of the material and inhibit heat transfer. Thus, the decomposition process would slow down causing a higher end temperature for the reaction.

Notably, the samples are of three different origins, therefore the minor difference in the conversion curves is negligible and to be expected. However, examples for coal-char thermal degradation where the differences in the T_{max} values are over 100 °C have been reported [121], [122]. These results are a strong indication that the inherent minerals do not exhibit a significant catalytic effect on the decomposition of organic matter in Estonian samples.

4 CONCLUSIONS

The aim of this thesis was to characterize different oil shales from Estonia, China, and the USA using modern chemical apparatus and to analyze the thermal behavior of the different samples. Although oil shale has been studied in Estonia for decades, earlier works often utilize methods that have become outdated. Long chemical analysis techniques that required days to produce results have now been substituted by significantly shorter (30 min) methods. Moreover, earlier works usually focus on one sample without comparing oil shales from other countries.

The main analytical methods used in this thesis are TGA-MS, elemental analysis, XRD, and WD-XRF. The data from this set of techniques enable the characterization of the composition of the material (both organic and inorganic components), investigation of its behavior during thermal degradation, and identification of the components that are released during its decomposition. The results of this thesis are described as follows:

- The samples were subjected to pyrolysis in a thermogravimetric analyzer and as expected, exhibited different thermal decomposition profiles due to their diverse compositions.

- The gases evaporating during the pyrolysis process were analyzed. The data for hydrocarbons and water was in good accordance with data reported in the literature. The release profiles of the sulfur-containing gases (H_2S and SO_2) were investigated and the profiles revealed important differences. The different forms of sulfur were quantified and the afforded results offered explanations on the differences in the release of sulfur-containing compounds. The total sulfur content ranged from 0.81 to 2.16%. With the exception of the Green River sample, sulfide sulfur prevailed in the samples. For the Green River sample, which also displayed the lowest sulfur content, most of the sulfur was found in organic form.

- The regulations on fuels, especially those regarding sulfur concentrations, have become stricter over the past few years. This has led to the question of whether it is possible to manipulate the pyrolysis temperature so that the resulting oil would contain less sulfur. The data suggest that it would be beneficial to lower the pyrolysis temperature ($<480\text{ }^\circ\text{C}$) to reduce the sulfur content in the produced oil. The samples from Estonia and Colorado would benefit less from this, as the H_2S evaporation maximum for both samples approaches $400\text{ }^\circ\text{C}$. The sulfur compounds in the Green River sample exhibited totally different behavior. In this sample, most of the sulfur-containing compounds had already evolved at temperatures $<500\text{ }^\circ\text{C}$. These results strongly suggest that the quality of the oil produced from this shale has a high sulfur content.

- The kinetic parameters of the decomposition of organic matter were calculated using the DAEM. The samples fell into two groups with different activation energy distributions. The first group (Chinese 1 and 2 and the Kentucky samples) exhibited a flat normal distribution with the maximal percentage of a single apparent activation energy of $<30\%$. In this case the amount of independent reactions was higher than that observed for the other group. The distribution of the second group (Estonia, Colorado, and Green River samples) was dominated by a single peak with apparent activation energy percentages ranging from 68 to 74%, depending on the sample. These results are in accordance with the TGA decomposition curves, strongly suggesting that they are dependent on the sample composition.

- To offer practical use for the acquired kinetic data, the parameters were used to predict the conversion of organic matter in isothermal conditions. The integral of the

Arrhenius equation for first order reactions was used. The conversions were calculated for a temperature of 450 °C. The Chinese 1 sample exhibited the highest initial activity (during the first 10 s); however, its conversion after 10 minutes was the lowest (only 70%). The Estonia and Green River samples exhibited a similar conversion curve with a conversion of ~90% in 10 minutes. The Colorado sample also exhibited a similar conversion (87% in 10 minutes); however, its conversion profile was steadier. The Chinese samples exhibited the lowest conversions during the calculated time. The conversions were also calculated for a temperature of 480 °C. As expected, the reactions were much faster and the total conversions after 10 minutes were higher. All the analyzed samples exhibited fast initial reactivities, with conversions ranging from 21 to 31% in the first 5 seconds. Although the Chinese 1 sample presented the highest conversion in the first few seconds, its total conversion after 10 minutes was the lowest. The sample from Estonia exhibited an opposite profile, being initially slower but reaching a higher total conversion after 10 minutes. These results are a clear representation of how kinetic calculations can be used to predict the actual processes in industrial retorts. They offer a good opportunity of comparing processes at different temperatures and gaining preliminary knowledge on the degradation process of the samples.

- Oil shale samples with varying organic matter contents were used to determine the existence of the catalytic effect in pyrolysis conditions. Selected samples with 30, 49, 68, and 88% organic matter (determined by TGA), afforded mineral carbon dioxide amounts of 18, 11, 5 and 0%, respectively. The mineral composition was quantified by XRD and WD-XRF analyses. To better compare the decomposition profiles of the organic matter, organic matter conversion curves were created and plotted against temperature. The results revealed that the sample composition did not affect the organic matter decomposition profile. Although there was a minor shift in the characteristic temperatures, it was too small to be an indication of a catalytic effect. Therefore, it was concluded that the inherent and removed minerals had no evident catalytic effect on the decomposition of organic matter.

List of Figures

Figure 1. Possible structure of kerogen [21]	13
Figure 2. H/C atomic ratios in various hydrocarbon materials [37]	15
Figure 3. Flow diagram illustrating the mechanism of oil shale retorting [39]	16
Figure 4. Demineralization process of oil shale	20
Figure 5. Thermogram of Estonian oil shale	22
Figure 6. Preparation of the samples	28
Figure 7. Thermograms of the analyzed oil shale samples	30
Figure 8. Activation energy distributions for the analyzed samples	35
Figure 9. Calculated conversions of the organic matter at 450 °C.....	36
Figure 10. Calculated conversions of the organic matter at 480 °C.....	37
Figure 11. Thermograms of the Estonian samples.....	38
Figure 12. Derivatives of thermograms.....	39
Figure 13. Organic matter conversion curves	39

List of Tables

Table 1. Proximate and ultimate analytical results of some oil shales, wt%	14
Table 2. Oil shale pyrolysis temperatures [17].....	17
Table 3. Oil shale ash composition, wt% on dry basis [62]	18
Table 4. Thermochemical properties of common minerals in oil shale deposits [91]	22
Table 5. Ultimate analysis results, wt%, dry base	27
Table 6. Proximate analysis results, as-received basis.....	27
Table 7. Mineral composition of the analyzed samples, wt%.....	28
Table 8. XRF analysis results of the analyzed samples, wt%.....	28
Table 9. Elemental composition of oil shales with different amounts of organic matter, wt%	29
Table 10. Characteristic parameters of TGA measurements	29

References

- [1] A. Siirde, M. Eldermann, P. Rohumaa, and J. Gusca, "Analysis of Greenhouse Gas Emissions From Estonian Oil Shale Based Energy Production Processes. Life Cycle Energy Analysis Perspective," *Oil Shale*, vol. 30, no. 2S, pp. 268–282, 2013.
- [2] A. Konist, T. Pihu, D. Neshumayev, and A. Siirde, "Oil Shale Pulverized Firing: Boiler Efficiency, Ash Balance and Flue Gas Composition," *Oil Shale*, vol. 30, no. 1, pp. 6–18, 2013.
- [3] J. Soone and S. Doilov, "Sustainable utilization of oil shale resources and comparison of contemporary technologies used for oil shale processing," *Oil Shale*, vol. 20, no. 3 S, pp. 311–323, 2003.
- [4] A. Ots, *Oil shale fuel combustion*. Tallinn: Tallinna Raamatutrükikoda, 2006.
- [5] T. Pihu, A. Konist, D. Neshumayev, J. Loosaar, A. Siirde, T. Parve, and A. Molodtsov, "Short-Term Tests on Firing Oil Shale Fuel Applying Low-Temperature Vortex Technology," *Oil Shale*, vol. 29, pp. 3–17, 2012.
- [6] A. Siirde, "Oil shale - global solution or part of the problem?," *Oil Shale*, vol. 25, no. 2, pp. 201–202, 2008.
- [7] G. L. Baughman, *Synthetic Fuels Data Handbook*, Second edi. Cameron Engineers, Inc., 1978.
- [8] F. Yan and Y. Song, "Properties Estimation of Main Oil Shale in China," *Energy Sources, Part A*, vol. 31, no. 4, pp. 372–376, 2009.
- [9] World Energy Council, "World Energy Resources: 2013 survey," *World Energy Council*, 2013. [Online]. Available: http://www.worldenergy.org/wp-content/uploads/2013/09/Complete_WER_2013_Survey.pdf.
- [10] A. Konist, A. Valtsev, L. Loo, T. Pihu, M. Liira, and K. Kirsimäe, "Influence of oxy-fuel combustion of Ca-rich oil shale fuel on carbonate stability and ash composition," *Fuel*, vol. 139, no. September, pp. 671–677, 2015.
- [11] I. Külaots, J. L. Goldfarb, and E. M. Suuberg, "Characterization of Chinese, American and Estonian oil shale semicokes and their sorptive potential," *Fuel*, vol. 89, no. 11, pp. 3300–3306, 2010.
- [12] X. Yu, Z. Luo, X. Yang, H. Jiang, E. Zhou, B. Zhang, and L. Dong, "Oil shale separation using a novel combined dry beneficiation process," *Fuel*, vol. 180, pp. 148–156, 2016.
- [13] B. K. Dutta, S. Khanra, and D. Mallick, "Leaching of elements from coal fly ash: Assessment of its potential for use in filling abandoned coal mines," *Fuel*, vol. 88, no. 7, pp. 1314–1323, 2009.
- [14] S. Lee, J. G. Speight, and S. K. Loyalka, *Handbook of Alternative Fuel Technologies*, vol. 9, no. 12. CRC Press, Taylor & Francis Group, 2015.
- [15] E. Väli, I. Valgma, and E. Reinsalu, "Usage of Estonian Oil Shale," *Oil Shale*, vol. 25, no. 2s, pp. 101–114, 2008.
- [16] V. Kattai and U. Lökk, "Historical review of the kukersite oil shale exploration in Estonia," *Oil Shale*, vol. 15, no. 2S, pp. 102–110, 1998.
- [17] J. Qian and L. Yin, *Oil Shale: Petroleum Alternative*. China Petrochemical Press, 2010.
- [18] M. Koel, "Estonian oil shale," *Oil Shale*, 1999. [Online]. Available: <http://www.kirj.ee/public/oilshale/Est-OS.htm>.
- [19] M. Vandenbroucke and C. Largeau, "Kerogen origin, evolution and structure," *Org. Geochem.*, vol. 38, pp. 719–833, 2007.

- [20] Y. H. Khraisha, "Kinetics of isothermal pyrolysis of Jordan oil shales," *Energy Convers. Manag.*, vol. 39, no. 3, pp. 157–165, 1998.
- [21] Ü. Lille, I. Heinmaa, and T. Pehk, "Molecular model of Estonian kukersite kerogen evaluated by C-13 MAS NMR spectra," *Fuel*, vol. 82, pp. 799–804, 2003.
- [22] A. Karabakan and Y. Yürüm, "Effect of the mineral matrix in the reactions of shales. Part 2. Oxidation reactions of Turkish Göynük and US Western Reference oil shales," *Fuel*, vol. 79, pp. 785–792, 2000.
- [23] N. E. Altun, C. Hicyilmaz, J.-Y. Hwang, A. S. Bacgi, and M. V. Kök, "Oil shales in the world and Turkey; reserves, current situation and future prospects: A review," *Oil Shale*, vol. 23, pp. 211–227, 2006.
- [24] A. K. Burnham and R. L. Braun, "Global Kinetic Analysis of Complex Materials," *Energy & Fuels*, vol. 13, no. 1, pp. 1–22, 1999.
- [25] A. Hutton, T. Robl, and S. Bharati, "Chemical and Petrographic Classification of Kerogen / Macerals," *Energy & Fuels*, vol. 8, pp. 1478–1488, 1994.
- [26] W. E. Robinson, "Chapter 4 - origin and characteristics of Green River oil shale," in *Developments in Petroleum Science*, 1976, pp. 61–79.
- [27] D. Vučelić, V. Marković, V. Vučelić, D. Spiridonović, B. Jovančićević, and D. Vitorović, "Investigation of catalytic effects of indigenous minerals in the pyrolysis of Aleksinac oil shale organic matter," *Org. Geochem.*, vol. 19, no. 4–6, pp. 445–453, 1992.
- [28] J. L. Hillier, T. H. Fletcher, M. S. Solum, and R. J. Pugmire, "Characterization of Macromolecular Structure of Pyrolysis Products from a Colorado Green River Oil Shale," *Ind. Eng. Chem. Res.*, vol. 52, no. 44, pp. 15522–15532, 2013.
- [29] P. Tiwari, M. Deo, C. L. Lin, and J. D. Miller, "Characterization of oil shale pore structure before and after pyrolysis by using X-ray micro CT," *Fuel*, vol. 107, pp. 547–554, 2013.
- [30] G. Gerasimov, V. Khaskhachikh, and O. Potapov, "Experimental study of kukersite oil shale pyrolysis by solid heat carrier," *Fuel Process. Technol.*, vol. 158, pp. 123–129, 2017.
- [31] F. Bai, Y. Sun, Y. Liu, Q. Li, and M. Guo, "Thermal and kinetic characteristics of pyrolysis and combustion of three oil shales," *Energy Convers. Manag.*, vol. 97, pp. 374–381, 2015.
- [32] P. T. Williams and N. Ahmad, "Investigation of oil-shale pyrolysis processing conditions using thermogravimetric analysis," *Appl. Energy*, vol. 66, no. 2, pp. 113–133, 2000.
- [33] L. A. Aunela-Tapola, F. J. Frandsen, and E. K. Hasanen, "Trace metal emissions from the Estonian oil shale fired power plant," *Fuel Process. Technol.*, vol. 57, no. 1, pp. 1–24, 1998.
- [34] J. F. Saldarriaga, R. Aguado, A. Pablos, M. Amutio, M. Olazar, and J. Bilbao, "Fast characterization of biomass fuels by thermogravimetric analysis (TGA)," *Fuel*, vol. 140, pp. 744–751, 2015.
- [35] R. L. Braun and A. J. Rothman, "Oil-shale pyrolysis: Kinetics and mechanism of oil production," *Fuel*, vol. 54, no. 2, pp. 129–131, 1975.
- [36] National Research Council, *Refining Synthetic Liquids From Coal and Shale: Final Report of the Panel on R&D Needs in Refining of Coal and Shale Liquids*, Energy Engineering Board, Assembly of Engineering. National Academy Press, Washington D.C., 1980.
- [37] D. D. Whitehurst, "A Primer on the Chemistry and Constitution of Coal," in

- Organic Chemistry of Coal*, 1978, pp. 1–35.
- [38] Y. a. Strizhakova and T. V. Usova, "Current trends in the pyrolysis of oil shale: A review," *Solid Fuel Chem.*, vol. 42, no. 4, pp. 197–201, 2008.
- [39] X. Han, I. Külaots, X. Jiang, and E. M. Suuberg, "Review of oil shale semicoke and its combustion utilization," *Fuel*, vol. 126, pp. 143–161, 2014.
- [40] S. Bhargava, F. Awaja, and N. D. Subasinghe, "Characterisation of some Australian oil shale using thermal, X-ray and IR techniques," *Fuel*, vol. 84, pp. 707–715, 2005.
- [41] P. F. V Williams, "Thermogravimetry and decomposition kinetics of British Kimmeridge Clay oil shale," *Fuel*, vol. 64, no. 4, pp. 540–545, 1985.
- [42] A. Kahru and L. Põllumaa, "Environmental hazard of the waste streams of estonian oil shale industry: An ecotoxicological review," *Oil Shale*, vol. 23, no. 1, pp. 53–93, 2006.
- [43] Z. Chang, M. Chu, C. Zhang, S. Bai, H. Lin, and L. Ma, "Influence of inherent mineral matrix on the product yield and characterization from Huadian oil shale pyrolysis," *J. Anal. Appl. Pyrolysis*, vol. in press, 2018.
- [44] Y.-R. Huang, X.-X. Han, and X.-M. Jiang, "Comparison of fast pyrolysis characteristics of Huadian oil shales from different mines using Curie-point pyrolysis-GC/MS," *Fuel Process. Technol.*, vol. 128, pp. 456–460, 2014.
- [45] J. M. Nazzal, "The influence of grain size on the products yield and shale oil composition from the Pyrolysis of Sultani oil shale," *Energy Convers. Manag.*, vol. 49, no. 11, pp. 3278–3286, 2008.
- [46] N. Olukcu, J. Yanik, M. Saglam, M. Yuksel, and M. Karaduman, "Solvent effect on the extraction of Bey pazari oil shale," *Energy & Fuels*, vol. 13, pp. 895–902, 1999.
- [47] R. Yoshida, M. Miyazawa, T. Yoshida, H. Narita, and Y. Maekawa, "Chemical structure changes in Condor shale oil and catalytic activities during catalytic hydrotreatment," *Fuel*, vol. 75, no. 1, pp. 99–102, 1996.
- [48] E. S. Vaysoglu, O. B. Harput, B. R. Johnson, B. Frere, and K. D. Bartle, "Characterization of oil shales by extraction with N-methylpyrrolidone," *Fuel*, vol. 76, no. 4, pp. 353–356, 1997.
- [49] S. Deng, Z. Wang, Q. Gu, F. Meng, J. Li, and H. Wang, "Extracting hydrocarbons from Huadian oil shale by sub-critical water," *Fuel Process. Technol.*, vol. 92, no. 5, pp. 1062–1067, 2011.
- [50] O. M. Ogunsola and N. Berkowitz, "Extraction of oil shales with sub- and near-critical water," *Fuel Process. Technol.*, vol. 45, no. 2, pp. 95–107, 1995.
- [51] K. El Harfi, C. Bennouna, A. Mokhlisse, M. Ben Chanâa, L. Lemée, J. Joffre, and A. Amblès, "Supercritical fluid extraction of Moroccan (Timahdit) oil shale with water," *J. Anal. Appl. Pyrolysis*, vol. 50, no. 2, pp. 163–174, 1999.
- [52] Y. Lin, Y. Liao, Z. Yu, S. Fang, Y. Lin, Y. Fan, X. Peng, and X. Ma, "Co-pyrolysis kinetics of sewage sludge and oil shale thermal decomposition using TGA-FTIR analysis," *Energy Convers. Manag.*, vol. 118, pp. 345–352, 2016.
- [53] A. Aboulkas, K. El, M. Nadifiyine, and M. Benchanaa, "Pyrolysis Behaviour and Kinetics of Moroccan Oil Shale with Polystyrene," *Int. J. Eng.*, vol. 1, no. September, pp. 1–11, 2011.
- [54] T. Cordero, J. Rodríguez-Mirasol, J. Pastrana, and J. J. Rodríguez, "Improved solid fuels from co-pyrolysis of a high-sulphur content coal and different lignocellulosic wastes," *Fuel*, vol. 83, no. 11–12, pp. 1585–1590, 2004.
- [55] Eesti Keemiatööstuse Liit and SA Keskkonnainvesteeringute Keskus, "Estonian

- Shale Oil Production Best Available Technology (in Estonian),” Tallinn, 2013.
- [56] I. Kamenev, R. Munter, L. Pikkov, and L. Kekisheva, “Wastewater treatment in oil shale chemical industry,” vol. 20, no. 4, pp. 443–457, 2003.
- [57] A. Trikkel, R. Kuusik, A. Martins, T. Pihu, and J. M. Stencel, “Utilization of Estonian oil shale semicoke,” *Fuel Process. Technol.*, vol. 89, no. 8, pp. 756–763, 2008.
- [58] V. Yefimov, S. Doilov, and I. Pulemyotov, “Development of ecologically acceptable technology for processing large particle kukersite in vertical retorts,” *Oil Shale*, vol. 14, no. 1, pp. 77–83, 1997.
- [59] H. Arro, A. Prikk, T. Pihu, and I. Öpik, “Utilization of semi-coke of Estonian shale oil industry,” *Oil Shale*, vol. 19, no. 2, pp. 117–125, 2002.
- [60] T. Pihu, H. Arro, A. Prikk, R. Rootamm, A. Konist, K. Kirsimäe, M. Liira, and R. Mõtlep, “Oil shale CFBC ash cementation properties in ash fields,” *Fuel*, vol. 93, pp. 172–180, 2012.
- [61] J. Reinik, N. Irha, E. Steinnes, G. Urb, J. Jefimova, and E. Piirisalu, “Release of 22 elements from bottom and fly ash samples of oil shale fueled PF and CFB boilers by a two-cycle standard leaching test,” *Fuel Process. Technol.*, vol. 124, pp. 147–154, 2014.
- [62] L. Loo, B. Maaten, A. Siirde, T. Pihu, and A. Konist, “Experimental analysis of the combustion characteristics of Estonian oil shale in air and oxy-fuel atmospheres,” *Fuel Process. Technol.*, vol. 134, pp. 317–324, 2015.
- [63] T. Triisberg-Uljas, K. Vellak, and E. Karofeld, “Application of oil-shale ash and straw mulch promotes the revegetation of extracted peatlands,” *Ecol. Eng.*, vol. 110, pp. 99–106, 2018.
- [64] X. Zhao, X. Zhang, Z. Liu, Z. Lu, and Q. Liu, “Organic Matter in Yilan Oil Shale: Characterization and Pyrolysis with or without Inorganic Minerals,” *Energy & Fuels*, vol. 31, no. 4, pp. 3784–3792, 2017.
- [65] R. A. Nadkarni, “Analytical techniques for characterization of oil shales,” in *Symposium on Geochemistry and Chemistry of Oil Shale. American Chemical Society Meeting, March 20-25, 1983*, pp. 200–208.
- [66] Y. Yürüm and A. Karabakan, “Effect of the mineral matrix in the reactions of oil shales: 1. Pyrolysis reactions of Turkish Göynük and US Green River oil shales,” *Fuel*, vol. 77, no. 12, pp. 1303–1309, 1998.
- [67] A. Al-Harashseh, M. Al-Harashseh, A. Al-Otoom, and M. Allawzi, “Effect of demineralization of El-lajjun Jordanian oil shale on oil yield,” *Fuel Process. Technol.*, vol. 90, pp. 818–824, 2009.
- [68] L. Ballice, “Effect of demineralization on yield and composition of the volatile products evolved from temperature-programmed pyrolysis of Beypazari (Turkey) Oil Shale,” *Fuel Process. Technol.*, vol. 86, no. 6, pp. 673–690, 2005.
- [69] R. Palvadre and V. Ahelik, “Beneficiation of Estonian (Kukersite) oil shale,” *Oil Shale*, vol. 28, no. 2, pp. 353–365, 2011.
- [70] J. Yan, X. Jiang, X. Han, and J. Liu, “A TG-FTIR investigation to the catalytic effect of mineral matrix in oil shale on the pyrolysis and combustion of kerogen,” *Fuel*, vol. 104, pp. 307–317, 2013.
- [71] R. Gai, L. Jin, J. Zhang, J. Wang, and H. Hu, “Effect of inherent and additional pyrite on the pyrolysis behavior of oil shale,” *J. Anal. Appl. Pyrolysis*, vol. 105, pp. 342–347, 2014.
- [72] Y. Yürüm, Y. Dror, and M. Levy, “Effect of acid dissolution on the mineral matrix and organic matter of Zefa Efe oil shale,” *Fuel Process. Technol.*, vol. 11, pp. 71–

- 86, 1985.
- [73] M. Al-Harashsheh, O. Al-Ayed, J. Robinson, S. Kingman, A. Al-Harashsheh, K. Tarawneh, A. Saeid, and R. Barranco, "Effect of demineralization and heating rate on the pyrolysis kinetics of Jordanian oil shales," *Fuel Process. Technol.*, vol. 92, no. 9, pp. 1805–1811, 2011.
- [74] L. Pan, F. Dai, J. Huang, S. Liu, and G. Li, "Study of the effect of mineral matters on the thermal decomposition of Jimsar oil shale using TG – MS," *Thermochim. Acta*, vol. 627–629, pp. 31–38, 2016.
- [75] A. Suleimenova, K. D. Bake, A. Ozkan, J. J. Valenza, R. L. Kleinberg, A. K. Burnham, N. Ferralis, and A. E. Pomerantz, "Acid demineralization with critical point drying: A method for kerogen isolation that preserves microstructure," *Fuel*, vol. 135, pp. 492–497, 2014.
- [76] W. Song, Y. Dong, L. Xue, H. Ding, Z. Li, and G. Zhou, "Hydrofluoric acid-based ultrasonic upgrading of oil shale and its structure characterization," *Oil Shale*, vol. 29, no. 4, pp. 334–343, 2012.
- [77] S. Vyazovkin, A. K. Burnham, J. M. Criado, L. A. Pérez-Maqueda, C. Popescu, and N. Sbirrazzuoli, "ICTAC Kinetics Committee recommendations for performing kinetic computations on thermal analysis data," *Thermochim. Acta*, vol. 520, pp. 1–19, 2011.
- [78] M. E. Brown, *Handbook of Thermal Analysis and Calorimetry: Principles and Practice*, vol. 1. Elsevier Science, 1998.
- [79] W. F. Hemminger and H. K. Cammenga, *Methoden der Thermischen Analyse*. Heidelberg: Springer, 1990.
- [80] C. Eyraud, E. Robens, and P. Rochas, "Some comments on the history of thermogravimetry," *Thermochim. Acta*, vol. 160, pp. 25–28, 1990.
- [81] S. Vyazovkin, K. Chrissafis, M. L. Di Lorenzo, N. Koga, M. Pijolat, B. Roduit, N. Sbirrazzuoli, and J. J. Suñol, "ICTAC Kinetics Committee recommendations for collecting experimental thermal analysis data for kinetic computations," *Thermochim. Acta*, vol. 590, pp. 1–23, 2014.
- [82] A. Gałuszka, Z. Migaszewski, and J. Namieśnik, "The 12 principles of green analytical chemistry and the SIGNIFICANCE mnemonic of green analytical practices," *TrAC - Trends Anal. Chem.*, vol. 50, pp. 78–84, 2013.
- [83] M. Beneš, N. Milanov, G. Matuschek, A. Kettrup, V. Placek, and V. Balek, "Thermal degradation of PVC cable insulation studied by simultaneous TG-FTIR and TG-EGA methods," *J. Therm. Anal. Calorim.*, vol. 78, pp. 621–630, 2004.
- [84] P. Tiwari and M. Deo, "Compositional and kinetic analysis of oil shale pyrolysis using TGA-MS," *Fuel*, vol. 94, pp. 333–341, 2012.
- [85] G. Vanhoyland, A. Le Bail, J. Mullens, and L. C. Van Poucke, "Characterization and Structure Determination of Ammonium Bismuth Oxalate Hydrate, $\text{Bi}(\text{NH}_4)(\text{C}_2\text{O}_4)_2 \cdot x\text{H}_2\text{O}$," *Inorg. Chem.*, vol. 43, no. 3, pp. 785–789, 2004.
- [86] Z. Wang, S. Deng, Q. Gu, Y. Zhang, X. Cui, and H. Wang, "Pyrolysis kinetic study of Huadian oil shale, spent oil shale and their mixtures by thermogravimetric analysis," *Fuel Process. Technol.*, vol. 110, pp. 103–108, 2013.
- [87] W. Qing, S. Baizhong, H. Aijuan, B. Jingru, and L. Shaohua, "Pyrolysis characteristics of Huadian oil shales," *Oil Shale*, vol. 24, no. 2, pp. 147–157, 2007.
- [88] F. Bai, W. Guo, X. Lü, Y. Liu, M. Guo, Q. Li, and Y. Sun, "Kinetic study on the pyrolysis behavior of Huadian oil shale via non-isothermal thermogravimetric data," *Fuel*, vol. 146, no. January, pp. 111–118, 2015.

- [89] X. M. Jiang, Z. G. Cui, X. X. Han, and H. L. Yu, "Thermogravimetric investigation on combustion characteristics of oil shale and high sulphur coal mixture," *J. Therm. Anal. Calorim.*, vol. 85, no. 3, pp. 761–764, 2006.
- [90] H. Sütcü, "Structural characterization of oil shale occurring in Mengen, Turkey," *Pet. Chem.*, vol. 54, no. 1, pp. 78–82, 2014.
- [91] M. C. Branch, "In-situ combustion retorting of oil shale," *Prog. Energy Combust. Sci.*, vol. 193, 1979.
- [92] X. Lan, W. Luo, Y. Song, J. Zhou, and Q. Zhang, "Effect of the Temperature on the Characteristics of Retorting Products Obtained by Yaojie Oil Shale Pyrolysis," *Energy and Fuels*, vol. 29, no. 12, pp. 7800–7806, 2015.
- [93] A. K. Burnham, "Use and misuse of logistic equations for modeling chemical kinetics," *J. Therm. Anal. Calorim.*, pp. 1–10, 2015.
- [94] S. Arrhenius, "Über die Reaktionsgeschwindigkeit bei der Inversion von Rohrzucker durch Säuren," *Zeitschrift für Phys. Chemie*, vol. 4U, no. 1, 1889.
- [95] M. A. Raja, Y. Zhao, X. Zhang, C. Li, and S. Zhang, "Practices for modeling oil shale pyrolysis and kinetics," *Rev. Chem. Eng.*, vol. 34, no. 1, pp. 21–42, 2017.
- [96] K. Czajka, A. Kisiela, W. Moroń, W. Ferens, and W. Rybak, "Pyrolysis of solid fuels: Thermochemical behaviour, kinetics and compensation effect," *Fuel Process. Technol.*, vol. 142, pp. 42–53, 2016.
- [97] A. A. Jain, A. Mehra, and V. V. Ranade, "Processing of TGA data: Analysis of isoconversional and model fitting methods," *Fuel*, vol. 165, pp. 490–498, 2016.
- [98] E. Moukhina, "Determination of kinetic mechanisms for reactions measured with thermoanalytical instruments," *J. Therm. Anal. Calorim.*, vol. 109, no. 3, pp. 1203–1214, 2012.
- [99] O. S. Al-Ayed, M. Matouq, Z. Anbar, A. M. Khaleel, and E. Abu-Nameh, "Oil shale pyrolysis kinetics and variable activation energy principle," *Appl. Energy*, vol. 87, no. 4, pp. 1269–1272, 2010.
- [100] M. Djuricic, R. C. Murphy, D. Vitorovic, and K. Biemann, "Organic acids obtained by alkaline permanganate oxidation of kerogen from the Green River (Colorado) shale," *Geochim. Cosmochim. Acta*, vol. 35, no. 12, pp. 1201–1207, 1971.
- [101] D. K. Young and T. F. Yen, "The nature of straight-chain aliphatic structures in green river kerogen," *Geochim. Cosmochim. Acta*, vol. 41, no. 10, pp. 1411–1417, 1977.
- [102] R. Lemaire, D. Menage, and P. Seers, "Study of the high heating rate devolatilization of bituminous and subbituminous coals—Comparison of experimentally monitored devolatilization profiles with predictions issued from single rate, two-competing rate, distributed activation energy and chemical," *J. Anal. Appl. Pyrolysis*, vol. 123, pp. 255–268, 2017.
- [103] F. Bai, Y. Sun, Y. Liu, B. Liu, M. Guo, X. Lü, W. Guo, Q. Li, C. Hou, and Q. Wang, "Kinetic investigation on partially oxidized Huadian oil shale by thermogravimetric analysis," *Oil Shale*, vol. 31, no. 4, p. 377, 2014.
- [104] Q. Q. Liu, X. X. Han, Q. Y. Li, Y. R. Huang, and X. M. Jiang, "TG–DSC analysis of pyrolysis process of two Chinese oil shales," *J. Therm. Anal. Calorim.*, vol. 116, no. 1, pp. 511–517, 2013.
- [105] C. R. Yörük, T. Meriste, A. Trikkel, and R. Kuusik, "Oxy-fuel combustion of Estonian oil shale: Kinetics and modeling," *Energy Procedia*, vol. 86, pp. 124–133, 2016.
- [106] Z. Yao, X. Ma, Z. Wang, and L. Chen, "Characteristics of co-combustion and kinetic study on hydrochar with oil shale: A thermogravimetric analysis," *Appl. Therm.*

- Eng.*, vol. 110, pp. 1420–1427, 2017.
- [107] P. Tiwari and M. Deo, “Detailed Kinetic Analysis of Oil Shale Pyrolysis TGA Data,” *AIChE J.*, vol. 58, pp. 505–515, 2012.
- [108] A. Ots, A. Poobus, and T. Lausmaa, “Technical and ecological aspects of shale oil and power cogeneration,” *Oil Shale*, vol. 28, no. 1S, pp. 101–112, 2011.
- [109] A. Riboulleau, S. Derenne, G. Sarret, C. Largeau, F. Baudin, and J. Connan, “Pyrolytic and spectroscopic study of a sulphur-rich kerogen from the ‘Kashpir oil shales’ (Upper Jurassic, Russian platform),” *Org. Geochem.*, vol. 31, no. 12, pp. 1641–1661, 2000.
- [110] P. T. Williams and H. M. Chishti, “Reaction of nitrogen and sulphur compounds during catalytic hydrotreatment of shale oil,” *Fuel*, vol. 80, no. 7, pp. 957–963, 2001.
- [111] J. Antturi, O. Hänninen, J.-P. Jalkanen, L. Johansson, M. Prank, M. Sofiev, and M. Ollikainen, “Costs and benefits of low-sulphur fuel standard for Baltic Sea shipping,” *J. Environ. Manage.*, vol. 184, pp. 431–440, 2016.
- [112] I. Vierth, R. Karlsson, and A. Mellin, “Effects of more stringent sulphur requirements for sea transports,” *Transp. Res. Procedia*, vol. 8, pp. 125–135, 2015.
- [113] M. Zetterdahl, J. Moldanová, X. Pei, R. K. Pathak, and B. Demirdjian, “Impact of the 0.1% fuel sulfur content limit in SECA on particle and gaseous emissions from marine vessels,” *Atmos. Environ.*, vol. 145, pp. 338–345, 2016.
- [114] M. C. Torrente and M. a. Galán, “Kinetics of the thermal decomposition of oil shale from Puertollano (Spain),” *Fuel*, vol. 80, no. 3, pp. 327–334, 2001.
- [115] M. V. Kök and A. G. Iscan, “Oil Shale Kinetics By Differential Methods,” *J. Therm. Anal. Calorim.*, vol. 88, no. 3, pp. 657–661, 2007.
- [116] C. Wang, X. Zhang, Y. Liu, and D. Che, “Pyrolysis and combustion characteristics of coals in oxyfuel combustion,” *Appl. Energy*, vol. 97, pp. 264–273, 2012.
- [117] X. Yongjiang, X. Huaqing, W. Hongyan, L. Zhiping, and F. Chaohe, “Kinetics of isothermal and non-isothermal pyrolysis of oil shale,” *Oil Shale*, vol. 28, no. 3, pp. 415–424, 2011.
- [118] A. K. Burnham, “A Simple Kinetic Model of Oil Generation, Vaporization, Coking, and Cracking,” *Energy & Fuels*, vol. 29, no. 11, pp. 7156–7167, 2015.
- [119] B. Wang, S. Zhao, Y. Huang, and J. Zhang, “Effect of some natural minerals on transformation behavior of sulfur during pyrolysis of coal and biomass,” *J. Anal. Appl. Pyrolysis*, vol. 105, pp. 284–294, 2014.
- [120] C. Fan, J. Yan, Y. Huang, X. Han, and X. Jiang, “XRD and TG-FTIR study of the effect of mineral matrix on the pyrolysis and combustion of organic matter in shale char,” *Fuel*, vol. 139, pp. 502–510, 2015.
- [121] K. A. Leeuw, C. A. Strydom, J. R. Bunt, and D. van Niekerk, “The influence of K₂CO₃ and KCl on H₂ formation during heat treatment of an acid-treated inertinite-rich bituminous coal-char,” *J. Therm. Anal. Calorim.*, vol. 126, no. 2, pp. 905–912, 2016.
- [122] C. Zou, J. Zhao, X. Li, and R. Shi, “Effects of catalysts on combustion reactivity of anthracite and coal char with low combustibility at low/high heating rate,” *J. Therm. Anal. Calorim.*, vol. 126, no. 3, pp. 1469–1480, 2016.

List of other publications

1. **B. Maaten**, H. Pikkor, A. Konist, A. Siirde, "Determination of the total sulphur content of oil shale by using different analytical methods," *Oil Shale*, in press
2. M. Kolnes, A. Mere, J. Kübarsepp, M. Viljus, **B. Maaten**, M. Tarraste, "Microstructure Evolution of TiC Cermets with Ferritic AISI 430L Steel Binder," *Powder Metallurgy*, 2018
3. M. Tarraste, J. Kübarsepp, K. Juhani, A. Mere, M. Kolnes, M. Viljus, and **B. Maaten**, "Ferritic chromium steel as binder metal for WC cemented carbides," *Int. J. Refract. Met. Hard Mater.*, vol. 73, pp. 183–191, 2018
4. S. Ben Moussa, J. Lachheb, M. Gruselle, **B. Maaten**, K. Kriis, T. Kanger, K. Tõnsuaadu, and B. Badraoui, "Calcium, Barium and Strontium apatites: A new generation of catalysts in the Biginelli reaction," *Tetrahedron*, vol. 73, no. 46, pp. 6542–6548, 2017
5. D.-L. Yung, **B. Maaten**, M. Antonov, and I. Hussainova, "Oxidation of spark plasma sintered ZrC-Mo and ZrC-TiC composites," *Int. J. Refract. Met. Hard Mater.*, vol. 66, 2017
6. L. Loo, **B. Maaten**, D. Neshumayev, and A. Konist, "Oxygen influence on Estonian kukersite oil shale devolatilization and char combustion," *Oil Shale*, vol. 34, no. 3, pp. 219–231, 2017
7. E. Latosov, M. Loorits, **B. Maaten**, A. Volkova, and S. Soosaar, "Corrosive effects of H₂S and NH₃ on natural gas piping systems manufactured of carbon steel," *Energy Procedia*, vol. 128, pp. 316–323, 2017
8. L. Loo, **B. Maaten**, A. Konist, A. Siirde, D. Neshumayev, and T. Pihu, "Carbon dioxide emission factors for oxy-fuel CFBC and aqueous carbonation of the Ca-rich oil shale ash," *Energy Procedia*, vol. 128, pp. 144–149, 2017
9. A. Konist, **B. Maaten**, L. Loo, D. Neshumayev, and T. Pihu, "Mineral sequestration of CO₂ by carbonation of Ca-rich oil shale ash in natural conditions," *Oil Shale*, vol. 33, no. 3, 2016
10. L. Loo, **B. Maaten**, A. Siirde, T. Pihu, and A. Konist, "Experimental analysis of the combustion characteristics of Estonian oil shale in air and oxy-fuel atmospheres," *Fuel Process. Technol.*, vol. 134, pp. 317–324, 2015
11. A. Konist, L. Loo, A. Valtsev, **B. Maaten**, A. Siirde, D. Neshumayev, and T. Pihu, "Calculation of the amount of Estonian oil shale products from combustion in regular and oxy-fuel mode in a CFB boiler," *Oil Shale*, vol. 31, no. 3, 2014
12. **B. Maaten**, J. Moussa, C. Desmarests, P. Gredin, P. Beaunier, T. Kanger, K. Tõnsuaadu, D. Villemin, and M. Gruselle, "Cu-modified hydroxy-apatite as catalyst for Glaser–Hay CC homo-coupling reaction of terminal alkynes," *J. Mol. Catal. A Chem.*, vol. 393, pp. 112–116, 2014
13. K. Kreek, K. Kriis, **B. Maaten**, M. Uibu, A. Mere, T. Kanger, and M. Koel, "Organic and carbon aerogels containing rare-earth metals: Their properties and application as catalysts," *J. Non. Cryst. Solids*, vol. 404, pp. 43–48, 2014
14. M. Gruselle, T. Kanger, R. Thouvenot, A. Flambard, K. Kriis, V. Mikli, R. Traksmäa, **B. Maaten**, and K. Tõnsuaadu, "Calcium hydroxyapatites as efficient catalysts for the Michael C-C bond formation," *ACS Catal.*, vol. 1, no. 12, 2011

Acknowledgements

The author is eternally thankful to her colleagues at the Department of Energy Technology.

The author is also grateful to her family. Writing this thesis would not have been the same without your guidance and support.

“Behind every great daughter is a truly amazing dad.” May you rest in peace, Dad.

This work has been partially supported by ASTRA “TUT Institutional Development Programme for 2016-2022” Graduate School of Functional Materials and Technologies (2014-2020.4.01.16-0032).

Lühikokkuvõte

Erinevate põlevkivide koostis ja reaktiivsus ning nende termilisel töölusel tekkivad produktid

Hiljuti tähistati Eestis põlevkivi 100. aastapäeva kuna põlevkivi on Eestis intensiivselt kasutatud ja uuritud 1910ndatest aastatest. Kuigi kirjanduses leidub tohutult artikleid põlevkivi teemadel, on varasemates töödes kasutatud meetodikate asemel tänapäeval kasutusel uuemad ning täpsemad meetodid. Kuna tänapäeval on oluline analüüsi korratavus ning kiirus, võimaldavad uued ja kiiremad analüüsitehnikad erinevate keerukate materjalide koostise täpset määramist. Kiire arengu tõttu on nüüd võimalik põlevkivi koostist määrata täpsemalt ja väiksema ajakuluga kui varem. Selle tulemusena on tekkinud vajadus kompleksse analüüsitulemuste kogumi järele, mis kirjeldaks põlevkivi kui tervikut, uuriks selle pürolüüsi protsessi, identifitseerides sealjuures ka eralduvaid ühendeid, ning reaktiivsust.

Antud töö eesmärgiks oli analüüsida erinevate päritoluriikidega põlevkivisid (Eesti, Hiina ja USA) kasutades selleks termogravimeetrilist analüsaatorit, elementaaranalüüsi, röntgendifraktsioon-analüüsi ning laine-dispersiivset röntgenfluorestsents-spektroskoopiat. Käesoleva töö uudsuseks on kaasaegsete analüüsimeetodikate kasutamise abil erinevate põlevkivide võrdlemine. Näiteks Kentuckyst pärit proov omab avastamata potentsiaali kuna seda pole enne uuritud.

Lisaks koostise analüüsile uuriti erinevate põlevkivide pürolüüsi protsessi. Võrreldi erinevat päritolu põlevkivide termilist käitumist ning väävlit sisaldavate ühendite eraldumist, et leida võimalusi pürolüüsi käigus toodetava õli väävlisisalduse potentsiaalseks vähendamiseks. Järelduste tegemiseks ning materjali kirjeldamiseks määrati erinevates vormides sisalduva väävli kogused. Saadud tulemuste põhjal järeldati, et pürolüüsi protsessi temperatuuri tuleks alandada – sellisel juhul jääks rohkem väävlit protsessi käigus tekkivasse tahkesse jääki.

Termilise analüüsi käigus saadud andmete põhjal arvutati põlevkivis sisalduva orgaanilise aine lagunemise aktivatsioonenergia, et kirjeldada lagunemise protsessi. Kuigi teaduskirjanduses leidub tohutult andmeid vastavate väärtuste kohta, ei pakuta neile tihti praktilist rakendust. Antud töös näidati kuidas vastavaid parameetreid kasutades saab arvutuslikult kirjeldada põlevkivi orgaanilise osa lagunemise kulgu isotermaalsetel tingimustel. Tulemusi analüüsiti 450 °C ja 480 °C jaoks ning vastavaid lagunemisgraafikuid võrreldi ja analüüsiti.

Põlevkivi sisaldab suurel hulgal erinevaid mineraale, millest mõningatel võivad olla katalüütilised omadused. Seega uuriti põlevkivis sisalduvate mineraalide mõju Eesti põlevkivi orgaanilise aine lagunemisele. Leiti, et põlevkivis sisalduvad mineraalid ei mõjuta oluliselt pürolüüsi käigus põlevkivi orgaanilise aine lagunemise kulgu.

Abstract

The Composition and Reactivity of Different Oil Shales and the Products Formed During Thermal Treatment

Recently, the Estonian oil shale industry celebrated its 100th anniversary. Oil shale has been intensively used and investigated in Estonia since the 1910s. Although extensive literature on oil shale is available, methods employed in earlier works have become obsolete due to the development of more precise and faster analytical techniques. As the reproducibility and analysis time gain increasing importance, new and improved technologies enable the precise determination of the composition and structure of different complex materials. Due to this significant advancement, it is possible to analyze the composition of oil shale more precisely and faster than ever before. This has led to the necessity of a complex set of analytical results to describe oil shale as a whole, including its behavior during the pyrolysis process; the evolved products, mainly sulfur-containing compounds; and its reactivity.

This research focused on the complex analysis of different oil shales from Estonia, China and the USA using thermogravimetric analysis, elemental analysis, X-ray diffraction and wavelength dispersive X-ray fluorescence. The novelty of this work is the use of these methods and the comparison of oil shales of different origin. Additionally, the sample from Kentucky has undiscovered potential as it has not been investigated before.

The pyrolysis process was also investigated. The thermal behavior of oil shales of different origin was compared and the sulfur evolution was investigated to offer possible ways to decrease the sulfur content in the produced shale oil. The different forms of sulfur in the samples were quantified. The results indicated that the pyrolysis temperatures should be lowered so that more sulfur would be retained in the residues of the process instead of the produced oil.

Based on the thermal analysis data, the activation energy values for the decomposition of kerogen during pyrolysis were calculated to describe the decomposition process. Although numerous values are available in the literature, these often remain purely theoretical. This thesis identifies how these results can be applied to calculate the decomposition of organic matter under isothermal conditions. The results are presented for temperatures of 450 °C and 480 °C and the resultant conversion profiles are analyzed and compared.

As the composition of oil shale is rich in minerals, some of which are known to exhibit catalytic properties, their effect on the decomposition of Estonian oil shale decomposition was also investigated. Results revealed that the inherent minerals do not exhibit a significant effect on the decomposition of organic matter during the pyrolysis process.

Appendix 1

PUBLICATION I

B. Maaten, L. Loo, A. Konist, D. Nešumajev, T. Pihu, I. Külaots, D. Neshumayev, T. Pihu, and I. Külaots, "Decomposition kinetics of American, Chinese and Estonian oil shales kerogen," *Oil Shale*, vol. 33, no. 2, pp. 167–183, 2016

DECOMPOSITION KINETICS OF AMERICAN, CHINESE AND ESTONIAN OIL SHALES KEROGEN

BIRGIT MAATEN^{†(a)*}, LAURI LOO^(a), ALAR KONIST^(a,b),
DMITRI NEŠUMAJEV^(a), TÕNU PIHU^(a),
INDREK KÜLAOTS^(a,b)

^(a) Department of Thermal Engineering, Tallinn University of Technology, Ehitajate tee 5, 19086 Tallinn, Estonia

^(b) School of Engineering, Brown University, 184 Hope Street, Providence, Rhode Island 02912, United States

Abstract. *An investigation of the pyrolysis kinetics of American, Chinese and Estonian oil shales was conducted applying a non-isothermal thermogravimetric analysis (TGA). TGA weight loss curves clearly indicate that the pyrolysis of all oil shales tested is independent of their geographic origin, and is mainly taking place in the temperature range of 300 to 500 °C. As expected, at temperatures above 700 °C mass loss due to the decomposition of oil shale carbonates was detected, except for the Kentucky and Chinese 2 oil shale samples. The kinetic decomposition rate parameters such as activation energy and pre-exponential factor were calculated applying the Coats-Redfern integral and direct Arrhenius methods. Independent of the oil shale kerogen origin, pyrolysis occurs in two consecutive temperature zones with slightly dissimilar kinetic parameter values. The activation energy values obtained were in the range of 14 to 31 kJ/mol for the low and 70 to 149 kJ/mol for the high temperature zone.*

Keywords: *oil shale decomposition kinetics, kerogen, pyrolysis, reaction rate, pre-exponential factor, activation energy.*

1. Introduction

Oil shale, a sedimentary rock found in many regions of the world, is largely used as a fossil fuel to generate electrical energy or higher value fuels. More than 600 deposits are known all over the world [1], the most vast ones of which are found in U.S.A., China, Brazil and Estonia [2]. Oil shale offers a reasonable alternative to conventional energy resources such as crude oil, coal and natural gas. Estonia has large resources of oil shale and today,

* Corresponding author: e-mail birgit.maaaten@ttu.ee

approximately 90% of the country's electricity is produced in thermal power plants operating on oil shale as fuel [1, 3]. Oil shale consists of an insoluble organic part called kerogen and of a rich inorganic part, which consists mostly of a wide selection of mineral components (quartz, calcite, dolomite, etc.) [4]. The kerogen part has a complex cross-linked structure and high molecular weight up to 3000 [5]. For example, the kerogen from Estonian oil shale has the dominating functionalities of alcohols, ketones, amines and ethers, and also long aliphatic chains [6]. Compared to oil shale found in different countries, Estonian oil shale has a relatively high content of carbonate minerals [2]. The organic part has a relatively high content of hydrogen – the atomic ratio of H/C is 1.4–1.5 and the atomic ratio of O/C is 0.16–0.2 [2], which makes it hard to distinguish between Type I and Type II kerogens [7]. In comparison, the oil shale from Colorado, U.S.A., which originates from the Eocene age, has an organic carbon content of only 11–16%. The oil shale from Maoming, China, is known to have an organic carbon content of about 14% [8].

During pyrolysis upon heating in an inert atmosphere oil shale kerogen is first converted into a viscous mixture of hydrocarbons called bitumen, and then into final products such as shale oil (a mixture of shorter length hydrocarbons). The byproduct of the process is solid carbon rich oil shale semicoke [9]. Due to the complex structure of kerogen, several bonds are broken during the pyrolysis process, leading to multiple reactions [10]. Beside the oil shale thermal treatment, solvent extraction techniques can be used to extract shale oil from oil shale. The downside of the solvent extraction technique is that it requires solvents that are harmful to the environment and are problematic or expensive to use in the industry on a large scale [11].

Oil shale pyrolysis consists of three main processes: 1) water evaporation at lower temperatures (below 200 °C), 2) pyrolysis of kerogen (from 200 up to 600 °C), and 3) decomposition of carbonates (at temperatures above 700 °C) [12, 13]. Normally the pyrolysis process is studied in an inert atmosphere, for example such as N₂ gas, thereby avoiding the oxidation of the sample. There are numerous studies on the thermal decomposition and kinetic calculations of various oil shale samples available in the literature and therefore, several decomposition kinetic rate models have been suggested [12, 14–16]. The majority of those kinetic models consider kerogen decomposition in the pyrolysis process as a first order reaction. Previous research has shown that changing the carrier gas from N₂ to CO₂ does not considerably change the total weight loss or the mechanism of kerogen decomposition, since the oil shale semicoke's carbon oxidation in CO₂ occurs at way higher temperatures. In addition, the decomposition of carbonates in oil shale is reported to be retarded in CO₂ environment [17].

Thermogravimetric apparatus (TGA) is a widely used instrument to analyze the kinetics of thermal decomposition of various solids and liquids because of its clear advantages – ability to set a defined atmosphere and apply a wide range of heating rates. When TGA operates together with the

differential scanning calorimeter (DSC), the resulting reaction thermal effects can be identified and quantified. From the TGA raw data one can calculate kinetic rate parameters for the reaction by applying the existing theoretical model [18]. Isothermal and non-isothermal TGA approaches have been widely used to study oil shale thermal behavior [11, 13, 19–21] in various conditions. Most of the oil shale kerogen decomposition reaction rate kinetic data are fitted to a first order model from which the kinetic parameters such as pre-exponential factor and activation energy are calculated. It has been noted that the non-isothermal TGA approach can simulate the conditions in commercial-scale oil shale retorting systems [14].

In order to further optimize the process conditions and retort dimensions, there is a clear need to investigate oil shale pyrolysis kinetics. Analyzing US, Chinese and Estonian oil shale samples can provide answers to whether similar units and/or similar technological processes are applicable to oil shales of varying origin, age and composition. As of today, there are several studies, which have reported wall-to-wall kinetic parameter values (activation energy values from 13 to 215 kJ/mol) for the oil shale decomposition rate reaction [5, 18, 22–24]. Thus this research also aims to offer clarification to the range of kinetic parameter values for oil shale pyrolysis in the temperature range from 300 to 500 °C at modest heating rates.

2. Experimental

2.1. Materials tested

Oil shale samples used in this investigation were from the subsequent locations and are named in this research as follows: Estonian – from an underground mine called “Estonia” in Estonia; Green River 1 – from the Green River shale formation, Colorado, U.S.A.; Green River 2 – from the Green River shale formation, U.S.A.; Kentucky – from the New Albany shale formation, Kentucky, U.S.A.; Chinese 1 and Chinese 2 – from the Maoming mine, Guangdong Province, Southwest China with the local classifications of C and A, respectively.

All oil shale samples used in pyrolysis tests were previously dried, crushed (if needed) and sieved (1 mm opening). The results of elemental analysis of oil shales tested are given in Table 1.

Table 1. Elemental analysis results for oil shales tested. All percentages are offered per oil shale mass basis

Sample	N, %	C ^{total} , %	H, %	S, %
Estonian	0.0	27.3	2.7	1.5
Green River 1	0.9	27.7	3.2	1.4
Green River 2	0.4	17.2	1.7	0.8
Kentucky	0.5	15.4	1.7	1.8
Chinese 1	0.9	23.3	2.4	2.2
Chinese 2	0.9	23.0	3.0	2.0

2.2. Experimental setup and methods applied

The recommendations presented in [25] for collecting experimental thermal analysis data were followed in this study. The kinetics of all oil shale samples was investigated with the NETZSCH STA 449 F3 Jupiter[®] TG-DSC apparatus. In order to avoid mass transfer limitations, a thin layer of 20 ± 1 mg of oil shale was placed into Pt/Rh alloy crucibles with removable thin walled liners of Al_2O_3 during the pyrolysis experiments. Oil shale samples were heated from 40 to 950 °C using a linear heating rate of 20 °C min^{-1} . A carrier gas flow of 50 ml/min of high purity N_2 gas was used for all the experiments. Prior to each pyrolysis test the TGA system was flushed with high purity N_2 gas to remove any residual air. The temperature and enthalpy calibrations of the apparatus were done using In, Sn, Zn, Al and Au standards. In order to eliminate buoyancy effects during the furnace heat-up cycle, empty crucible experiment background mass data were recorded and subtracted from each oil shale measurement data set. Excellent reproducibility (for two or three parallel measurements) was observed for the mass loss curves. All the reported final results are the average values of the conducted repeated measurements.

Characteristic oil shale decomposition temperatures were recorded at the start of thermal decomposition (T_s), at the temperature when maximum mass loss rate occurred (T_{max}), and at the end of thermal decomposition (T_c). T_s and T_c temperatures were set according to the intersection of the tangents and T_{max} as the temperature value corresponding to the maximum decomposition rate. These characteristic temperatures can be seen in Figure 1.

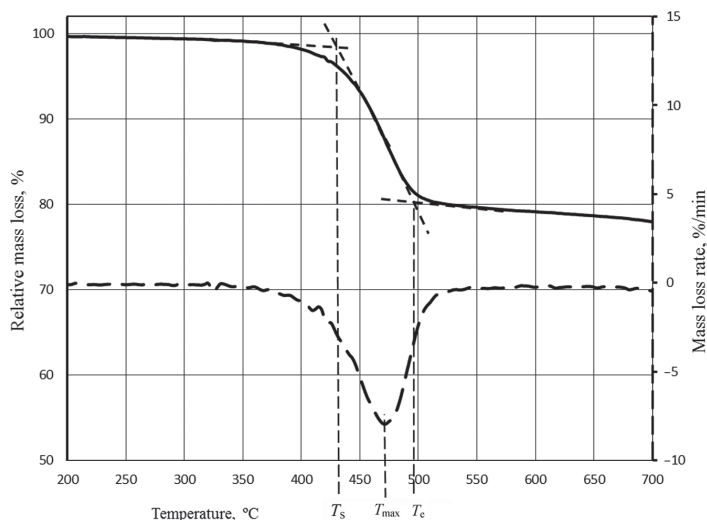
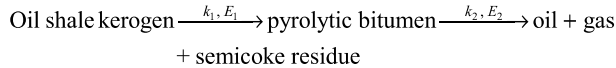


Fig. 1. Characteristic temperatures of an oil shale sample pyrolysis thermogravimetric (TG) profile.

2.3. Decomposition reaction kinetic parameters

According to Rajeshwar [15] the general reaction mechanism of oil shale kerogen decomposition is as follows:



In the initial stages of the decomposition process, species with low molecular weight are distilled and in the second step, long hydrocarbon chains are cracked into smaller hydrocarbon molecules [22]. Therefore, during oil shale decomposition the reaction occurs in two zones. This theory is supported by use of mass spectrometry for shale oil compositional measurements [20].

Kinetic parameters such as activation energy and pre-exponential factor of decomposition are often obtained from the decomposition reaction rate expression. The kinetics may be represented as follows [26]:

$$\frac{d\alpha}{dt} = kf(\alpha), \quad (1)$$

where α is the fraction reacted in time t , k is the rate constant and the function $f(\alpha)$ depends on the decomposition mechanism. The rate constant k can be explained by the Arrhenius equation:

$$k = A * \exp\left(\frac{-E}{RT}\right), \quad (2)$$

where A is the frequency or pre-exponential factor, E is the activation energy and R is the universal gas constant.

The conversion of kerogen to products at any time t can be defined as fractional weight loss (α):

$$\alpha = \frac{W_0 - W_t}{W_0 - W_f}, \quad (3)$$

where W_0 is the initial weight of the sample, W_t is the weight of the sample at time t (variable), and W_f is the final mass at the end of the reaction. Due to the moisture content of some samples, the conversion α was recalculated to zero at 200 °C, so that the kinetic parameters would only be representative of the pyrolysis of dry kerogen.

The Coats-Redfern integral method was used to determine whether the decomposition involves one or two zones and to obtain the respective activation energy and pre-exponential factor values [15]. Using the Arrhenius equation and combining it with a linear heating rate β , and integrating, one gets [27]:

$$\frac{1 - (1 - \alpha)^{1-n}}{1 - n} = \frac{ART^2}{\alpha E} \left[1 - \frac{2RT}{E} \right] \exp\left(-\frac{E}{RT}\right). \quad (4)$$

For the reaction order of $n = 1$, Equation 4 can be written as follows:

$$\ln\left[-\frac{\ln(1 - \alpha)}{T^2}\right] = \ln\frac{AR}{\beta E} \left[1 - \frac{2RT}{E} \right] - \frac{E}{RT}. \quad (5)$$

Therefore, a plot of $\ln[-\ln(1 - \alpha)/T^2]$ vs $1/T$ should result in a straight line with the slope of $-E/R$ and an intercept of $\ln(AR/\beta E)$. The presence of a 'breaking point' in the data confirms that there are two consecutive zones during the decomposition reaction.

The second kinetic analysis method used in this paper was the direct Arrhenius method [15]. When combining the aforementioned decomposition reaction (1) and combining it with the Arrhenius equation (2), in case of a non-isothermal measurement with a linear heating rate (β), the conversion can be described as:

$$\frac{d\alpha}{dt} = \frac{A}{\beta} \exp\left(-\frac{E}{RT}\right) (1 - \alpha)^n. \quad (6)$$

Therefore, in case of $n = 1$, a plot of $\ln[(d\alpha/dT)/(1 - \alpha)]$, also stated as $\ln k$ vs $1/T$, will yield a straight line from which E and A can be calculated from the slope and intercept, respectively.

3. Results and discussion

3.1. Oil shale organic and mineral contents

Figure 2 shows the weight loss data for the pre-dried samples of American, Chinese and Estonian oil shales as a function of temperature heated with a constant heating rate of $20 \text{ }^\circ\text{C min}^{-1}$ in a N_2 atmosphere. As can be seen from the figure, all the samples exhibit different mass loss magnitudes. Little if any mass loss below $200 \text{ }^\circ\text{C}$ is assigned to the evaporation of water and is not displayed in Figure 2. Estonian oil shale shows the greatest total mass loss of 47 %, including both organic matter and carbonate part decomposition. The Green River 1 oil shale exhibits a quite similar mass loss profile with a total mass loss of 42%. The Green River 2 sample can be considered somewhat similar to the abovementioned samples, since it shows similar steps but in smaller magnitude – the total mass loss is 35%. The mass losses of Kentucky, Chinese 1 and Chinese 2 oil shale samples are noticeably different from those of the aforesaid samples – these samples have a slightly smaller total mass loss (only up to 28 %). The Chinese 1 sample exhibits carbonate mineral decomposition of about just 6%, however, Chinese 2 and Kentucky oil shales do not seem to contain any carbonate mineral. It is worth noting that the mass loss of Chinese 2 and Kentucky oil shales does

not remain constant (a constant negative slope) during the heating at a temperature beyond 600 °C. This behavior of the sample might be due to the mineral portion reduction during the heating in an inert atmosphere. If compared to the other oil shale samples, Estonian oil shale has the highest carbonate mineral content (22%). As can be also seen from Figure 2 and Table 2, the total extractable kerogen content varies from 12 to 27%, respectively, for the samples of Kentucky and Green River 1.

As seen from the figure, most oil shale powders were dry prior to the analysis. The first mass loss (between 300 and 550 °C) is attributed to the pyrolysis of oil shale in inert N₂ gas atmosphere when heated at 20 °C/min. The second mass loss (between 650 and 850 °C) is ascribed to the decomposition of oil shale carbonates.

Characteristic temperatures for the decomposition reaction for oil shale samples tested are cumulatively shown in Table 2. As can be seen from the table, the Green River 1 oil shale sample exhibits the highest determined temperature values, indicating low kerogen reactivity or delayed decomposition reaction if compared to the other samples. On the contrary, the samples Kentucky and Green River 1 have the most delayed thermal decomposition and therefore the highest temperatures at maximum mass loss rate, although the extent of the reaction (temperature difference between the start and end of thermal decomposition) is the highest. It seems Kentucky oil shale kerogen is most reactive if compared to the rest of oil shales in the sample

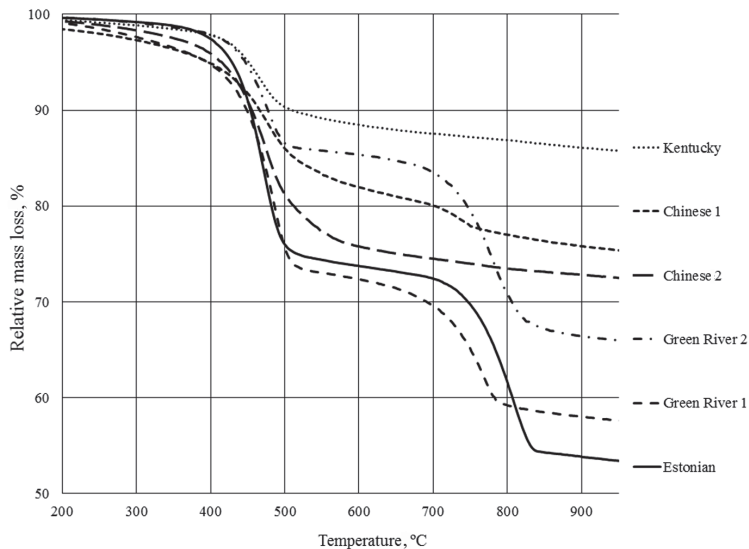


Fig. 2. TG profiles of the analyzed oil shale samples.

Table 2. Oil shale kerogen and carbonate contents and characteristic temperatures of pyrolysis obtained at the beginning, at the end and at maximum mass loss rate of the reaction

Result	Sample	Estonian	Green River 1	Green River 2	Kentucky	Chinese 1	Chinese 2
Residual mass, %		53	58	65	85	75	72
Total mass loss, %		47	42	35	15	25	28
Pyrolysis of organics, %		24	27	14	12	18	24
Fischer assay oil yield, %		17	19	10	8	13	17
Decomposition of carbonate minerals, %		22	14	19	0	6	0
Start of thermal decomposition of kerogen, °C		432	435	434	419	n.d	n.d
Temperature of maximum mass loss speed of kerogen, °C		471	483	476	465	475	473
End of thermal decomposition of kerogen, °C		495	504	498	501	n.d	n.d

* n.d – not determined due to curve shapes obtained

bank. Estonian and Green River 1 oil shale samples exhibit a higher organic content and a smaller residual mass. This is consistent with the Fischer Assay oil yield results (see results in Table 2), where it is shown that Estonian, Green River 1 and Chinese 2 oil shale samples exhibited the highest oil yields. Fischer Assay oil yield, in percent (%), was calculated from the kerogen content according to Cook [28]. The Fischer Assay oil yields in this study are quite comparable to those presented in the work of Goldfarb et al. [9], except the Estonian oil shale yield. It should be noted that the Estonian oil shale used in [9] was from “Aidu” mine, however, this study employed a sample from “Estonia” mine.

T_s and T_e temperatures were not determined for Chinese oil shale samples due to the shape of their mass loss curves – in this case the intersection of tangents would not give meaningful temperature values.

As Table 2 shows, the organic content is the highest in Estonian, Green River 1 and Chinese 2 oil shale samples, however, the highest carbonate content is in Estonian and Green River 2 oil shale samples.

The main mass loss occurring at temperatures below around 600 °C is attributed to the decomposition of kerogen present in oil shale [22]. It is known that the pyrolysis process temperature is related to the rate of weight loss, since higher temperatures cause greater weight loss or higher oil yields [14]. In our case, complete decomposition of organics occurs at temperatures up to 550 °C. Above 650 °C, the decomposition of carbonate minerals as well as changes in the chemical structure of clay minerals takes place. As can be seen from the results in Table 2, the mass loss originating from the decomposition of Green River 1 carbonates is smaller than for the decomposition of the same oil shale kerogen. It is interesting that for the Green

River 2 sample, in opposite, the magnitude of kerogen decomposition is smaller than the step of decomposition of carbonates. The temperature values, between which the kerogen decomposition reaction occurs, are about the same for Estonian and both Green River samples. The results in Table 2 also reveal that the organic content is more or less the same for Estonian, Green River 1 and Chinese 2 samples, ranging from 24 to 27%.

Figure 3 depicts the differential TGA rate curves of the analyzed samples. As seen from the graph (and results in Table 2), the maxima of various oil shale decomposition rates are more or less similar ranging from 465 to 483 °C. There seems to be no correlation between the extent of the kerogen decomposition and the temperatures recorded at maximum rate. Although, Chinese 2 and Kentucky oil shales exhibit a continuous very slow mass loss and therefore the differential mass loss curve does not show any peaks. Additionally, it can be seen that the larger the carbonate mineral decomposition step (in %), the more intense the peak and the more delayed the peak maximum. The results in Table 2 demonstrate that the characteristic thermal temperatures of oil shale kerogen decomposition are in more or less the same range, and therefore it seems that the reaction rate is independent of the origin, age and composition of oil shale.

As seen from Figure 3, pyrolysis in all oil shale samples tested begins at around 300 °C, and is over at about 530 °C. Estonian and US Green River 1 are the highest kerogen oil shales. Independent of the origin of oil shale, as expected, the decomposition of carbonate minerals begins at around 650 °C.

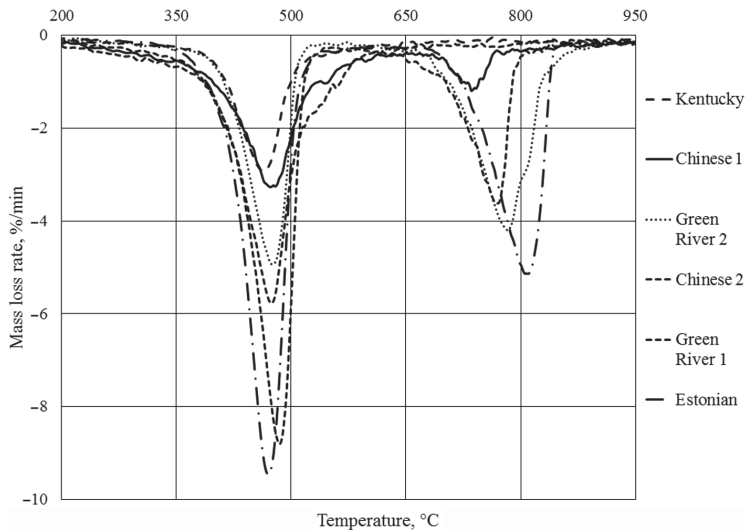


Fig. 3. Differential TG curves of the analyzed oil shale samples.

Estonian, US Green River 2 and US Green River 1 samples have the highest carbonate content.

The assumption of first-order reactions seems reasonable due to uniform Gaussian distribution style differential rate curves (see Fig. 3) for all oil shales. Long tail of the differential rate curve would suggest rate order to be over 1, and long heads of the curve would suggest rate order to be below 1. None of this is the case, and therefore assumption of first order kinetics during decomposition seems reasonable.

As a summary of this section, oil shale samples investigated in this work have different mass loss and differential mass loss rate profiles due to their different origin and composition. However, oil shale kerogen decomposition reaction rates seem to be independent of oil shale origin and composition.

3.2. Oil shale decomposition kinetic parameters and their comparison to literature data

As mentioned in the Experimental section, the Coats-Redfern integral and direct Arrhenius plot methods were used to calculate the kinetic rate parameters such as pre-exponential factor and activation energy. Their common advantage is that the presence of a distinct “breaking point” at certain temperatures (see Figs. 4 and 5) in the data plot verifies that there might be two consecutive reaction zones with slightly different temperature ranges. This can be explained as a change in the rate of decomposition at some critical temperature. The difficulties associated with clearly determining this “breaking point” are related to various reactions taking place during oil shale decomposition, which do overlap to some extent and could therefore influence the calculated rate parameters.

Figure 4 represents the direct Arrhenius plot method analysis results. As can be seen from the presented results, the decomposition rate proceeds in two zones where firstly the kerogen decomposes into pyrolytic bitumen, which is then further converted to complicated hydrocarbons with varying length as previously seen in the literature [22, 29]. It should be noted that in the lower temperature zone for each oil shale, the data dispersion is the highest (R^2 values are relatively low) if compared to the second reaction zone. In addition it can be seen from the graph that Estonian oil shale seems to be slightly different from the other samples – the “breaking point” is at a lower temperature.

Figure 4 shows that the uncertainty of kinetic parameter values obtained in the z1 zone is relatively high when the Arrhenius method is applied. The correlation factors in z1 range from 0.66 up to 0.91, however, in the z2 temperature zone the correlation factors are relatively high, ranging from 0.98 up to 0.99, suggesting excellent kinetic parameters for all oil shales tested.

Figure 5 displays the results of the Coats-Redfern integral method – a plot of $\ln[-\ln(1-\alpha)/T^2]$ vs $1/T$. Three of the oil shale samples are depicted – Estonian, Green River 2 and Kentucky, since they all exhibit slightly

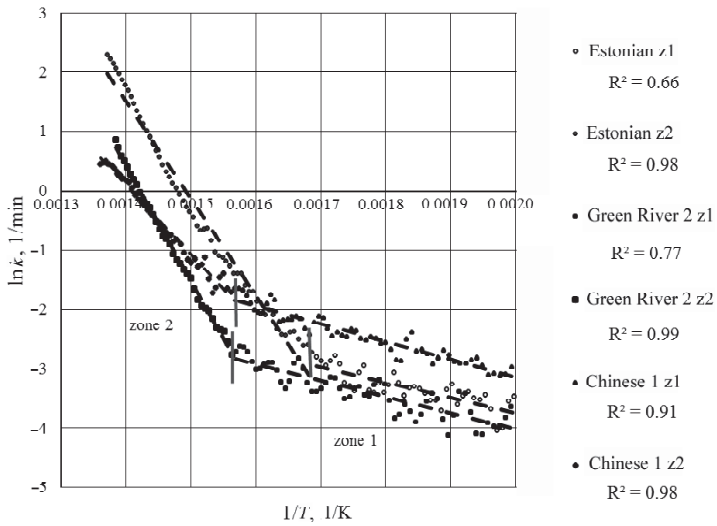


Fig. 4. The direct Arrhenius plot method results for Estonian, US and Chinese oil shale samples, z1 and z2 denoting the reaction zones at lower and higher temperatures, respectively.

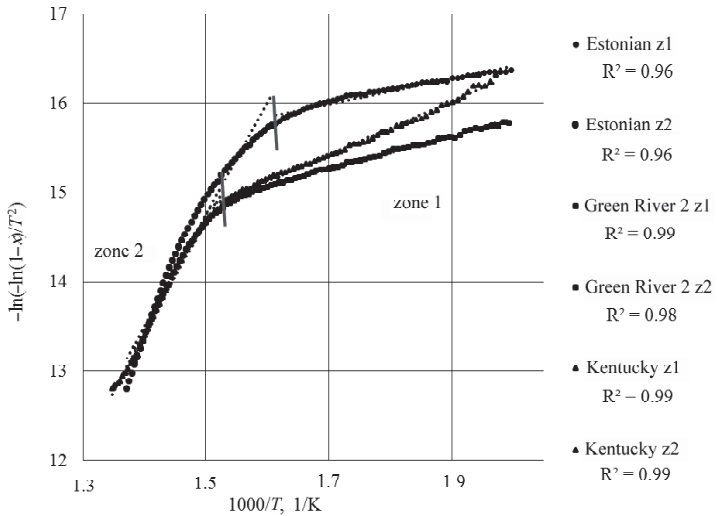


Fig. 5. The Coats-Redfern integral method results for Estonian and US oil shale samples, z1 and z2 denoting the reaction zones of lower and higher temperature range, respectively.

differently shaped rate curves. The other three oil shale data sets show significant overlapping in the two zone “breaking point” temperature region and therefore are not shown. Similarly to the direct Arrhenius method, the results in Figure 5 reveal the existence of two consecutive rate zones during the decomposition reaction. Both zones in Figure 5 are separated with a vertical brown line, which divides “zone 1” and “zone 2” data. The results demonstrate a close linear fitting with R^2 coefficients ranging from 0.96 to 0.99 over the used temperature ranges. Similarly to the results shown in Figure 4 and Figure 5, Estonian oil shale seems to exhibit a higher rate of decomposition. This is due to the higher organic/mineral ratio in oil shale.

Figure 5 shows that the uncertainty of kinetic parameter values obtained in the z1 zone is relatively low, the linear correlation factors range from 0.96 to 0.99. The correlation factors in the z2 temperature zone range from 0.96 up to 0.99, suggesting excellent kinetic parameters for all oil shales tested. It is noticeable that the R^2 values are considerably higher for the Coats-Redfern method (Fig. 5) than for the direct Arrhenius plot method (Fig. 4), which suggests that the Coats-Redfern model fits oil shale decomposition data more precisely than the Arrhenius method. The latter method gives a closer correlation between kinetic parameters in the higher temperature zone (zone 2) in which the cracking of hydrocarbons occurs. It is evident that when using the direct Arrhenius plot method for the lower temperature zone, the correlation coefficients are quite low for Estonian and Green River 2 oil shales. As both of the samples contain about 20% carbonate minerals, the mineral matrix may have a catalytic effect on the on-going reactions in the organic portion. This will be discussed later. For the Estonian oil shale sample, the dispersion of the obtained kinetic parameters is significantly higher than for the other oil shale samples. This might be due to the difference in the composition of oil shale samples, but also possibly due to the different chemical and physical behavior of organic and inorganic portions, since it is not exactly known which chemical or physical changes or molecular rearrangements take place during the heating process.

Qing et al. [29] have reported Chinese Huadian oil shale decomposition kinetics, applying similarly both the direct Arrhenius plot and Coats-Redfern methods. That study shows better rate data correlation with the Arrhenius method, which supports the findings of the current paper. The main difference is that Qing et al. have calculated their kinetic parameters for a single reaction zone, combining all organics decomposition data, but in this research we present activation energy calculations for two reaction zones without eliminating any data points near the breaking point.

The activation energy values calculated both in low and high temperature zones for all oil shales tested are presented in Figure 6. In this figure “zone 1” denotes the lower temperature region reaction zone and “zone 2” the higher temperature region reaction zone.

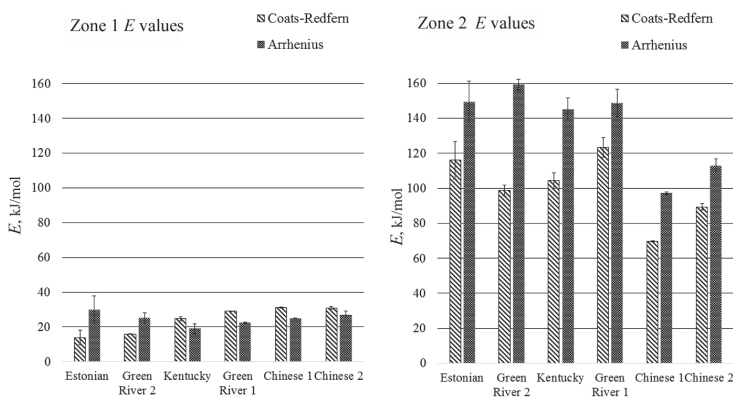


Fig. 6. A comparison of the calculated activation energy values for oil shales tested in two reaction zones.

As seen from the results in Figure 6, independent of the origin of oil shale, the activation energy values in zone 1 are significantly lower, ranging from 14 up to 31 kJ/mol, however, those in zone 2 range from 70 up to 149 kJ/mol. Also, Figure 6 shows that the Coats-Redfern method yields a lower deviation of the obtained kinetic parameter values and a better fit to the data for all oil shales tested, especially for the lower temperature range reaction zone. However, consistently for all oil shales, the direct Arrhenius plot method yields higher activation energy values. An issue that has been discussed in several articles before is the possible catalytic effect of minerals on the pyrolysis of organics in oil shale. It has been shown by Yan et al. [30] that the mineral matrix (mostly carbonates and silicates) in oil shale promotes the decomposition of organic matter during the pyrolysis process – the minerals can affect the organic matter decomposition, and therefore alter kinetic parameter values.

The comparison of activation energy and pre-exponential factor values with the data presented in the literature is shown in Table 3 [12, 31–34]. These results demonstrate that the activation energy values obtained in this work are very similar to those reported by Braun and Rothman (44.6 to 177.6 kJ/mol) for Green River oil shale [31]. The researchers indicated that the activation energy values of the decomposition reaction low temperature zone are lower because of the weaker bonds existing in organics decomposing in the early stages of the process. With the decomposition reaction progressing, the stronger bond organics decompose and the activation energy increases. These results are in correlation with those obtained by Kök and Iscan [23], who reported activation energy calculation for different oil shale samples from Turkey with results falling into the same range. Tiwari and Deo [10] have shown the activation energy values for Green River oil shale

decomposition ranging from 95 to 245 kJ/mol, with uncertainties of about 10%. Liu et al. [13] have calculated the activation energy values for three steps of decomposition of Chinese oil shale samples and obtained the figures in the range of 54 to 277 kJ/mol. The results obtained in this paper are smaller than those reported in the literature. This is not surprising since the samples have different origins and are found in different geological environments.

Table 3. A comparison of the obtained activation energy values with literature data

Zone 1	Coats-Redfern method		Direct Arrhenius plot method		Literature data	Reference
Sample	E_a , kJ/mol	$\log A$	E_a , kJ/mol	$\log A$	E_a , kJ/mol	No
Estonian	13.9	10.33	29.8	2.52	31.0	[33]
Green River 1	29.0	8.98	22.5	2.51	44.6	[31]
Green River 2	15.9	9.86	25.1	2.05	50.7 ^x	[34]
Kentucky	24.7	9.30	19.0	1.43	–	–
Chinese 1	31.2	8.72	24.9	2.48	54.0	[12]
Chinese 2	30.9	4.92	26.8	2.70		
Zone 2	Coats-Redfern method		Direct Arrhenius plot method		Literature data	Reference
Sample	E_a , kJ/mol	$\log A$	E_a , kJ/mol	$\log A$	E_a , kJ/mol	No
Estonian	115.9	3.13	149.3	12.43	–	–
Green River 1	123.4	2.61	148.7	12.41	177.6	[31]
Green River 2	98.9	4.26	159.3	12.70		
Kentucky	104.4	3.84	145.1	11.49	211–226 ^y	[32]
Chinese 1	69.7	6.16	97.2	8.21	277.0	[12]
Chinese 2	89.4	5.25	112.8	9.66		

^x – calculated using different heating rates, ^y – total mean value

As the table shows, the zone 1 activation energy values obtained in this research are in good agreement with the literature data, however, the activation energy values for zone 2 reported in this paper are somewhat lower than the ones published previously.

The kinetic parameter values presented above could potentially differ if common catalysts were eliminated from oil shale prior to its pyrolysis experiment. In this study, we did not eliminate the mineral part prior to the pyrolysis and therefore, our kinetic parameter values represent kinetics with potential catalytic effects. As evidenced from the results presented in Table 3, the activation energy of Kentucky oil shale (which contains no carbonate minerals) has no clear trend if compared to that of Green River 1 (14% carbonates). However, it has been reported that carbonate minerals provide a catalytic effect on pyrolysis kinetics and thereby, lower the

activation energy [22]. In our investigations, such a clear catalytic effect of the carbonate part has not been observed. According to Rajeshwar [15], there should not be any difference in the calculated kinetic parameter values depending on whether kerogen was previously extracted from oil shale or not. Another study has reported that when oil shale vs pure kerogen decomposition TGA curves are compared at different heating rates, the decomposition of oil shale is faster if compared to pure kerogen decomposition, suggesting catalytic effects of minerals present in oil shale [22]. However, Aboulkas and El Harfi [18] observed delayed kinetics for oil shale if compared to the kinetics of pure kerogen. As stated by Al-Harashsheh et al. [22], the minerals could offer catalytic effects and therefore enhance heat transfer in oil shale particles, thereby increasing the cracking during pyrolysis. Further study is needed to investigate the catalytic effects of minerals present in oil shale on its pyrolysis kinetics.

The oil shale pyrolysis kinetic parameter values obtained in this investigation were more or less the same for all oil shales tested in either decomposition temperature zone if a heating rate of $20\text{ }^{\circ}\text{C min}^{-1}$ was applied. Indeed, altering the heating rate might somewhat provide different kinetic parameter values, however, more practical use heating rates (such as in an actual oil shale retort) cannot be obtained with the conventional TGA method. Further study is required to investigate the effect of heating rates applied (heating rates which are more comparable to those of the actual retort process) on oil shale decomposition kinetics.

4. Conclusions

This paper offers the results of the pyrolysis kinetics of American, Chinese and Estonian oil shales applying TGA. The oil shales tested exhibited dissimilar thermal decomposition extents depending on their kerogen content. The activation energy and pre-exponential factor values were obtained applying the direct Arrhenius plot and Coats-Redfern integral methods. Independent of the origin of oil shale the decomposition of kerogen portion proceeds in two temperature zones – in the low temperature zone (kerogen decomposition to bitumen), and in the consequent high temperature zone (a cracking step and the formation of various hydrocarbons). As evidenced from the presented results, both temperature zones exhibit considerably dissimilar activation energy and pre-exponential factor values. There were no clear relationships between the kinetic parameter values recorded if the results from two methods were compared. The Arrhenius plot method yielded the activation energy values in the range of 19 to 30 kJ/mol and 97 to 159 kJ/mol, respectively, for the two occurring temperature zones. The respective figures for the Coats-Redfern integral method were in the range of 14 to 31 kJ/mol and 70 to 116 kJ/mol.

Acknowledgements

This research was supported by the European Union through the European Regional Development Fund.

REFERENCES

1. Siirde, A. Oil shale – global solution or part of the problem? *Oil Shale*, 2008, **25**(2), 201–202.
2. Altun, N. E., Hicyilmaz, C., Hwang, J.-Y., Bagci, A. S., Kk, M. Oil shales in the world and Turkey; reserves, current situation and future prospects: a review. *Oil Shale*, 2006, **23**(3), 211–227.
3. Konist, A., Loo, L., Valtsev, A., Maaten, B., Siirde, A., Neshumayev, D., Pihu, T. Calculation of the amount of Estonian oil shale products from combustion in regular and oxy-fuel mode in a CFB boiler. *Oil Shale*, 2014, **31**(3), 211–224.
4. Konist, A., Valtsev, A., Loo, L., Pihu, T., Liira, M., Kirsime, K. Influence of oxy-fuel combustion of Ca-rich oil shale fuel on carbonate stability and ash composition. *Fuel*, 2015, **139**, 671–677.
5. Torrente, M. C., Galn, M. C. Kinetics of the thermal decomposition of oil shale from Puertollano (Spain). *Fuel*, 2001, **80**(3), 327–334.
6. Lille, . Current knowledge on the origin and structure of Estonian kukersite kerogen. *Oil Shale*, 2003, **20**(3), 253–263.
7. Hutton, A., Bharati, S., Robl, T. Chemical and petrographic classification of kerogen/macerals. *Energ. Fuel*, 1994, **8**(6), 1478–1488.
8. Yan, F., Song, Y. Properties estimation of main oil shale in China. *Energ. Source. Part A*, 2009, **31**(4), 372–376.
9. Klaots, I., Goldfarb, J. L., Suuberg, E. M. Characterization of Chinese, American and Estonian oil shale semicokes and their sorptive potential. *Fuel*, 2010, **89**(11), 3300–3306.
10. Tiwari, P., Deo, M. Detailed kinetic analysis of oil shale pyrolysis TGA data. *AIChE J.*, 2012, **58**(2), 505–515.
11. Wang, Z., Deng, S., Gu, Q., Zhang, Y., Cui, X., Wang, H. Pyrolysis kinetic study of Huadian oil shale, spent oil shale and their mixtures by thermogravimetric analysis. *Fuel Process. Technol.*, 2013, **110**, 103–108.
12. Bai, F., Sun, Y., Liu, Y., Liu, B., Guo, M., L, X., Guo, W., Li, Q., Hou, C., Wang, Q. Kinetic investigation on partially oxidized Huadian oil shale by thermogravimetric analysis. *Oil Shale*, 2014, **31**(4), 377–393.
13. Liu, Q. Q., Han, X. X., Li, Q. Y., Huang, Y. R., Jiang, X. M. TG–DSC analysis of pyrolysis process of two Chinese oil shales. *J. Therm. Anal. Calorim.*, 2014, **116**(1), 511–517.
14. Jaber, J. O., Probert, S. D. Non-isothermal thermogravimetry and decomposition kinetics of two Jordanian oil shales under different processing conditions. *Fuel Process. Technol.*, 2000, **63**(1), 57–70.
15. Rajeshwar, K. The kinetics of the thermal decomposition of Green River oil shale kerogen by non-isothermal thermogravimetry. *Thermochim. Acta*, 1981, **45**(3), 253–263.
16. Williams, P. T., Ahmad, N. Investigation of oil-shale pyrolysis processing conditions using thermogravimetric analysis. *Appl. Energ.*, 2000, **66**(2), 113–133.

17. Fang-Fang, X., Ze, W., Wei-Gang, L., Wen-Li, S. Study on thermal conversion of Huadian oil shale under N₂ and CO₂ atmospheres. *Oil Shale*, 2010, **27**(4), 309–320.
18. Aboulkas, A., El Harfi, K. Study of the kinetics and mechanisms of thermal decomposition of Moroccan Tarfaya oil shale and its kerogen. *Oil Shale*, 2008, **25**(4), 426–443.
19. Thakur, D. S., Nuttall, H. E., Cha, C. Y. The kinetics of the thermal decomposition of Moroccan oil shale by thermogravimetry. *Prepr. Pap. Am. Chem. Soc., Div. Fuel Chem.*, 1982, **27**, 131–142.
20. Tiwari, P., Deo, M. Compositional and kinetic analysis of oil shale pyrolysis using TGA–MS. *Fuel*, 2012, **94**, 333–341.
21. Zanoni, M. A. B., Massard, H., Martins, M. F., Salvador, S. Application of inverse problem and thermogravimetry to determine the kinetics of oil shale pyrolysis. *High Temp.-High Press.*, 2012, **41**(3), 197–213.
22. Al-Harahsheh, M., Al-Ayed, O., Robinson, J., Kingman, S., Al-Harahsheh, A., Tarawneh, K., Saeid, A., Barranco, R. Effect of demineralization and heating rate on the pyrolysis kinetics of Jordanian oil shales. *Fuel Process. Technol.*, 2011, **92**(9), 1805–1811.
23. Kök, M. V., Iscan, A. G. Oil shale kinetics by differential methods. *J. Therm. Anal. Calorim.*, 2007, **88**(3), 657–661.
24. Wang, C., Zhang, X., Liu, Y., Che, D. Pyrolysis and combustion characteristics of coals in oxyfuel combustion. *Appl. Energ.*, 2012, **97**, 264–273.
25. Vyazovkin, S., Chrissafis, K., Di Lorenzo, M. L., Koga, N., Pijolat, M., Roduit, B., Sbirrazzuoli, N., Suñol, J. J. ICTAC Kinetics Committee recommendations for collecting experimental thermal analysis data for kinetic computations. *Thermochim. Acta*, 2014, **590**, 1–23.
26. Jacobs, P. W. M., Tompkins, F. C. Classification and theory of solid reactions. In: *Chemistry of the Solid State* (Garner, W. E., ed.). Butterworths, London, 1955, 184–212.
27. Coats, A. W., Redfern, J. P. Kinetic parameters from thermogravimetric data. *Nature*, 1964, **201**, 68–69.
28. Cook, E. W. Oil-shale technology in the USA. *Fuel*, 1974, **53**(3), 146–151.
29. Qing, W., Baizhong, S., Aijuan, H., Jingru, B., Shaohua, L. Pyrolysis characteristics of Huadian oil shales. *Oil Shale*, 2007, **24**(2) 147–157.
30. Yan, J., Jiang, X., Han, X., Liu, J. A TG-FTIR investigation to the catalytic effect of mineral matrix in oil shale on the pyrolysis and combustion of kerogen. *Fuel*, 2013, **104**, 307–317.
31. Braun, R. L., Rothman, A. J. Oil-shale pyrolysis: kinetics and mechanism of oil production. *Fuel*, 1975, **54**(2), 129–131.
32. Knauss, K. G., Copenhaver, S. A., Braun, R. L., Burnham, A. Hydrous pyrolysis of New Albany and Phosphoria shales: production kinetics of carboxylic acids and light hydrocarbons and interactions between the inorganic and organic chemical systems. *Org. Geochem.*, 1997, **27**(7–8), 477–496.
33. Ots, A. *Oil Shale Fuel Combustion*. Tallinna Raamatutrukikoda, 2006.
34. Schenk, H. J., Dieckmann, V. Prediction of petroleum formation: the influence of laboratory heating rates on kinetic parameters and geological extrapolations. *Mar. Petrol. Geol.*, 2004, **21**(1), 79–95.

Presented by A. Siirde and O. Trass

Received November 30, 2015

Appendix 2

PUBLICATION II

B. Maaten, L. Loo, A. Konist, T. Pihu, and A. Siirde, "Investigation of the evolution of sulphur during the thermal degradation of different oil shales," *J. Anal. Appl. Pyrolysis*, vol. 128, pp. 405–411, 2017



Contents lists available at ScienceDirect

Journal of Analytical and Applied Pyrolysis

journal homepage: www.elsevier.com/locate/jaap

Investigation of the evolution of sulphur during the thermal degradation of different oil shales



Birgit Maaten*, Lauri Loo, Alar Konist, Tõnu Pihu, Andres Siirde

Department of Energy Technology, Tallinn University of Technology, Ehitajate tee 5, Tallinn, 19086, Estonia

ARTICLE INFO

Keywords:

Oil shale
Pyrolysis
Decomposition
Distributed activation energy model
Mass spectrometry
Sulphur behaviour

ABSTRACT

This paper presents the results of the pyrolytic decomposition of six different oil shale samples with different sulphur contents from Estonia, USA and China using non-isothermal thermogravimetry coupled with a mass spectrometer (TGA-MS). Mass spectrometry (MS) was used to analyse the evaporating gases. The results showed a major difference in the evolution of sulphur containing substances. The sulphur behaviour was found to be in excellent correlation with the composition of the sample. H₂S and SO₂, the problematic components forming during the pyrolysis process, both exhibited evaporation in two peaks. The kinetic distribution supported the findings of MS – samples with a higher sulphur content exhibited more parallel reactions that had similar weight percentages. SO₂ evolution intensifies above 500 °C. H₂S is released in the temperature range of 350–500 °C, depending on the sample. The samples Kentucky, Green River, Estonia and Chinese 2 also have an additional peak at 500–570 °C. This is in good accordance with the aforementioned samples having a relatively high amount of sulphur in the forms of organics and sulphides. Based on the results, an important conclusion is that changing the pyrolysis temperature can reduce the sulphur content of the oil produced. The experimental curves obtained were used to calculate the kinetic parameters using a distributed activation energy model. The obtained activation energy values were in the range of 134–276 kJ/mol with the frequency factors ranging from 1.89E10¹² to 1.20E10¹⁴ s⁻¹. In order to validate the obtained kinetic parameters, the decomposition curves were compared to modelled ones. The dependence of total conversion on reaction time was calculated at isothermal conditions to show the effect of pyrolysis temperature.

1. Introduction

Oil shale is an unconventional fossil fuel, often described as a complex material consisting of an organic part (called kerogen) and an inorganic part, which consists of a wide range of minerals [1–4]. When oil shale particles are heated to a certain critical temperature, the organic part starts to decompose and vaporize, leading to the production of gas, oil and residual carbon [5]. In addition to being an energy source, the exploitation of oil shale in, for example, China represents a valuable source of liquid hydrocarbons. The pyrolysis process of oil shale involves complex reactions and its end products are dependent on numerous factors like heating rate, final temperature, etc. [6]. Therefore, in order to maximize the potential, the conversion process of oil shale to oil should be studied and optimized [7].

There are several different devices and methods to conduct studies about kinetics, but thermogravimetry is the most used technique [8]. Since the decomposition of oil shale is complex and consists of a large number of parallel and series reactions, thermal analysis describes the

overall weight loss due to these reactions instead of describing individual reactions [9]. The factors that are considered to influence the thermal behaviour of oil shale have been widely discussed in the literature [2,5,6,10–13]. Non-isothermal methods are usually preferred to isothermal ones due to not having a thermal induction period and permitting a more rapid scan of the whole temperature range [2,7,14]. As an additional advantage, using a non-isothermal approach helps to more closely simulate the conditions of a large-scale retorting process [3]. Using different models to analyse the devolatilization process can help predict the burnout of a particle, the heating value of pyrolysis products and the overall process efficiency [15]. Additionally, one can calculate the time a particle should be in a retort in order to obtain complete decomposition, which is useful in industry.

Another big advantage of thermal analysis is the possibility to couple it with other analytical devices, for example FTIR, GC or MS. Thermal analysis helps to understand the process of oil shale pyrolysis process, but understanding the mechanism is still tricky due to the potential effect of various minerals and without additional analysis, it is

* Corresponding author.

E-mail address: birgit.maaten@ttu.ee (B. Maaten).<http://dx.doi.org/10.1016/j.jaap.2017.09.007>

Received 18 January 2017; Received in revised form 8 September 2017; Accepted 12 September 2017

Available online 18 September 2017

0165-2370/© 2017 Elsevier B.V. All rights reserved.

quite often hypothetical. For example, MS data enables us to study gas evolution [16], molecular characterization [17], the kinetics of hydrocarbon generation [18], etc. Pan, et al. has used TG-MS to investigate the effect of mineral matter on the thermal decomposition of Jimsar oil shale [10] – using MS they showed that pyrites can react with organic matter to form H₂S and SO₂ in the temperature range of 510–650 °C. Lan, et al. found that the content of sulphur-containing gases in non-condensable gases changes when increasing the retorting temperature [19]. They found that H₂S is the primary component in non-condensable gases and the release of this gas begins even at low temperatures. Therefore, MS offers valuable information regarding the evolution of gases and the behaviour of the components in the samples.

There are numerous methods to calculate and analyse the experimental data in order to calculate the kinetic parameters of different processes. Their advantages and disadvantages have been critically evaluated by the International Confederation for Thermal Analysis and Calorimetry (ICTAC) Kinetics Committee, with the most important principle being that methods that use only a single heating rate should not be used. The choice of a good method is important, since good kinetic data is essential to accurately model various processes, which in the case of oil shale pyrolysis is the oil-evolution step [14].

As opposed to the considerable research that has been devoted to publishing single sample results or articles comparing several samples [18,20–24], the objective of this paper is to describe the decomposition of samples from all over the world using simultaneous thermogravimetric analysis and mass spectrometry (MS). Sulphur behaviour and evolution is investigated in light of potential benefits to oil plants. In Estonia oil is produced at temperatures of 450–500 °C [25]. The solid heat carrier technology utilizes lower temperatures than the gaseous heat carrier technology making it the preferred technology [26]. Since this directly influences emissions, sulphur behaviour was analysed in order to see whether the sulphur content in the oil could be reduced for oil shales of other origins. It is necessary to investigate the limits of the sulphur release to determine the optimal temperature for the pyrolysis process. To overcome the shortcomings of previous research [27], this study offers the calculation of kinetic parameters based on experiments with different heating rates, analyses the decomposition products and their profiles and also focuses on modelling. The effect of sulphur and heating rate on the pyrolysis kinetics and evolved products of different oil shales is studied.

2. Experimental

2.1. Materials

Six oil shale samples from the USA, China and Estonia were investigated. The samples exhibited different sulphur concentrations (0.81–2.16%), both in the mineral and organic part. The samples were chosen due to China and USA having the largest resources (1600 and 354 million barrels, respectively [28]) and Estonia being highly dependent on oil shale for power production (about 90% of electricity is produced from oil shale [29,30]). The sampling locations are as follows: Estonia – from an underground mine called “Estonia” in Estonia; Colorado – from Green River shale formation, Colorado, USA; Green River – from the Uinta basin of the Green River shale formation, Utah, USA; Kentucky – from the New Albany shale formation, Kentucky, USA; Chinese 1 and Chinese 2—from the Maoming mine, Guangdong Province, Southwest China with the local classifications of C and A, respectively. All oil shale samples used in pyrolysis tests were previously dried and crushed to less than 1 mm. The elemental analysis results can be seen in Table 1 and the proximate analysis in Table 2. As sulphur in oil shale exists in the form of sulphide, sulphate and organic sulphur the organic sulphur content has been calculated by difference (from the total sulphur content and sulphide and sulphate forms) [31,32].

Table 1

Ultimate analysis results (wt%, dry base) and characteristics of the tested oil shale samples.

Sample	N	C	H	S ^{total}	S _{sulphide}	S _{sulphate}	S _{organic}
Estonian	0.1	27.3	2.7	1.46	0.96	0.07	0.43
Colorado	0.9	27.7	3.2	1.39	0.67	0.30	0.42
Green River	0.4	17.2	1.7	0.81	0.20	0.03	0.58
Kentucky	0.5	15.4	1.7	1.76	0.76	0.33	0.67
Chinese 1	0.9	23.3	2.4	2.16	1.17	0.30	0.69
Chinese 2	0.9	23.0	3.0	1.96	1.26	0.23	0.47

Table 2

Proximate analysis results, presented on an as received basis.

	Estonian	Colorado	Green River	Kentucky	Chinese 1	Chinese 2
Ash (wt%)	51.3	61.9	66.8	76.6	56.1	61.0
Moisture (wt%)	0.5	1.9	0.3	0.9	0.6	1.2
Volatile matter (wt%)	47.5	26.9	33.2	14.9	42.8	28.9
Fixed carbon (wt%)	1.3	11.2	0.0	8.6	1.2	10.1
Higher heating value (MJ/kg)	9.85	11.34	5.51	6.41	11.40	10.14

2.2. Experimental setup and methods

The samples were analysed using a NETZSCH STA 449 F3 Jupiter[®] TG-DSC apparatus coupled with a NETZSCH QMS Aëolos[®] mass spectrometer. The samples were heated in a pure nitrogen atmosphere from 200 °C to 650 °C using constant heating rates set to 2, 5, 10, 20 and 35 °C/min. For comparison of the MS data, the measurements with a heating rate of 5 °C/min were chosen to ensure that there were no overlaps between the peaks. In order to correctly interpret the results it was checked that the ratio of the mass-to-charge-ratio (m/z) at 34 to that at 33 is 2.38 to ensure that the compound is indeed H₂S. m/z 34 was selected for comparison due to its higher intensity. For the analysis of SO₂ m/z 64 was investigated and m/z 48 was also checked. The data was normalized starting from 200 °C to remove background noise and smoothed with a 5 point moving average. The results of kerogen decomposition with a heating rate of 20 °C/min can be seen on Fig. 1. A protective gas flow of 50 mL/min of high purity nitrogen was used. In order to eliminate buoyancy effects during the furnace heat-up cycle, background mass data were recorded during empty crucible experiments and subtracted from the each of the oil shale measurement data set. The temperature calibration of the apparatus was done using In, Sn, Zn, Al and Au standards. Excellent reproducibility (temperature differences less than 2 °C and mass change differences less than 0.7% for parallel measurements) was observed for the mass loss curves. All the reported results are the average values of the conducted repeated measurements.

2.3. Kinetic computations

Due to the complexity of oil shale composition [17,33,34], a distributed reactivity model was used to calculate the activation energy values. The reactivity distribution corresponds to a set of independent and parallel reactions and an activation energy value and a frequency factor are calculated for each of them [35]. As a further validation, the reactions are described with a single frequency factor, thereby representing the reactivity distribution by a continuous distribution of activation energy values. The calculations and recreation of the curves were done using Kinetics2015. Although the earliest model of sequential decomposition of kerogen to bitumen and then bitumen to oil and gas is still the most cited one, an alternate pathway is believed to be

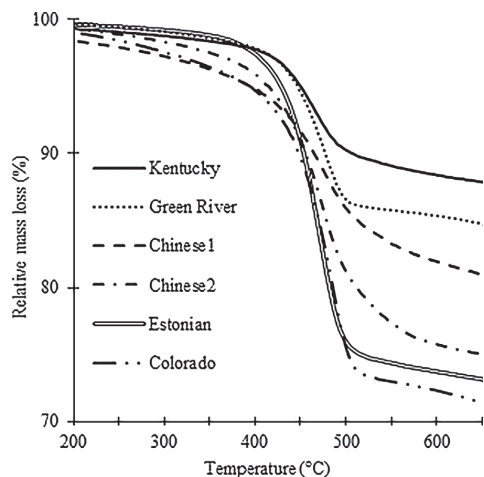


Fig. 1. The thermal decomposition profiles of the analysed samples [27].

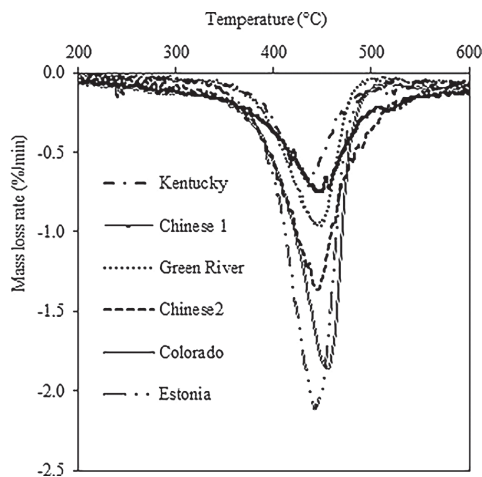


Fig. 2. The mass loss rates for all the samples [27].

correct [36]. Therefore a variety of different data can be found in the literature. As noted in the literature, most reactions of practical importance occur at nominally isothermal conditions – there is usually a finite heat-up time during which some part of the material has already reacted [35]. Kinetics2015 uses time-dependent temperature and numerically integrates the calculated rate over the thermal history, thereby offering precise results. A distributed activation energy model (DAEM) was used. Distributed reactivity models assume that the reactivity distribution is represented by a set of independent and parallel reactions. Each one of them has their own frequency factor and activation energy [35]. The rate constants follow an Arrhenius-type relation and the according activation energy is distributed following a given function [37]. Therefore, DAEM enables the calculation of activation energies for tens of simultaneous first-order reactions. The formula derivation can be found in [35]. According to Burnham [35], DAEM is the most appropriate model for calculating the activation energy values for oil shale as it is a complex material. The activation energy distributions are calculated with a step of 4.184 kJ/mol (1 kcal/mol). In order to compare the data of the different samples, the reaction with the highest activation energy value and percentage was chosen.

3. Results and discussion

3.1. Thermal analysis and kinetics

Tiwari and Deo showed that the derivatives of the weight loss curves show mostly a single major peak in the temperature region that corresponds to organic matter decomposition [38]. Our results follow the same trend, as can be seen from Fig. 2, although it was noticed that some of the peaks are more flat than sharp and have some fluctuations near the maxima. This might be an indication that the parallel reactions that are taking place are temperature-dependent, not evenly distributed and that there is not one dominant reaction.

This is also supported by the results of the calculations. The activation energy distributions are illustrated on Fig. 3. When analysing the activation energy distributions, it was noticed that the samples fall into two groups. Both of the Chinese samples and the Kentucky oil shale form a group where the activation energy distribution follows a flat type of normal distribution, whereas the weights (percentages of the respective activation energy) of the reactions are less than 30% and evenly distributed. It should be noted that the distribution is not perfectly symmetric, but tilted towards higher energy values. The second

group consists of the samples Estonia, Colorado and Green River. Their results are dominated by one reaction (representing a normal distribution with a very sharp peak) with the weight percentage of the dominant reaction being about 70%. For the first group, the values are more even and it was noted that the amount of independent reactions was higher (30 for Chinese 2 and 25 for Green River). For the second group, the dominant reaction's energy value is a bit smaller than that of the first group. For the first group, the three biggest activation energy values account for only 35–46% of the overall yield, for the second group the percentage lies between 79 and 88%. As can be expected, there is a linear dependence between $\log A$ and the selected activation energy value. The two sample groups exhibit different results in this aspect as well – the groups form two linear lines with slightly different slopes indicating once again that the samples can be divided into two groups.

According to the ICTAC Committee guidelines, increasing the heating rate by the same factor should cause a nearly constant shift of the TG curves [39]. Although it is considered common knowledge, several authors have shown that when increasing the heating rate the decomposition is shifted to a higher heating rate [3,33,40–42]. This was noticed in this paper as well. The results can be seen on Fig. 4, which compares the thermal decomposition of kerogen and the modelled curves. As stated by Brown, the final test of every kinetic analysis should be constructing modelled curves in order to compare the experimental results over a wide range [43].

The decomposition curve profiles of the tested samples are different, as can be seen from Fig. 4. For Chinese 2, the end of the decomposition is less sharp, but for the Estonian sample the end is steeper. This explains why the activation energy distributions are different – for the Chinese 2 sample there are many parallel reactions with similar energy values which might be quenched at different times, making the curve smoother at higher reacted fraction values. In contrast, for the Estonian sample, when the dominating reaction is over, the curve will follow a steeper course. The beginning of the decomposition follows respectively the same paths for both of the groups. This difference in the samples can also be noticed in the MS measurements. The differences might be due to the fact that the kerogens are of different types. According to the van Krevelen diagram, kerogen from Green River oil shale should be Type I (relatively high H/C) and that from Estonia is on the border between Types I and II [44]. The shales also have different origins and histories, and might therefore react differently.

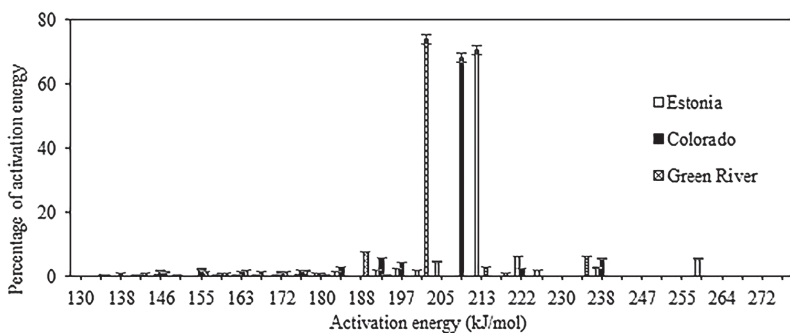


Fig. 3. The characteristic activation energy distributions of all the analysed samples.

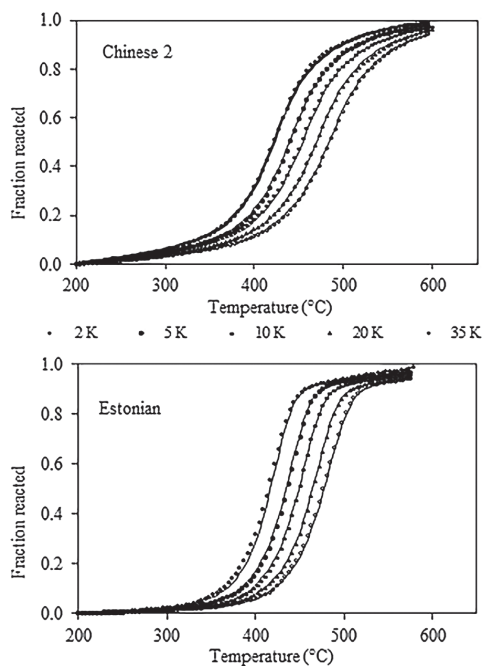
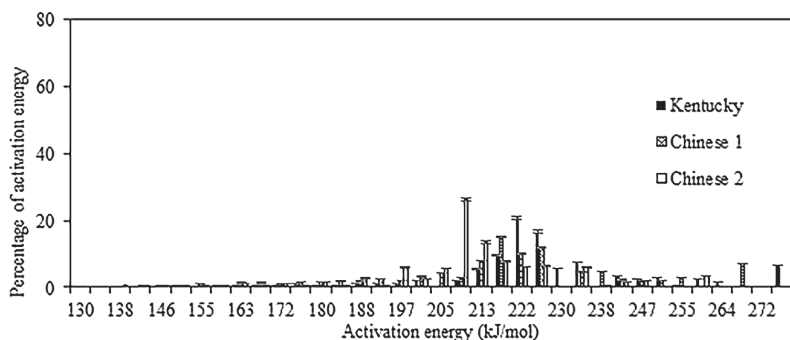
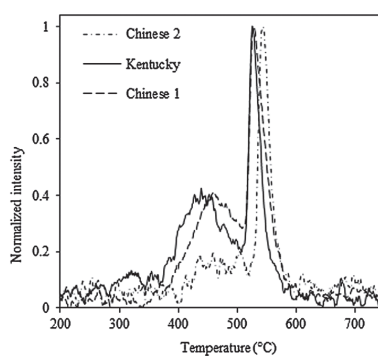
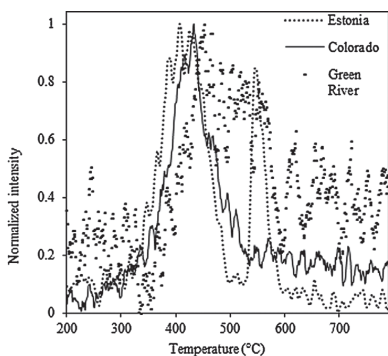
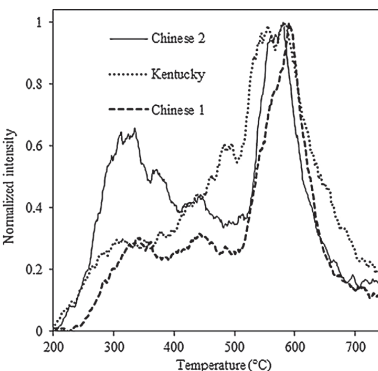
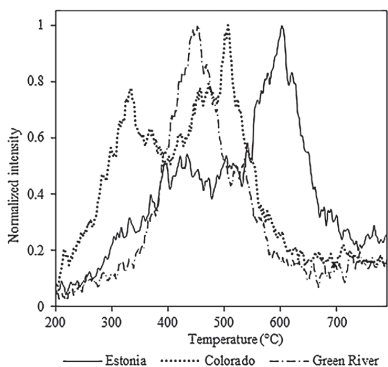


Fig. 4. Characteristic curves of the experimental and modelled data. The dots represent the experimental data and the solid lines the results from the model. Heating rate for the different experiments increases from left to right.

3.2. Mass spectrometry

As stated in the previous paragraph, the MS results for the evolving gases also indicate a difference in the samples. All the samples exhibited m/z 12, 16, 17, 18 and 44 during the organic decomposition phase. Water (m/z 18 and 17) was released in all cases with significant intensities, especially for the Chinese samples. The carbon and oxygen fragment and carbon dioxide (m/z 12, 16 and 44, respectively) were also noticeable for all samples but with a much smaller intensity. m/z 39, 41, 42, 43, 55 and 56 had high intensities and were detected during organic decomposition. These account for the release of organic compounds like hydrocarbons (for example, butane and pentane or their isomers).

An important difference is noticed when investigating the evolution of sulphur-containing compounds. m/z 33 and 34, which correspond to the release of the H_2S fragment, exhibited substantially different evolution profiles than those seen with hydrocarbons and water. The results can be seen on Fig. 5. For the sample from Colorado, m/z 34 was registered only in the organic decomposition region, whereas with the Green River sample no clear peak was identified. This is also expected since the Green River sample has the lowest total sulphur content (see Table 1). Most of the sulphur is also in the organic form for the Green River sample. For the Estonian sample two major peaks were identified – the first in the organic decomposition region (320–500 °C) and an additional, more narrow peak in the temperature region of 520–570 °C. This is expected, since most of the sulphur is in sulphide and organic forms in the Estonian sample. On the contrary, for the Chinese and the Kentucky samples the evolution of m/z 34 during organic decomposition is low and there is a sharp intense peak in the temperature region of 500–600 °C. This is in good accordance with the composition of the samples – the Chinese samples have a relatively large amount of sulphur in sulphide form (1.17 and 1.26%, respectively). As pyrite is known to decompose in the temperature range of 450–650 °C during pyrolysis [45], this is an indication of the decomposition of pyrite. This

Fig. 5. The evolution of m/z 34, indicating H_2S .Fig. 6. The evolution of m/z 64, indicating SO_2 .

is also supported by the measurement of m/z 64, which can be seen on Fig. 6. As shown by Hu [46], when oil shale is pyrite-free, sulphur evolves only in the form of SO_2 .

The results of thermal analysis should be interpreted with caution as they generally include the contributions of minerals when kerogen is not separated from the mineral part. The catalytic effect of minerals has been broadly discussed [10,13,31,40]. For example, Hu et al. have investigated the effect of inherent and additional pyrite on the pyrolysis behaviour of oil shale [46] and found that inherent pyrite can improve oil yields. Although the samples from Estonia and China mostly contain sulphur in the form of sulphides and organic sulphur and have similar H_2S evaporation profiles, the second peak is delayed in the case of the Estonian sample. The reason lies in the composition of the samples – the Estonian sample has almost no sulphur in the sulphate form (see Table 1). Respectively, the Chinese 1 and 2 samples exhibit more sulphide and sulphate forms of sulphur. This is an indication of a possible catalytic effect due to the composition of the sample. This still needs some research, especially for the Estonian sample.

The presented results are important for optimizing the temperatures of the pyrolysis process to lower sulphur contents in the produced oil. When comparing the graphs one can determine the optimal temperature which allows the sulphur content in the products to be reduced for oil produced using different technologies. From Fig. 5 and 6 it can be deduced that the temperature should definitely be kept below 480 °C to decrease the resulting sulphur content. More precisely, according to the MS measurements, a temperature of 400–450 °C would be optimal. Above that temperature sulphur evolution intensifies, especially for m/z 64, resulting in higher sulphur concentrations in the end products. However, this temperature would not be optimal for the samples from Estonia and Colorado since the evaporation maximum is near 400°, but for the other samples it would decrease the sulphur contents drastically.

Another exception is the Green River sample for which most of the sulphur has already evolved by 500 °C. This leads to the conclusion that the quality of the oil produced from Green River oil shale results in an oil with a higher sulphur content.

As the pyrolysis process in oil plants usually takes place at 480 °C, according to the spectra presented here, the sulphur content in the oil could be reduced by using different oil shales and also by changing the pyrolysis temperature. As the International Maritime Organization (IMO) has mandated a reduction of the global maximum fuel sulphur content from 4.5% to 0.5% by 2020, or even to 0.1% depending on the country, oil producing companies need to reduce the sulphur content in their products [47,48]. It has been proposed that one of the most reasonable strategies would be to use scrubbers to reduce the sulphur emissions. On the downside, this calls for big additional investments and increases the costs for the old ships that would need to be retrofitted. Based on our measurements, when using for example Colorado oil shale, a large amount of the sulphur would end up in the ash, thereby making the oil more environmentally friendly without the use of any additional technologies. Looking at the results obtained, one can conclude that when using Estonian or Green River oil shale, the sulphur content of the oil could be reduced substantially, which is not the case when using Chinese oil shale.

3.3. Calculation of conversion in isothermal conditions

Since TGA may not always be available and in order to implement the calculated kinetic triplet to real life, the total conversion dependence on the reaction time was calculated at isothermal conditions using the integral of the Arrhenius equation for first order reactions. The results can be seen on Fig. 7. 450 °C was chosen as the reaction temperature since by then the decomposition has already started but is

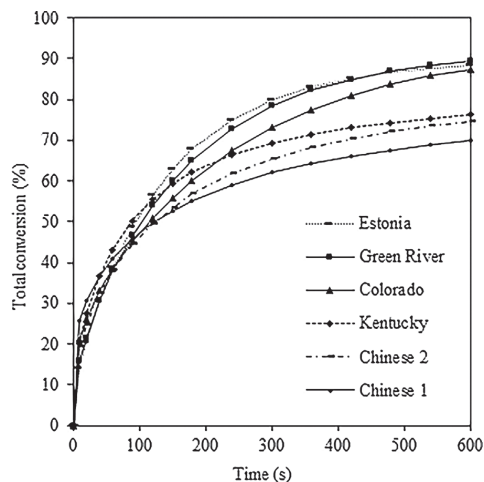


Fig. 7. Dependence of the calculated total conversion on reaction time at 450 °C.

not yet at the maximum rate. As this is calculated based on the data from TGA, the results apply to similar conditions – particle size of less than 1 mm. During the first minute the samples exhibit some differences in the conversion rate. The highest conversion in the first 10 s is for the Chinese 1 sample with the percentage being about 26%, being an indication of high initial reactivity. Although the start of the reaction is fast, the total conversion within 10 min is rather modest – only 79%. The samples from Estonia and Green River show a nearly identical profile – for the first 10 s they reach a conversion of 13.8 and 15.7%, respectively. They also resemble each other in reaching a total conversion of 90% in 10 min. The sample from Colorado also reaches nearly 90% but with a flatter profile. The Chinese 2 and Kentucky samples reach a small total conversion in 10 min – the conversions being near 75%, showing another principal difference between the samples.

4. Conclusions

This paper describes the decomposition parameters and analyses the evaporating substances for the pyrolysis process of six different oil shale samples from the US, Estonia and China. TGA-MS was applied using five different heating rates. The sulphur behaviour was investigated in light of the desire to reduce sulphur content in oil production process – H₂S and SO₂ were investigated. Due to the different composition of the samples the sulphur evaporation temperature range was studied. As expected, the differences in sulphur content largely determine sulphur evaporation. The activation energy distributions were calculated using a distributed activation energy model. In order to validate the parameters the experimental curves were recreated using the model. The fit of the modelled curves was found to be in very good correlation with the experimental data. The activation energy distributions displayed roughly two different kinds of distribution patterns, which was in correlation with the sulphur behaviour based on the sulphur content. Firstly, the samples that had a larger sulphur content (Chinese 1 and 2 and Kentucky) had more reactions with similar weight values. For these samples H₂S is released less in the organic decomposition region and there is a sharp main peak in the temperature range of 500–600 °C. The release of SO₂ follows a similar profile. Secondly, for the samples that had a smaller sulphur content (Estonian, Green River and Colorado) only one activation energy value was dominant, with a percentage of 68–74%. For these samples H₂S mostly evolved in the organic decomposition region. The release of SO₂ was different for these three samples

and no single conclusion can be drawn. These results indicate an important conclusion: the sulphur content in oil could be reduced during oil production when using different oil shales and optimizing the pyrolysis temperature accordingly.

References

- [1] W. Wang, S. Li, C. Yue, Y. Ma, Multistep pyrolysis kinetics of North Korean oil shale, *J. Therm. Anal. Calorim.* 119 (2015) 643–649, <http://dx.doi.org/10.1007/s10973-014-4191-7>.
- [2] J.O. Jaber, S.D. Probert, Pyrolysis and gasification kinetics of Jordanian oil-shales, *Appl. Energy* 63 (1999) 269–286, [http://dx.doi.org/10.1016/S0306-2619\(99\)00033-1](http://dx.doi.org/10.1016/S0306-2619(99)00033-1).
- [3] P.T. Williams, N. Ahmad, Investigation of oil-shale pyrolysis processing conditions using thermogravimetric analysis, *Appl. Energy* 66 (2000) 113–133, [http://dx.doi.org/10.1016/S0306-2619\(99\)00038-0](http://dx.doi.org/10.1016/S0306-2619(99)00038-0).
- [4] F. Yan, Y. Song, Properties estimation of main oil shale in China, *Energy Sources Part A* 31 (2009) 372–376, <http://dx.doi.org/10.1080/15567030701530347>.
- [5] M.C. Torrente, M.a. Galán, Kinetics of the thermal decomposition of oil shale from Puertollano (Spain), *Fuel* 80 (2001) 327–334, [http://dx.doi.org/10.1016/S0016-2361\(00\)00101-0](http://dx.doi.org/10.1016/S0016-2361(00)00101-0).
- [6] X. Lü, Y. Sun, T. Lu, F. Bai, M. Viljanen, An efficient and general analytical approach to modelling pyrolysis kinetics of oil shale, *Fuel* 135 (2014) 182–187, <http://dx.doi.org/10.1016/j.fuel.2014.06.009>.
- [7] X. Yongjiang, X. Huaqing, W. Hongyan, L. Zhiping, F. Chaohu, Kinetics of isothermal and non-isothermal pyrolysis of oil shale, *Oil Shale* 28 (2011) 415–424, <http://dx.doi.org/10.3176/oil.2011.3.05>.
- [8] R. Ebrahimi-Kahrizsangi, M.H. Abbasi, Evaluation of reliability of Coats-Redfern method for kinetic analysis of non-isothermal TGA, *Trans. Nonferrous Met. Soc. China (English Ed.)* 18 (2008) 217–221, [http://dx.doi.org/10.1016/S1003-6326\(08\)60039-4](http://dx.doi.org/10.1016/S1003-6326(08)60039-4).
- [9] O.S. Al-Ayed, M. Matouq, Z. Anbar, A.M. Khaleel, E. Abu-Nameh, Oil shale pyrolysis kinetics and variable activation energy principle, *Appl. Energy* 87 (2010) 1269–1272, <http://dx.doi.org/10.1016/j.apenergy.2009.06.020>.
- [10] L. Pan, F. Dai, J. Huang, S. Liu, G. Li, Study of the effect of mineral matters on the thermal decomposition of Jimbar oil shale using TG – MS, *Thermochim. Acta* 627–629 (2016) 31–38, <http://dx.doi.org/10.1016/j.tca.2016.01.013>.
- [11] C. Pan, A. Geng, N. Zhong, J. Liu, L. Yu, Kerogen pyrolysis in the presence and absence of water and minerals. 1. gas components, *Energy Fuels* 22 (2008) 416–427.
- [12] J.G. Stainforth, Practical kinetic modeling of petroleum generation and expulsion, *Mar. Pet. Geol.* 26 (2009) 552–572, <http://dx.doi.org/10.1016/j.marpetgeo.2009.01.006>.
- [13] C. Pan, A. Geng, N. Zhong, J. Liu, L. Yu, Kerogen pyrolysis in the presence and absence of water and minerals: amounts and compositions of bitumen and liquid hydrocarbons, *Fuel* 88 (2009) 909–919, <http://dx.doi.org/10.1016/j.fuel.2008.11.024>.
- [14] J.H. Campbell, G.H. Koskinas, N.D. Stout, Kinetics of oil generation from Colorado oil shale, *Fuel* 57 (1978) 372–376.
- [15] K. Czajka, A. Kisiela, W. Moron, W. Ferens, W. Rybak, Pyrolysis of solid fuels: thermochemical behaviour, kinetics and compensation effect, *Fuel Process. Technol.* 142 (2016) 42–53, <http://dx.doi.org/10.1016/j.fuproc.2015.09.027>.
- [16] J.G. Reynolds, R.W. Crawford, A.K. Burnham, Analysis of oil shale and petroleum source rock pyrolysis by triple quadrupole mass spectrometry: comparisons of gas evolution at the heating rate of 10 °C/min, *Energy Fuels* (1991) 507–523.
- [17] R. Kumar, V. Bansal, R.M. Badhe, I.S.S. Madhira, V. Sugumaran, S. Ahmed, J. Christopher, M.B. Patel, B. Basu, Characterization of Indian origin oil shale using advanced analytical techniques, *Fuel* 113 (2013) 610–616, <http://dx.doi.org/10.1016/j.fuel.2013.05.055>.
- [18] E.W. Tegelaar, R.A. Noble, Kinetics of hydrocarbon generation as a function of the molecular structure of kerogen as revealed by pyrolysis-gas chromatography, *Org. Geochem.* 22 (1994) 543–574, [http://dx.doi.org/10.1016/0146-6380\(94\)90125-2](http://dx.doi.org/10.1016/0146-6380(94)90125-2).
- [19] X. Lan, W. Luo, Y. Song, J. Zhou, Q. Zhang, Effect of the temperature on the characteristics of retorting products obtained by yaojie oil shale pyrolysis, *Energy Fuels* 29 (2015) 7800–7806, <http://dx.doi.org/10.1021/acs.energyfuels.5b01645>.
- [20] R.L. Braun, A.K. Burnham, J.G. Reynolds, J.E. Clarkson, Pyrolysis kinetics for lacustrine and marine source rocks by programmed micro-pyrolysis, *Energy Fuels* 5 (1991) 192–204.
- [21] D.M. Jarvie, Factors affecting Rock-Eval derived kinetic parameters, *Chem. Geol.* 93 (1991) 79–99, [http://dx.doi.org/10.1016/0009-2541\(91\)90065-Y](http://dx.doi.org/10.1016/0009-2541(91)90065-Y).
- [22] K.E. Peters, A.E. Cunningham, C.C. Walters, J. Jiang, Z. Fan, Petroleum systems in the Jiangling-Dangyang area, Jianghan Basin, China, *Org. Geochem.* 24 (1996) 1035–1060, [http://dx.doi.org/10.1016/S0146-6380\(96\)00080-0](http://dx.doi.org/10.1016/S0146-6380(96)00080-0).
- [23] M.D. Lewan, T.E. Ruble, Comparison of petroleum generation kinetics by isothermal hydrous and nonisothermal open-system pyrolysis, *Org. Geochem.* 33 (2002) 1457–1475, [http://dx.doi.org/10.1016/S0146-6380\(02\)00182-1](http://dx.doi.org/10.1016/S0146-6380(02)00182-1).
- [24] K.E. Peters, C.C. Walters, P.J. Mankiewicz, Evaluation of kinetic uncertainty in numerical models of petroleum generation, *Am. Assoc. Pet. Geol. Bull.* 90 (2006) 387–403, <http://dx.doi.org/10.1306/10140505122>.
- [25] A. Ots, A. Poobus, T. Lausmaa, Technical and ecological aspects of shale oil and power cogeneration, *Oil Shale* 28 (2011) 101–112, <http://dx.doi.org/10.3176/oil.2011.1S.03>.
- [26] J. Soone, S. Doilov, Sustainable utilization of oil shale resources and comparison of contemporary technologies used for oil shale processing, *Oil Shale* 20 (2003)


- 311–323.
- [27] B. Maaten, L. Loo, A. Konist, D. Neshumajev, T. Pihu, I. Külaots, Decomposition kinetics of American, Chinese and Estonian oil shales kerogen, *Oil Shale* 33 (2016) 167–183, <http://dx.doi.org/10.3176/oil.2016.2>.
- [28] World Energy Council, World Energy Resources: 2013 Survey, World Energy Council, 2013 (11), http://www.worldenergy.org/wp-content/uploads/2013/09/Complete_WER_2013_Survey.pdf.
- [29] T. Pihu, A. Konist, D. Neshumajev, J. Loosaar, A. Siirde, T. Parve, A. Molodtsov, Short-Term tests on firing oil shale fuel applying low-Temperature vortex technology, *Oil Shale* 29 (2012) 3–17, <http://dx.doi.org/10.3176/oil.2012.1.02>.
- [30] A. Siirde, Oil shale – global solution or part of the problem? *Oil Shale* 25 (2008) 201, <http://dx.doi.org/10.3176/oil.2008.2.01>.
- [31] J. Yan, X. Jiang, X. Han, J. Liu, A TG-FTIR investigation to the catalytic effect of mineral matrix in oil shale on the pyrolysis and combustion of kerogen, *Fuel* 104 (2013) 307–317, <http://dx.doi.org/10.1016/j.fuel.2012.10.024>.
- [32] H. Arro, A. Prikk, T. Pihu, Calculation of qualitative and quantitative composition of Estonian oil shale and its combustion products Part 2. Calculation on the basis of technical analysis data, *Fuel* 82 (2003) 2197–2204, [http://dx.doi.org/10.1016/S0016-2361\(03\)00196-0](http://dx.doi.org/10.1016/S0016-2361(03)00196-0).
- [33] J.O. Jaber, S.D. Probert, Non-isothermal thermogravimetry and decomposition kinetics of two Jordanian oil shales under different processing conditions, *Fuel Process. Technol.* 63 (2000) 57–70, [http://dx.doi.org/10.1016/S0378-3820\(99\)00064-8](http://dx.doi.org/10.1016/S0378-3820(99)00064-8).
- [34] S. Li, C. Yue, Study of pyrolysis kinetics of oil shale, *Fuel* 82 (2003) 337–342.
- [35] A.K. Burnham, R.L. Braun, Global kinetic analysis of complex materials, *Energy Fuels* 13 (1999) 1–22.
- [36] A.K. Burnham, Chemistry and kinetics of oil shale retorting, in: O.I. Oguniola, A.M. Hartstein, O. Oguniola (Eds.), *Oil Shale A Solut. to Liq. Fuel Dilemma*, ACS Symposium Series, Washington DC, 2010, pp. 115–134.
- [37] R. Lemaire, D. Menage, P. Seers, Study of the high heating rate devolatilization of bituminous and subbituminous coals—Comparison of experimentally monitored devolatilization profiles with predictions issued from single rate, two-competing rate, distributed activation energy and chemical, *J. Anal. Appl. Pyrolysis*. 123 (2017) 255–268, <http://dx.doi.org/10.1016/j.jaap.2016.11.019>.
- [38] P. Tiwari, M. Deo, Detailed kinetic analysis of oil shale pyrolysis TGA data, *AIChE J.* 58 (2012) 505–515, <http://dx.doi.org/10.1002/aic>.
- [39] S. Vyazovkin, K. Chrissafis, M.L. Di Lorenzo, N. Koga, M. Pijolat, B. Roduit, N. Sbirrazzuoli, J.J. Suñol, ICTAC Kinetics Committee recommendations for collecting experimental thermal analysis data for kinetic computations, *Thermochim. Acta*. 590 (2014) 1–23, <http://dx.doi.org/10.1016/j.tca.2011.03.034>.
- [40] M. Al-Harashsheh, O. Al-Ayed, J. Robinson, S. Kingman, A. Al-Harashsheh, K. Tarawneh, A. Saeid, R. Barranco, Effect of demineralization and heating rate on the pyrolysis kinetics of Jordanian oil shales, *Fuel Process. Technol.* 92 (2011) 1805–1811, <http://dx.doi.org/10.1016/j.fuproc.2011.04.037>.
- [41] C. Wang, X. Zhang, Y. Liu, D. Che, Pyrolysis and combustion characteristics of coals in oxyfuel combustion, *Appl. Energy* 97 (2012) 264–273, <http://dx.doi.org/10.1016/j.apenergy.2012.02.011>.
- [42] Z. Wang, S. Deng, Q. Gu, Y. Zhang, X. Cui, H. Wang, Pyrolysis kinetic study of Huadian oil shale, spent oil shale and their mixtures by thermogravimetric analysis, *Fuel Process Technol.* 110 (2013) 103–108, <http://dx.doi.org/10.1016/j.fuproc.2012.12.001>.
- [43] H. Tanaka, The theory and practice of thermoanalytical kinetics of solid-state reactions, *J. Therm. Anal. Calorim.* 80 (2005) 795–797 <http://www.springerlink.com/index/N424566V4K31440L.pdf>.
- [44] N.E. Altun, C. Hicilymaz, J.-Y. Hwang, A.S. Bacgi, M.V. Kög, Oil shales in the world and Turkey; reserves, current situation and future prospects: a review, *Oil Shale* 23 (2006) 211–227.
- [45] H.L. Zhao, Z.Q. Bai, J.C. Yan, J. Bai, W. Li, Transformations of pyrite in different associations during pyrolysis of coal, *Fuel Process Technol.* 131 (2015) 304–310, <http://dx.doi.org/10.1016/j.fuproc.2014.11.035>.
- [46] R. Gai, L. Jin, J. Zhang, J. Wang, H. Hu, Effect of inherent and additional pyrite on the pyrolysis behavior of oil shale, *J. Anal. Appl. Pyrolysis*. 105 (2014) 342–347, <http://dx.doi.org/10.1016/j.jaap.2013.11.022>.
- [47] J. Antturi, O. Hänninen, J.-P. Jalkanen, L. Johansson, M. Prank, M. Sofiev, M. Ollikainen, Costs and benefits of low-sulphur fuel standard for Baltic Sea shipping, *J. Environ. Manage.* 184 (2016) 431–440, <http://dx.doi.org/10.1016/j.jenvman.2016.09.064>.
- [48] I. Vierth, R. Karlsson, A. Mellin, Effects of more stringent sulphur requirements for sea transports, *Transp. Res. Procedia*. 8 (2015) 125–135, <http://dx.doi.org/10.1016/j.trpro.2015.06.048>.

Appendix 3

PUBLICATION III

B. Maaten, L. Loo, A. Konist, and A. Siirde, "Mineral matter effect on the decomposition of Ca-rich oil shale," *J. Therm. Anal. Calorim.*, vol. 131, no. 3, pp. 2087–2091, 2018

Mineral matter effect on the decomposition of Ca-rich oil shale

Birgit Maaten¹  · Lauri Loo¹ · Alar Konist¹ · Andres Siirde¹

Received: 16 July 2017 / Accepted: 1 November 2017 / Published online: 9 November 2017
© Akadémiai Kiadó, Budapest, Hungary 2017

Abstract Four oil shale samples with different amounts of organic and mineral matter were analysed through non-isothermal thermogravimetric analysis using a heating rate of 50 °C min⁻¹ in nitrogen. The goal of the paper is to study the supposed catalytic effect of the indigenous and removed minerals. The samples contained 30, 49, 70 and 90% of organic matter, respectively. X-ray diffraction analysis was used to identify the minerals in the samples. Thermal analysis experiments were carried out up to temperatures of 850 °C in pyrolysis conditions. The mass loss data were used to study the variations in the conversion profiles of the organic matter depending on the content of the mineral matter. The obtained data and the comparison of the sample composition show that the effect of the mineral matter amount on the course of the pyrolysis processes is insignificant.

Keywords Oil shale · Pyrolysis · Mineral matter effect · Thermal decomposition · Thermogravimetric analysis

Introduction

Oil shale (OS) is a complex solid fuel that consists of an insoluble organic part, called kerogen, a sandy-clay part and a mineral part [1, 2]. Being one of the largest hydrocarbon reserves in the world, oil shale has offered scientific interest to groups around the world. On a wider scale, the inorganic part of OS mainly consists of carbonates,

silicates and also pyrite. To be more precise, the composition depends strongly on the origin and heritage of the shale [1]. For example, the oil shale that is used for power production in Estonia has an ash content of about 46% and contains up to 17% of carbonate minerals [3, 4]. As a comparison, OS from Maoming, China may contain 74% ash and only 1.4% of carbonates [5, 6]. It is important to note that the organic material is heterogeneously and finely dispersed in the mineral matrix [7]. As OS is widely used for both power and oil production processes like combustion and pyrolysis, these processes must be thoroughly investigated. As the mineral matter content of oil shale is one of the most crucial parameters in oil production—it affects the product yield and quality—its influence requires deeper research.

As the indigenous content of kerogen in sedimentary rocks is quite small, both physical and chemical methods are used to isolate it [2]. Chemical methods usually involve a non-oxidant acid attack at temperatures. There are different methodologies to demineralize oil shale—acid demineralization with critical point drying, subcritical water extraction, etc. [8, 9]. Flotation is also used, although this does not enable the removal of all minerals [10]. The most common is the sequential use of HCl and HF, since it is effective in removing most carbonates, silicates and oxides [11, 12]. It is also widely used since it is known that using HF and HCl acid dissolution does not alter the structure of the organic matter [13]. Boric acid is also often used in order to remove any fluorides formed during the acid wash [14]. Sometimes, HNO₃ is additionally used to remove pyrite [15, 16]. There are also combinations of different methods, for example Al-Harabsheh et al. [14] successfully used solvent extraction followed by HCl/HF acid wash, thereby increasing the kerogen content from 20 to 74%. Pan et al. [17] also successfully used a similar

✉ Birgit Maaten
birgit.maaten@ttu.ee

¹ Department of Energy Technology, Tallinn University of Technology, Ehitajate tee 5, 19086 Tallinn, Estonia

methodology in order to study the evaporating hydrocarbons.

Although there is a lot of similar data about the effectiveness of the kerogen separation, the subsequent tests offer controversial results. Yan et al. [11] studied the catalytic effect on both the pyrolysis and combustion of Huadian oil shale and found that the catalytic effect of the minerals increases the oxidation of the organic matter in the first oxidation stage. Contrary to this, Vučelić et al. [12] investigated the same phenomena with oil shale from Yugoslavia and concluded that the catalytic effect of indigenous mineral matters in the decomposition of organic matter is negligible. Additionally, the interaction between kerogen and the inorganic matrix is not well understood. To the best of our knowledge, there is no data on this issue for Estonian oil shale. Therefore, this paper investigates the pyrolysis of four Estonian oil shale samples with different organic matter contents in order to analyse the existence of the catalytic effect of indigenous minerals.

Experimental

Materials

Oil shale samples used in this paper were all from Estonia. For the following experiments, the samples were prepared as follows—the raw oil shale sample was dried at 105 °C, crushed and sieved to a particle size of below 1 mm. This is marked as sample A. Additionally from another sample with the initial particle size of up to 8 mm, the fraction of below 90 µm was separated (sieved) in order to determine whether there was a difference in the composition and reactivity. This is indicated as sample B. Two samples with the respective amounts of 70 and 90% of organic matter were prepared via flotation and HNO₃ wash from another batch of oil shale. These are marked as C and D, respectively. This means that the samples were of three different origins. The elemental analysis results of the samples can be seen in Table 1, XRD analysis results in Table 2 and X-ray fluorescence (XRF) analysis results in Table 3. As can be seen from Table 1, sample B contained a remarkably higher amount of sulphur than the other samples. This might be due to the fact that for samples C and D, the sulphur containing minerals, like

Table 1 Elemental composition of the used samples, mass%

Component	A	B	C	D
C	27.3	40.1	54.3	68.8
H	2.7	4.1	6.4	8.3
N	0.07	0.08	0.23	0.32
S	1.46	2.24	1.58	1.42

Table 2 Mineral composition of the analysed samples, analysed with XRD, mass%

Component	A	B	C	D
Dolomite	22.2	26.3	11.7	1.5
Calcite	31.7	17.8	26.6	tr.*
Quartz	11.8	11.5	12.1	6.7
K-feldspar	8.5	11.7	12.5	15.2
Illite	17.5	22	25.1	59.9
Chlorite	2.1	3.3	5.1	12.3
Kaolinite	4.4	4.3	4.5	tr.*
Anatase	tr.*	0.6	0.5	1.2
Apatite	tr.*	0.9	0.0	tr.*

* tr < 0.5 mass%

Table 3 XRF analysis results of the oil shale samples, mass%

Component	A	B	C	D
Na ₂ O	0.13	0.17	0.14	0.08
MgO	3.69	3.43	1.41	0.47
Al ₂ O ₃	5.02	4.36	2.79	1.42
SiO ₂	15.35	12.98	8.71	3.73
P ₂ O ₅	0.10	0.07	0.05	0.02
SO ₃	1.98	2.10	2.41	0.24
K ₂ O	1.87	1.82	0.84	0.86
CaO	20.71	11.96	7.33	0.85
TiO ₂	0.32	0.24	0.18	0.10
MnO	0.04	0.03	0.02	0.00
Fe ₂ O ₃	2.21	2.24	1.14	0.39
LOI ^a	48.54	60.54	74.92	91.82

* *n/d* not detected

^aLoss on ignition at 920 °C

pyrite, were removed with acid wash. Sample B was not treated with any acidic compounds but contained less mineral matter, thereby increasing the sulphur content.

Equipment and procedure

The chemical composition of the samples was determined with XRF. The analysis was performed with a Rigaku Primus II WD-XRF spectrometer. X-ray source was Rhodium anode 4 kW X-Ray tube with 30 µm window. The list of crystals in use was as follows: RX25, PET, LiF(200), LiF(220), RX61F, RX75, Ge, RX4 and RX40. For mineralogical composition, the XRD analysis was done using a Bruker Advance D8 system using Cu K α radiation in the 2 h range of 3°–72°, with a step size of 0.02° 2 θ and a counting time of 0.1 s per step using a LynxEye detector. The X-ray tube was operated at 40 kV and 40 mA. Elemental analysis results were obtained using an Elementar

Table 4 Characteristic temperatures and parameters of oil shale thermal decomposition

Characteristic	A	B	C	D
$T_{\text{onset}}/^{\circ}\text{C}$	417	415	419	419
$T_{\text{max}}/^{\circ}\text{C}$	466	461	464	472
$T_{\text{e}}/^{\circ}\text{C}$	489	485	492	496
Organic matter/mass%	30.3	49.0	68.3	88.3
Mineral CO_2 /mass%	18.4	11.5	5.0	0.0

Analyser System Vario MACRO CHNS apparatus. The TGA analysis was conducted on a NETZSCH STA 449 F3 Jupiter[®] TG-DSC apparatus. The samples were heated in a pure nitrogen atmosphere. A protective gas flow of 50 mL min^{-1} of high-purity nitrogen was used. A constant heating rate of $50 \text{ }^{\circ}\text{C min}^{-1}$ was applied in the temperature range of 40–850 $^{\circ}\text{C}$. In order to eliminate buoyancy effects, correction runs with empty crucibles were run and subtracted from the measurement data. The samples were analysed in Pt/Rh alloy crucibles with removable thin-walled liners of Al_2O_3 . An isothermal step at 105 $^{\circ}\text{C}$ was used in order to remove moisture. The temperature calibration of the apparatus was done using In, Sn, Zn, Al and Au standards. Measurements were repeated at least twice to ensure reproducibility (temperature difference did not exceed 1.6 $^{\circ}\text{C}$). Additionally, the amount of organic matter and mineral carbon dioxide (see Table 4) were quantified. These were obtained from the results of thermal analysis in an atmosphere of 80% N_2 and 20% O_2 .

Calculation of conversion

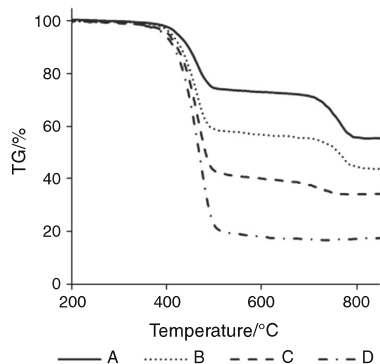
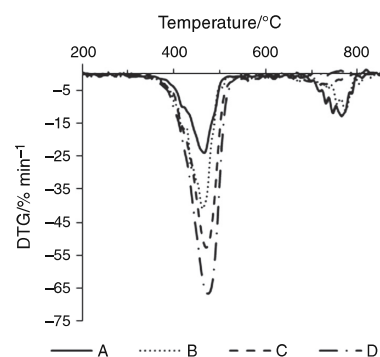
In order to compare the possible effect of the minerals on the organic matter thermal decomposition, the conversion in relation to temperature was investigated. The extent of conversion, x , was defined as the fractional mass loss at any time, t . It was calculated as follows:

$$x = \frac{W_0 - W_t}{W_0 - W_f} \quad (1)$$

W_0 was the initial mass of the sample, W_t the mass of the sample at time t , and W_e was the final mass at the end of the reaction (burnout). Therefore, it was a dimensionless value in the range of 0–1. In order to avoid any effects of moisture, conversion calculation was started as 0 at 200 $^{\circ}\text{C}$.

Results and discussion

The analysed samples contained different amounts of organic matter and minerals, and this was very well illustrated by their thermal degradation profiles. Figure 1 shows

**Fig. 1** Thermal degradation curves for the pyrolysis process of the analysed oil shale samples**Fig. 2** Derivatives of mass loss of the analysed oil shale samples

the total mass loss (TG) curves of the analysed samples for the pyrolysis process. Figure 2 exhibits the derivatives of total mass loss (DTG).

The pyrolysis process is complex, with many competing processes contributing to thermal curves [14]. As can be seen from Fig. 1, the main mass loss step is in the temperature range of 410–500 $^{\circ}\text{C}$. This is attributed to the pyrolysis of bitumen and kerogen and additionally the cracking of kerogen and the release of hydrocarbons [14]. This is in good accordance with literature data [18–20]. The second mass loss step (700–800 $^{\circ}\text{C}$) was the result of decomposition of carbonate minerals. For the sample D, containing no carbonate minerals no second step was recorded as expected.

The significant temperatures derived from TG and DTG are shown in Table 4. For comparison, the onset of mass loss (T_{onset}), the temperature of maximal devolatilization ($T_{\text{max}1}$ and $T_{\text{max}2}$) and the temperature of the end of the decomposition (T_{e}) are shown.

As can be seen from these data, the beginning of the pyrolysis process is not affected by the mineral and organic matter amount— T_{onset} varies in a very small range, only 4 °C and T_b varies 11 °C. The samples with higher mineral matter amount content exhibited a lower end of reaction temperature. This may indicate the existence of a catalytic effect of additives. Nevertheless, the difference between characteristic temperatures of raw oil shale, containing 70% mineral matter, and upgraded oil shale, containing only 12% mineral matter, was less than 10 °C. Zou et al. and Leeuw et al. [21, 22] have investigated effects of catalysts on coal-char thermal degradation and found difference in T_{max} to be even over 100 °C. As the samples contain different amounts of organic matter, the TG curves displayed in Fig. 1 were difficult to compare. Plotting conversion of organic matter against temperature simplifies the comparison of the samples.

The research about the possible catalytic effect of minerals on the decomposition of Estonian oil shale is scarce. Therefore, samples with containing different amounts of organic and mineral matter were chosen and subjected to thermal analysis in pyrolysis conditions. The results of the comparison of organic matter conversion can be seen in Fig. 3.

As the curves exhibit very similar profiles and the difference is minimal, this result is strongly suggestive that the catalytic effect of the minerals on the decomposition of the organic matter in oil shale during the pyrolysis process was neglectable. It should be noted that the samples were of different origin. With that in mind, the differences were negligible. Although pyrolysis is catalysed by alkaline earth metal cations and carbonates, the reactions are at the same time inhibited by silicates [23]. As there was no change in the conversion, it seems that the inhibiting effect

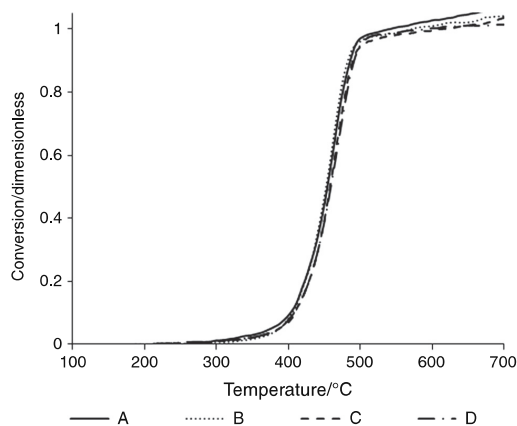


Fig. 3 Comparison of the conversion change for pyrolysis analysis results

is greater than the catalytic effect. This is in good accordance with the results obtained with other oil shales [15, 23]. If there would be a catalytic effect of the minerals, the reaction temperature (maximum mass loss rate temperature T_{max}) would be shifted to lower regions. However, this phenomenon does not apply here. As noted in Table 3, the T_{max} values were very similar for all the samples, varying only by 6 °C and the conversion curves were almost identical. As T_{max} was shifted to a lower temperature in case of sample B but not for sample C, which contains significantly less mineral matter, there was no reason to believe that such a small change would result in a noticeable effect. This was also explained by the fact that during the sieving process some parts of the mineral matter remained bound with the organic matter, thereby decreasing the overall porosity and inhibiting heat transfer. Ultimately, this slowed the decomposition process and increased the end temperature. As the oil shales used to produce the samples analysed in this paper are of three different origins, these results correlate very well with each other. Therefore, we can conclude that there is no significant catalytic effect of the minerals in Estonian oil shale on the decomposition of organic matter for the pyrolysis process.

Conclusions

This paper presents the results of the thermogravimetric analysis of four oil shale samples with different amounts of organic and mineral matter. The analysed samples contained 30, 49, 70 and 90% organic matter and 18, 12, 5 and 0% of carbonate minerals, respectively. The samples were subjected to thermal analysis in pyrolysis conditions. TGA data were used to calculate the conversion of the organic matter in relation to temperature in order to determine whether the inherent and removed minerals have a catalytic effect on the decomposition. It was concluded that for the pyrolysis process, the minerals had no evident catalytic effect.

Acknowledgements This work has been partially supported by ASTRA “TUT Institutional Development Program for 2016-2022” Graduate School of Functional materials and technologies (2014-2020.4.01.16-0032). Special thanks go to Gert Preegel, Ph.D., for the procurement of some of the samples.

References

- Altun NE, Hicyilmaz C, Hwang J-Y, Baççi AS, Kök MV. Oil shales in the world and Turkey; reserves, current situation and future prospects: a review. *Oil Shale*. 2006;23:211–27.
- Vandenbroucke M, Largeau C. Kerogen origin, evolution and structure. *Org Geochem*. 2007;38:719–833.

3. Konist A, Pihu T, Neshumayev D, Siirde A. Oil shale pulverized firing: boiler efficiency, ash balance and flue gas composition. *Oil Shale*. 2013;30:6–18.
4. Kaljuvee T, Trass O, Pihu T, Konist A, Kuusik R. Activation and reactivity of Estonian oil shale cyclone ash towards SO₂ binding. *J Therm Anal Calorim*. 2015;121:19–28.
5. Qian J, Li S, Wang J. Oil shale development in China. *Oil Shale*. 2003;20:356–9.
6. Li S, Yue C. Study of pyrolysis kinetics of oil shale. *Fuel*. 2003;82:337–42.
7. Karabakan A, Yürüm Y. Effect of the mineral matrix in the reactions of shales. Part 2. Oxidation reactions of Turkish Göynük and US western reference oil shales. *Fuel*. 2000;79:785–92.
8. Suleimenova A, Bake KD, Ozkan A, Valenza JJ, Kleinberg RL, Burnham AK, et al. Acid demineralization with critical point drying: a method for kerogen isolation that preserves microstructure. *Fuel*. 2014;135:492–7.
9. Luong D, Sephton MA, Watson JS. Subcritical water extraction of organic matter from sedimentary rocks. *Anal Chim Acta*. 2015;879:48–57.
10. Palvadre R, Abelik V. Beneficiation of Estonian (Kukersite) oil shale. *Oil Shale*. 2011;28:353–65.
11. Yan J, Jiang X, Han X, Liu J. A TG-FTIR investigation to the catalytic effect of mineral matrix in oil shale on the pyrolysis and combustion of kerogen. *Fuel*. 2013;104:307–17.
12. Vučelić D, Marković V, Vučelić V, Spiridonović D, Jovančičević B, Vitorović D. Investigation of catalytic effects of indigenous minerals in the pyrolysis of Aleksinac oil shale organic matter. *Org Geochem*. 1992;19:445–53.
13. Aboulkas A, El Harfi K. Effects of acid treatments on Moroccan Tarfaya oil shale and pyrolysis of oil shale and their kerogen. *J Fuel Chem Technol*. 2009;37:659–67.
14. Al-Harashsheh M, Al-Ayed O, Robinson J, Kingman S, Al-Harashsheh A, Tarawneh K, et al. Effect of demineralization and heating rate on the pyrolysis kinetics of Jordanian oil shales. *Fuel Process Technol*. 2011;92:1805–11.
15. Pan L, Dai F, Huang J, Liu S, Li G. Study of the effect of mineral matters on the thermal decomposition of Jimsar oil shale using TG–MS. *Thermochim Acta*. 2016;627–629:31–8.
16. Ballice L. Effect of demineralization on yield and composition of the volatile products evolved from temperature-programmed pyrolysis of Beypazari (Turkey) oil shale. *Fuel Process Technol*. 2005;86:673–90.
17. Pan C, Geng A, Zhong N, Liu J, Yu L. Kerogen pyrolysis in the presence and absence of water and minerals. 1. Gas components. *Energy Fuels*. 2008;22:416–27.
18. Bai F, Sun Y, Liu Y, Li Q, Guo M. Thermal and kinetic characteristics of pyrolysis and combustion of three oil shales. *Energy Convers Manag*. 2015;97:374–81.
19. Aboulkas A, El Harfi K. Study of the kinetics and mechanisms of thermal decomposition of Moroccan Tarfaya oil shale and its kerogen. *Oil Shale*. 2008;25:426.
20. Tiwari P, Deo M. Detailed kinetic analysis of oil shale pyrolysis TGA data. *AIChE J*. 2012;58:505–15.
21. Zou C, Zhao J, Li X, Shi R. Effects of catalysts on combustion reactivity of anthracite and coal char with low combustibility at low/high heating rate. *J Therm Anal Calorim*. 2016;126:1469–80.
22. Leeuw KA, Strydom CA, Bunt JR, van Niekerk D. The influence of K₂CO₃ and KCl on H₂ formation during heat treatment of an acid-treated inertinite-rich bituminous coal-char. *J Therm Anal Calorim*. 2016;126:905–12.
23. Yürüm Y, Karabakan A. Effect of the mineral matrix in the reactions of oil shales: 1. Pyrolysis reactions of Turkish Göynük and US Green River oil shales. *Fuel*. 1998;77:1303–9.

Curriculum vitae

Personal data

Name	Birgit Maaten
Date of birth	05.10.1990
Place of birth	Viljandi
Citizenship	Estonian

Contact data

E-mail	birgit.maaten@ttu.ee
--------	--

Education

2014– 2018	Tallinn University of Technology—PhD
2013 autumn	Semester abroad at Pierre and Marie Curie University
2014– 2018	Tallinn University of Technology, Applied Chemistry and Biotechnology (<i>cum laude</i>) – MSc
2009– 2012	Tallinn University of Technology, Applied Chemistry and Biotechnology – BSc
1997– 2009	Viljandi Paalalinna Gymnasium – High school

Language competence

Estonian	Native speaker
English	Fluent
German	Fluent
French	Beginner

Professional employment

01.09.2017-...	Tallinn University of Technology, School of Engineering, Department of Energy Technology, early stage researcher
01.01.2017-31.08.2017	Tallinn University of Technology, School of Engineering, Department of Energy Technology, researcher
01.09.2014-31.12.2016	Tallinn University of Technology, Faculty of Mechanical Engineering, Department of Thermal Engineering, researcher
10.06.2013-31.08.2014	Tallinn University of Technology, Faculty of Mechanical Engineering, Department of Thermal Engineering, other staff

Projects in progress

LEP17084 "Fundamental Research studies on thermochemical conversion of local biomass in Utilitas Tallinn powerplant (9.08.2017–8.08.2020)", Alar Konist, Tallinn University of Technology, School of Engineering, Department of Energy Technology.

Lep17006 "Fundamental Research studies on Oil Shale Technologies (1.01.2017–31.12.2018)", Alar Konist, Tõnu Pihu, Tallinn University of Technology, School of Engineering, Department of Energy Technology.

KIK16064 "The survey of the emission of heavy metals of the ashes formed by thermal treatment and burning of the solid fuels - oil shale, semi-coke gas, biomass etc. (26.10.2016–3.06.2018)", Andres Siirde, Tallinn University of Technology , School of Engineering, Department of Energy Technology.

Elulookirjeldus

Isikuandmed

Nimi	Birgit Maaten
Sünniaeg	05.10.1990
Sünnikoht	Viljandi
Kodakondsus	Eesti

Kontaktandmed

E-post	birgit.maaten@ttu.ee
--------	--

Hariduskäik

2014–2018	Tallinna Tehnikaülikool – PhD
2013 sügis	Välispraktika Pierre ja Marie Curie nimelises ülikoolis
2012–2014	Tallinna Tehnikaülikool, rakenduskeemia ja biotehnoloogia – MSc (<i>cum laude</i>)
2009–2012	Tallinna Tehnikaülikool, rakenduskeemia ja biotehnoloogia – BSc
1997–2009	Viljandi Paalalinna Gümnaasium – keskharidus

Keelteoskus

Eesti keel	Emakeel
Inglise keel	Kõrgtase
Saksa keel	Kõrgtase
Prantsuse keel	Algtase

Teenistuskäik

01.09.2017-...	Tallinna Tehnikaülikool, Inseneriteaduskond, Energiatehnoloogia instituut, doktorant-nooremteadur
01.01.2017-31.08.2017	Tallinna Tehnikaülikool, Inseneriteaduskond, Energiatehnoloogia instituut, teadur
01.09.2014-31.12.2016	Tallinna Tehnikaülikool, Mehaanikateaduskond, Soojustehnika instituut, teadur
10.06.2013-31.08.2014	Tallinna Tehnikaülikool, Mehaanikateaduskond, Soojustehnika instituut, insener

Jooksvad projektid

LEP17084 "Biomassi termokeemiliste protsesside alased teadusuuringud OÜ Utilitas Tallinna Elektrijaamas (9.08.2017–8.08.2020)", Alar Konist, Tallinna Tehnikaülikool, Inseneriteaduskond, Energiatehnoloogia instituut.

Lep17006 "Põlevkivitehnoloogiate alased teadusuuringud Enefit Energiatootmise AS-ile (1.01.2017–31.12.2018)", Alar Konist, Tõnu Pihu, Tallinna Tehnikaülikool, Inseneriteaduskond, Energiatehnoloogia instituut.

KIK16064 "Tahkete segukütuste- põlevkivi, uttegaasi, biomassi jt termilisel käitlemisel ja (26.10.2016–3.06.2018)", Andres Siirde, Tallinna Tehnikaülikool, Inseneriteaduskond, Energiatehnoloogia instituut.